THESIS FOR THE DEGREE OF DOCTOR OF PHILOSOPHY

Design, Synthesis and Characterization of Conjugated Polymers for Photovoltaics and Electrochromics

KIM BINI

Department of Chemistry and Chemical Engineering

CHALMERS UNIVERSITY OF TECHNOLOGY

Gothenburg, Sweden 2018

Design, Synthesis and Characterization of Conjugated Polymers for Photovoltaics and Electrochromics
Kim Bini
ISBN 978-91-7597-834-5

Doktorsavhandlingar vid Chalmers tekniska högskola
Ny serie nr 4515
ISSN 0346-718X

Division of Applied Chemistry
Department of Chemistry and Chemical Engineering
Chalmers University of Technology
SE-412 96 Gothenburg
Sweden
Telephone + 46 (0)31-772 1000

Cover:
An series of photos of the electrochromic transition of the polymer PIDTT from red/pink and absorbing to faint blue transmissive, along with schematic polymer structure and arbitrary CIE 1931 color coordinate system transition.

Chalmers Reproservice
Gothenburg, Sweden 2018

Design, Synthesis and Characterization of Conjugated Polymers for Photovoltaics and Electrochromics

Kim Bini

Department of Chemistry and Chemical Engineering

Chalmers University of Technology

Abstract

With the invention of organic electronics, a new class of materials needed to be explored and suitable applications found. The use as semiconductors in many different devices has been explored, where photovoltaics, light-emitting diodes and field-effect transistors have been prominent. For most applications the organic semiconductors have some advantages when compared to their inorganic counterpart, such as molecular design variability, solution processing and flexible mechanical properties. These advantages are quickly making organic semiconductors an interesting alternative in a wide variety of fields.

Organic photovoltaics (OPV) have developed rapidly the last decade and is currently close to being commercially viable for niche applications. There are still some problems to overcome, however, such as device lifetimes, upscaling to large scale production and preferably a higher power conversion efficiency (PCE) as well. A major disadvantage is the use of toxic and environmentally negative solvents during processing. With the rapid rise of OPVs with polymeric donor and acceptors, so called all-polymer solar cells (all-PSC), some old assumptions about the devices are not valid anymore. Rational design of molecules can be used to achieve desired molecular properties in an attempt to overcome these problems.

To address these problems, side chain modification of conventional conjugated polymers was used to produce several series of functional polymers. A set of fluorene-based polymers with polar side chain pendant groups was used as alcohol-soluble cathode interfacial layers. This study managed to prove design principles previously used for polymer:fullerene based solar cells are still valid for all-PSCs. A separate set of polymers, based on isoindigo, included thermocleavable side chains in an effort to address the inherently unstable bulk-heterojunction structures between polymers and fullerenes. This series of polymers managed to show almost complete stabilization of the blend films upon thermal treatment.

In parallel with the developing OPV field, similar conjugated polymers have shown dramatic electrochromism, meaning they change color when an electrical field is applied over them. This peculiar property has possible uses in devices which could either switch between absorbing and transmitting such as windows or sunglasses, or switch between non-emissive coloration and transparent, useful in displays with energy consumption restrictions. The polymers used for organic electrochromics (OEC) need to show a large degree of electrochromic contrast, fast switching speeds and electrochemical stability. These two fields will be treated in this thesis with a focus on design and synthesis of functional polymers to solve the problems and material requirements for their future successful application.

Keywords: *all-polymer solar cells, conjugated polymers, electrochromic polymers, organic electronics, polymer solar cells, side chain engineering*

List of Publications

This thesis is based on the following publications:

Paper I. Synthesis and Characterization of Isoindigo-Based Polymers with Thermocleavable Side Chains
Kim Bini; Xiaofeng Xu; Mats R. Andersson; Ergang Wang
Macromolecular Chemistry and Physics, (2018), p. 1700538

Paper II. Alcohol-Soluble Conjugated Polymers as Cathode Interlayers for All-Polymer Solar Cells
Kim Bini; Xiaofeng Xu; Mats R. Andersson; Ergang Wang
ACS Applied Energy Materials, Vol. 1 (2018), p. 2176-2182

Paper III. Conjugated Polymers with Tertiary Amine Pendant Groups for Organic Electronic Applications
Kim Bini; Anirudh Sharma; Xiaofeng Xu; Mats R. Andersson; Ergang Wang
Manuscript in preparation.

Paper IV. Broad Spectrum Absorption and Low-Voltage Electrochromic Operation from Indacenodithieno[3,2-b]thiophene-Based Copolymers
Kim Bini; Petri Murto; Sait Elmas; Mats R. Andersson; Ergang Wang
Submitted.

Paper V. Orange to Green Switching Anthraquinone-Based Electrochromic Material
Kim Bini; Desta Gedefaw; Caroline Pan; Jonas M. Bjuggren; Sait Elmas; Anirudh Sharma; Ergang Wang, Mats R. Andersson
Submitted.

Contribution Report

Paper I. Responsible for planning experiments and writing the article, as well as performing all synthesis and most characterization with the exception of molecular weight determination.

Paper II. Responsible for planning experiments and writing the article, as well as performing all synthesis and most characterization with the exception of molecular weight determination, device production and photovoltaic performance measurements.

Paper III. Responsible for planning, synthesis, characterization except for device manufacturing and photovoltaic measurements. Writing the manuscript as first author.

Paper IV. Responsible for electrochromic measurements and data analysis, as well as writing the manuscript as first author with equal contribution to Petri Murto.

Paper V. Responsible for electrochromic measurements and data analysis, and parts of manuscript writing as shared first author with Desta Gedefaw.

Publications not included in this thesis

Effects of side chain isomerism on the physical and photovoltaic properties of indacenodithieno[3,2-b]thiophene–quinoxaline copolymers: toward a side chain design for enhanced photovoltaic performance
Xiaofeng Xu; Zhaojun Li; Olof Bäcke; Kim Bini; David I. James; Eva Olsson; Mats R. Andersson; Ergang Wang
Journal of Materials Chemistry, Vol. 2 (2014), 44, p. 18988-18997.

Pyrrolo[3,4-g]quinoxaline-6,8-dione-based conjugated copolymers for bulk heterojunction solar cells with high photovoltages
Xiaofeng Xu; Chuanfei Wang; Olof. Bäcke; David I. James; Kim Bini; Eva Olsson; Mats R. Andersson; Mats Fahlman; Ergang Wang
Polymer Chemistry, Vol. 6 (2015), 25, p. 4624-4633.

Synthesis and characterization of benzodithiophene and benzotriazole-based polymers for photovoltaic applications
Desta Antenehe Gedefaw; M. Tessarolo; M. Bolognesi; M. Prosa; Renee Kroon; Wenliu Zhuang; Patrik Henriksson; Kim Bini; Ergang Wang; M. Muccini; M. Seri; Mats R. Andersson
Beilstein Journal of Organic Chemistry, Vol. 12 (2016), p. 1629-1637.

Low Band Gap Polymer Solar Cells With Minimal Voltage Losses
Chuanfei Wang; Xiaofeng Xu; Wei Zhang; Jonas Bergqvist; Yuxin Xia; Xiangyi Meng; Kim Bini; Wei Ma; Arkady Yartsev; Koen Vandewal; Mats R. Andersson; Olle Inganäs; Mats Fahlman; Ergang Wang
Advanced Energy Materials, Vol. 6 (2016), p. 1600148.

High-Performance Organic Photodetectors from a High-Bandgap Indacenodithiophene-Based π‑Conjugated Donor−Acceptor Polymer
Cindy Montenegro Benavides; Petri Murto; Christos L. Chochos; Vasilis G. Gregoriou; Apostolos Avgeropoulos; Xiaofeng Xu; Kim Bini; Anirudh Sharma; Mats R. Andersson; Oliver Schmidt; Christoph J. Brabec; Ergang Wang; Sandro F. Tedde
ACS Applied Materials & Interfaces, Vol. 10 (2018), p. 12937-12946

List of Acronyms

AFM - Atomic Force Microscopy

All-PSC - All-polymer solar cell

BHJ - Bulk heterojunction

t-BOC - *tert*-butyloxycarbonyl

BT - Benzothiadiazole

BTz - Benzotriazole

CIM - Cathode Interface Material

CV - Cyclic Voltammetry

DA - Donor-Acceptor

DArP – Direct Arylation Polymerization

DFT - Density Functional Theory

DMAP - Dimethylamino pyridine

DMF - Dimethylformamide

DMSO - Dimethyl sulfoxide

DPP - Diketopyrrolopyrrole

DSC - Differential scanning calorimetry

EA – Electron Affinity

ECP – Electrochromic Polymer

E_{CT} – Charge-Transfer Energy

E^{ec}- Electrochemical Band Gap

E^{opt}- Optical Band Gap

EPBT – Energy Payback time

ETL – Electron Transport Layer

FF - Fill-factor

Fl - Fluorene

FTIR - Fourier-transform infrared spectroscopy

GPC - Gel permeation chromatography

HOMO - Highest occupied molecular orbital

$HOMO_D$ - Donor HOMO

HTL – Hole Transport Layer

II - Isoindigo

IP – Ionization Potential

J_{SC} - Short-circuit current

LiF - Lithium Fluoride

LUMO - Lowest Unoccupied Molecular Orbital

$LUMO_A$ - Acceptor LUMO

MEH-PPV - poly(2-methoxy-5-(2'-ethyl-hexyloxy)-1,4-phenylene vinylene

M_n - Number-Average Molecular Weight

M_w - Weight-average molecular weight

OEC - Organic Electrochromic

OED – Organic Elechtrochromic Device

OLED – Organic Light-emitting diode

OPV - Organic Photovoltaics

P3HT – Poly(3-hexylthiophene-2,5-diyl)

PCBM - Phenyl-C61-butyric acid methyl ester

PCE - Power conversion efficiency

$Pd_2(dba)_3$ - tris(dibenzylideneacetone)dipalladium(0)

PDI - Polydispersity index

PEDOT:PSS - poly(3,4-ethylenedioxythiophene): polystyrene sulfonate

PFN - polyfluorene amine

N2200 – Poly[[*N*,*N*′-bis(2-octyldodecyl)-naphthalene-1,4,5,8-bis(dicarboximide)-2,6-diyl]-*alt*-5,5′-(2,2′-bithiophene)]

PSC - Polymer solar cell

P(*o*-Tol)$_3$ - tri(*o*-tolyl)phosphine

SMA – Small molecule acceptor

SWV - Square wave voltammetry

TEA - triethylamine

TEM - Transmission electron microscopy

TGA - Thermogravimetric analysis

V_{oc} - Open-circuit voltage

Table of contents

1. Introduction

1.1. Aim and Outline of the Thesis

This thesis will treat the synthesis and characterization of a wide array of conjugated polymers used in various organic electronics applications, mainly photovoltaics and electrochromics. A recurring theme will be the modification of side chains, instead of just the polymer backbones. Initially a general background to organic semiconductors will be presented with a focus on the history and theory of conjugated polymers. This is followed by a more theoretical section discussing the properties of conjugated polymers, how the structures can be modified to change their properties and lastly how to synthesize and characterize them. The following chapter introduced some core concepts of organic photovoltaics, which is been a main focus area of the thesis. A background to the purpose of the field of organic photovoltaics will be presented followed by an introduction to the working mechanism, as well as a description of the device structure and figures of merit. This chapter contains the necessary knowledge needed for the following chapters.

In chapter 3 and 4 Paper II and Paper III will be presented, respectively. The first one treats the production of alcohol-soluble cathode interfacial layer polymers used in all-polymer solar cell devices with good effect. It will in detail describe the interface between the active layer and the electrodes in devices and show the synthesis, characterization and performance of the produced polymers. Chapter 4 will treat the content of an unpublished manuscript in which a series of seven polymers bearing tertiary amine pendant groups aimed for the active layer will be presented. While the polymers are similar to the preceding chapter, their application is different.

After the focus on organic photovoltaics, chapter 5 will introduce the concept of organic electrochromics. This is the field of materials with color changes associated with changes in external potential. The materials are closely related to the conjugated polymers used in photovoltaics and sometimes the material produced for one application performs better in the other. The differences in desired properties will also be discussed. After the necessary background has been presented in chapter 5, chapter 6 will present the work in Paper IV and Paper V. These papers contain the synthesis and characterization of two sets of polymers for electrochromic applications. The first consists of four polymers based on the IDTT-block and the last polymer is based on anthraquinone.

Chapter 7, the last chapter, treats the first Paper I. This counterintuitive ordering is because it fits into neither of the previous sections, or possibly both. It presents the synthesis and extensive characterization of a series of isoindigo-based polymers with an increasing content of cleavable side-chains. Since the polymers were applied in neither solar cells nor electrochromics, but could be relevant in both, it was placed after the other chapters last.

The final chapter contains some conclusions drawn from this research, a general view of the present position of the fields discussed and outlook for the future.

1.2. A Brief History of Organic Semiconductors

The development of organic semiconductors started with the work of Heeger, MacDiarmid and Shirakawa, for which they shared the Nobel Prize in Chemistry year 2000.[1] In their original paper from 1977, they present the dramatically increased conductivity of polyacetylenes by halogen doping, which was followed by a large amount of publications.[2-3] In 1984, the same group managed to make a conjugated polymer with a narrow band gap with the use of the lower energy resonance quinoidal structure to reach a narrower band gap.[4] The understanding of the band gap-narrowing effect of the quinoidal resonance structure came from calculations by Brédas two years later, who produced good agreement between experimental and calculated band gap values when comparing poly(thiophene) to poly(isothianaphtalene).[5] They also predicted that even lower band gaps could be reached with intermediate aromatic-quinoidal structure, leading to copolymers with alternating aromatic and quinoidal structures.[6] A different approach to achieve a smaller band gap was to include a “push-pull” structure with electron rich thiophene units and electron poor pyridine units in a copolymer.[7] Further studies by Havinga *et al.* managed to produce polymers with remarkably small band gaps of around 0.5 eV.[8-9] This was then used as a design tool to customize the optical or electrochemical properties of polymers and to further improve the understanding of the new class of material.[10-11] In the 1990s, knowledge of organic semiconductor had progressed enough for investigations into semiconductor applications starting to show up. This was the beginning of organic electronics such as photovoltaics, transistors, photodetectors, light-emitting diodes, applications where inorganic materials dominated.

Organic Solar Cells

The first organic solar cells used one-component active layers, which yielded small photocurrents, but in 1986, Tang made a bilayer device with energy level offset, which gave

significantly improved performance.[12] This was later explained by the energy level differences creating a driving force for charge separation of excitons. In 1992, the extremely fast photoinduced electron transfer from an excited conducting polymer to fullerene was shown.[13] The interest in fullerenes as electron acceptor molecule was large, but the limited solubility was a problem. By introducing the chemically modified fullerene derivative phenyl-C61-butyric acid methyl ester (PCBM), the solubility issue was significantly improved in 1995.[14] Later the same year, PCBM was successfully used in blends with conducting polymers.[15] Blends of poly(2-methoxy-5-(2'-ethyl-hexyloxy)-1,4-phenylene vinylene (MEH-PPV) with PCBM were used in organic solar cells with a PCE of 2.9%, which at the time was an incredible improvement compared to earlier pure MEH-PPV based polymer solar cells (PSC). The improvement is mainly attributed to the charge separation in the blend and a "bicontinous network of internal donor-acceptor heterojunctions", introducing the bulk-heterojunction (BHJ) which quickly became the almost universally used active layer morphology. In 2005, new record OPV devices of 4 - 5% were produced with the use of greatly improved understanding of the morphology of the BHJ systems.[16-17] These rapid advances have led to new records in performance almost every year, and single junction solar cells reached 13% in 2017, with a current record of over 14% PCE.[18-19] They are expected to soon reach over 15%, and possibly 20% within a few years.[20-21] This is quickly approaching what people calculated as a soft maximum efficiency just a few years ago, and means the structures are rapidly approaching commercial viability with calculated energy payback times (EPBT) of just days.[22-25]

Other applications

In parallel with the development of OPVs, the field of organic light-emitting diodes (OLED) was developing. OLEDs have not been the focus of this thesis, but will be referenced occasionally and require an introduction. The first reports of organic electroluminescence was in the 1960s,[26-27] but the large advancements came later. The reports showed that electroluminescence required injection of electrons and holes via electrodes to generate radiative recombination of the charge carriers. A highly influential review article, published by Friend *et al.* in Nature in 1999, presented the rapid advances in OLED from the 1980s and forward.[28] In 1987, Tang and VanSlyke published a landmark paper where a double-layer organic thin film device showed significant electroluminescence.[29] This led to rapid development in the field, with pioneering works to improve the efficiency of the organic emitters led by Adachi, Tsutsui and Saito.[30] The use of conjugated polymers in OLEDs was proposed by Burroughes *et al.* in 1990.[31] OLEDs are the most commercially successful

application for organic semiconductors today, with plenty finished consumer products such as monitors in TVs and smartphones containing OLED technology.

The growing research into organic electronics made major advancements for other applications as well, such as organic molecules in transistors,[32-35] and photodiodes,[15,36] and the field of organic electrochromics, which will be further discussed in chapter 5 & 6. A common theme for the interest in the organic electronics, which directly competes with more mature technology based on inorganic compounds, is their lightness, flexibility, ease of processing and relative price advantage.

1.3. Properties and Molecular Design of Conjugated Polymers

A semiconducting compound is one which requires excitation to conduct a charge. The energy required to excite the semiconductor is called the band gap (E_g). The E_g of a polymer is the most fundamental property that governs its use as a semiconductor and corresponds to the difference between the top of the valence band and the bottom of the conduction band, the polymer's ionization energy (IP) and electron affinity (EA).[37] The relationship of these factors are summarized in an energy level diagram in Figure 1.1. A conducting material has overlapping levels of IP and EA, which means they do not have a band gap, resulting in a ground state conduction. Insulators, on the other hand, possess a very large band gap making the transition require very high energies. The lowest energy required for a photon to excite an electron in the molecule from the ground state (S_0) to the lowest singlet state (S_1) is called the optical band gap (E^{opt}) and is generally smaller than the E_g due to electrostatic interaction between the electron and the electron hole, together called an exciton. The difference between E_g and E^{opt} is called the binding energy (E_B) and can be seen as the energy required to separate the exciton.

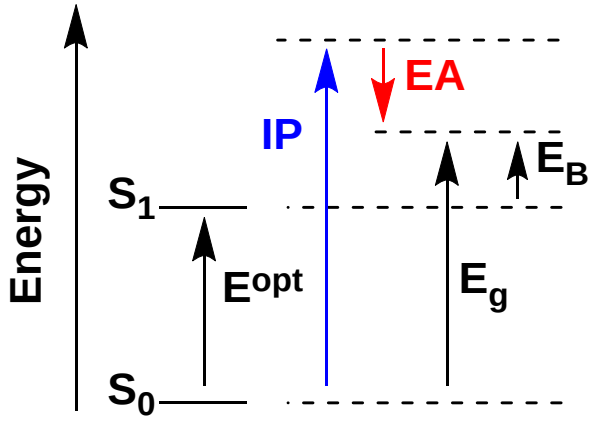

Figure 1.1. Energy level diagram illustrating energy levels and band gaps.

The energy levels of the electrons of molecules are generally presented as molecular orbitals. The most relevant energies are the frontier orbitals, i.e. the highest occupied molecular orbital (HOMO) and the lowest unoccupied molecular orbital (LUMO). The energy levels relative to vacuum position of the HOMO and LUMO levels define how much energy is needed for the material to lose an electron or gain an electron, respectively.

Quinoidal Structure

Conjugated polymers tend to have large band gaps, which needs to be reduced to be used as practical semiconductors. As will be discussed in section 2.2, two primary tools have been developed to reduce the band gap: alternating aromatic and quinoidal units in copolymers and using donor-acceptor structure with push-pull effect. Scheme 1.1 shows examples of the quinoidal resonance structures for three polymers. The quinoidal structure tends to have more delocalized electrons, which gives a more planar structure with smaller bond length difference between the single bonds and double bonds. This effect lowers the band gap, red-shifting the absorption of the polymer.[4] Part of the drastic difference in the band gaps of the three polymers can be ascribed to this effect, where poly(isothianaphtalene) has a very stable quinoidal structure and poly(*p*-phenylene) an unstable one.

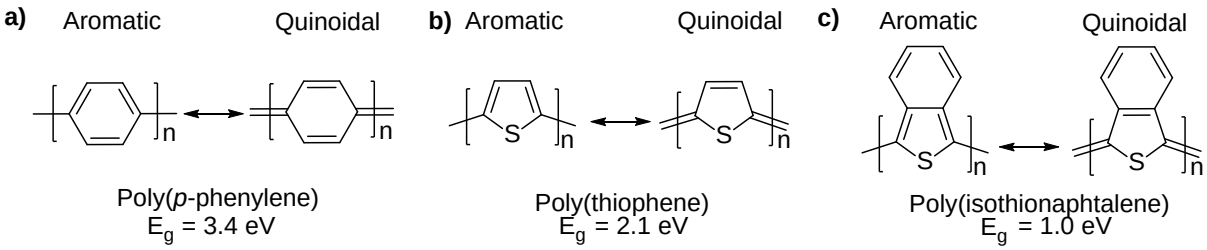

Scheme 1.1. Examples of three aromatic and quinoidal structures.

Donor Acceptor Structure

For conjugated polymers with alternating segments of electron rich and electron deficient substituents (DA), it has been observed that the HOMO-level is mostly affected by donor (D), while LUMO is more affected more by the acceptor (A).[38] One explanation of this effect has been the suggestion that the DA structure gives rise to intramolecular charge transfer within the molecule, increasing the double bond structure of the bonds, stabilizing the quinoidal form of the molecules.[39-40] An example of this effect is illustrated in Scheme 1.2 together with examples of electron rich and electron deficient substituents.

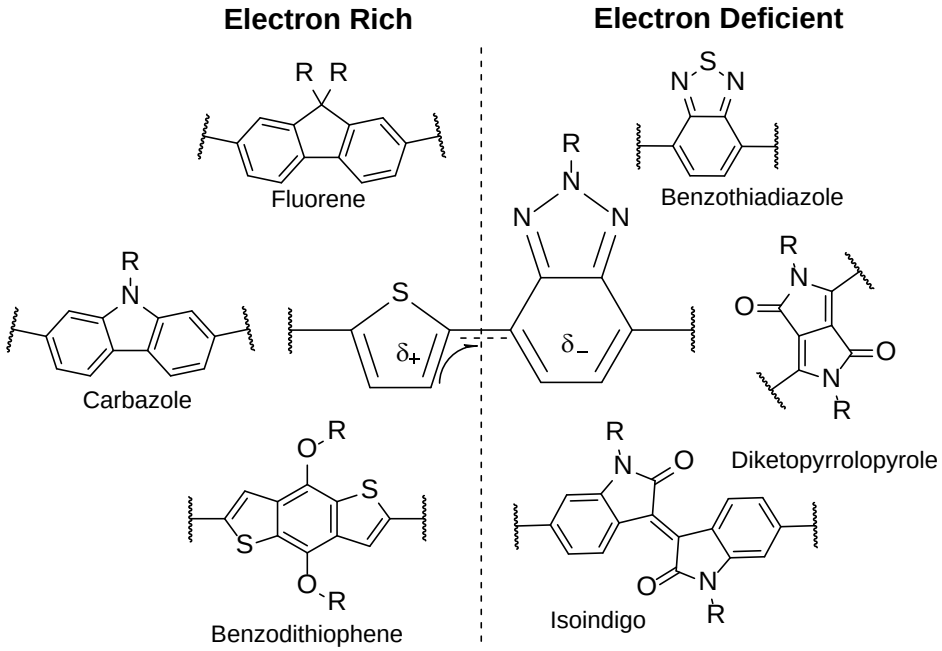

Scheme 1.2. Intramolecular Charge Transfer between electron rich and electron deficient units and examples of both types.

Another explanation, probably closer to the truth, depends on frontier orbital hybridization. When there is significant orbital overlap between neighboring sp2-hybridized carbons, an orbital hybridization between them forms and electrons can delocalize over the hybrid orbital. An illustration of this using an energy level diagram is shown in Figure 1.2. The acceptor has both HOMO and LUMO levels shifted away from the vacuum energy level relative to the donor. Since the donor contributes more to the HOMO of the hybridized orbital while the acceptor contributes more to the LUMO, the final molecular orbital will have a significantly decreased E_g. This is also a slightly simplified view, since a large difference in energy levels between two substituents affect the amount of orbital overlap. The HOMO levels tend to be closer between donors and acceptors, which leads to more delocalized HOMO states over a molecule, while the LUMO is often more localized on the acceptor.

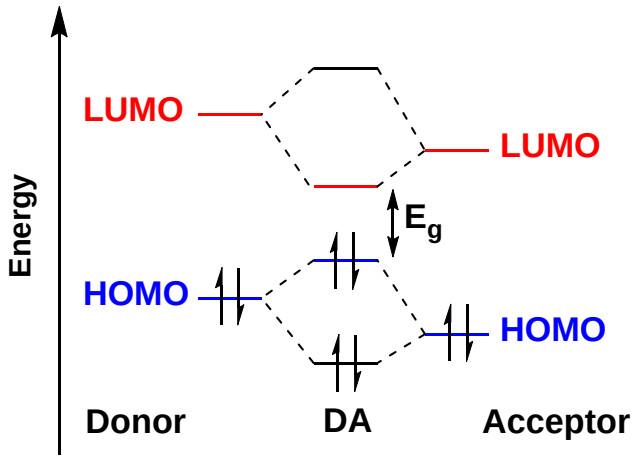

Figure 1.2. Energy level diagram illustrating the molecular orbital hybridization leading to a smaller band gap.

By combining donor and acceptor segments with suitable energy levels, the DA effect is used to tune the HOMO, LUMO and E_g of polymers. The alternating DA motif is the simplest case, and many different combinations of donors and acceptors are used, such as D-A-A, D-A-D or D-A_1-D-A_2 Donor segments generally include aromatic groups such as phenyls, thiophenes and fused versions of them, such as benzodithiophene, fluorene and carbazole, as shown in Figure 1.2. The electron poor unit contains electron-withdrawing groups and has often been a benzothiadiazole,[41] diketopyrrolopyrrole,[42] or isoindigo.[43-44] Modern materials often include fluorinated acceptor groups, due to the ability to lower both the HOMO and LUMO of a material, positioning them better as acceptor structures.[45]

Effect of backbone planarity

The orbital overlap is negatively affected by high dihedral angles between the substituents, which reduces conjugation length. This means coplanarity between the substituents lead to higher delocalization and a smaller bandgap. Another factor affecting the conjugation length is the torsion angle along the backbone. Twisting of the backbone reduce the conjugation length by hindering the orbital overlap required. This hinders the narrowing of the band gap which comes with delocalization, leading to a band gap closer to that of the individual monomer and the benefit of polymerization might be smaller, depending on the application. An example of this effect is the previously mentioned polyphenylene, which has repeating units of six-membered phenyls, which give large dihedral angles between the units and consequently a large band gap as well.

Effect of side chains

The side chains of conjugated polymers provide necessary solubility to an otherwise quite insoluble class of molecules. They serve several important functions in the polymer and a critical one is to keep them in solution during polymerization. Since polymers are less soluble than their monomer constituents, a common problem with conjugated polymers with short side chains is precipitation during polymerization. This limits the final molecular weight of the polymer, which is usually undesirable. The design of these side chains vary with the polymer backbone and therefore the optimal side chain can't be generalized and is hard to predict. Design elements that are commonly used are alkyl chains of different lengths, branched alkyl chains, alkoxy chains, thiophene spacers between the backbone and alkyl chain, and several more.[46] It is also possible to include other functionalities such as highly polar groups or ionized groups,[47] often used in interfacial polymers, cleavable side chains,[48] and crosslinks.[49] Since they don't directly affect the backbone properties, it is a suitable place to functionalize a polymer.

1.4. Synthesis of Conjugated Polymers

Increasing the amount of repeating units in a conjugated polymer increases the conjugation length over the backbone. This tends to reduce the band gap as well up to at least about ten repeating units.[39,50-51] For this reason, the polymerization reaction is critical to produce conjugated polymers. Luckily, the synthesis of conjugated polymers has improved significantly over the past few decades. Much is related to the many new and improved methods of efficiently forming carbon-carbon bonds. Especially important is the selective bonding of aromatic groups and other unsaturated carbons, which is the main type of reaction performed to synthesize conjugated molecules. Some commonly used polymerization reactions have been summarized in Figure 1.3 a). To self-polymerize a monomer, the nickel-catalyzed Yamamoto dehalogenation reaction is often used.[52] Poly(3-hexyl thiophene-2,5-diyl) (P3HT) has been important in developing new ways to synthesize conjugated polymers, since the regioregularity was found to greatly affect how well the polymer could transport charges.[53-56] There is now a wide variety of methods to produce the polymer.[57] Highly regioregular P3HT, so called head-to-tail structure, tends to stack more and enable more efficient charge transfer than regiorandom polymers. This can be achieved using nickel catalyzed Grignard Couplings.[57]

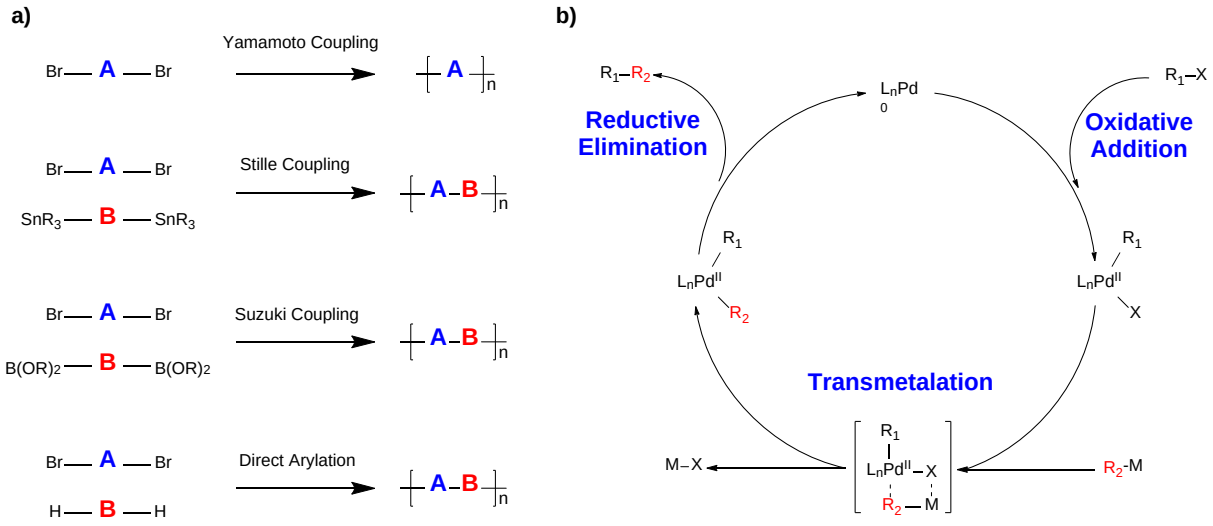

Figure 1.3. a) Schematic of common polymerization reactions **b)** Simplified catalytic cycle of palladium catalyzed reactions.

Palladium Catalyzed Polymerization Reactions

The development of the DA motif polymers made palladium catalyzed reactions such as Stille polycondensation and Suzuki polycondensation highly useful. Since they make use of difunctional monomers, this is a practical way to ensure the desired alternating copolymer structure. Some tendencies of homo-coupling still remains however, and has been studied in depth to see the cause and effect.[58-60] It is generally regarded as unfavorable in PSCs, since it can reduce the efficiency but can be mitigated to some degree, if not completely avoided by careful control of polymerization conditions such as catalyst to ligand ratio and reaction temperature.

A simplified version of the catalytic cycle of palladium-catalyzed reactions, such as Stille or Suzuki reactions is shown in Figure 1.3 b). The cycle begins at the top with the palladium catalyst in the metallic form. In the oxidative addition step, a halide bonded compound, generally an aryl halide, comes and adds two ligands, oxidizing the catalyst to Pd^{II}. Then transmetalation takes place when a metal-bonded compound, such as a stannylated monomer, is exchanged for the halide. The metal halide leaves and in the final step, the Pd undergoes reductive elimination where the two aryl groups are joined together, forming a C-C bond. The Pd catalyst is regenerated into the initial Pd^{0} metallic form, and the cycle can start over.

Stille Polymerization

The Migita-Kosugi-Stille coupling reaction (or Stille reaction) is one of the primary coupling reactions used for producing conjugated polymers.[61] It uses organostannane compounds, which has both advantages and disadvantages. An example of this reaction is shown in Scheme

1.3. The reaction has proven to be able to produce very high molecular weight polymers with few defects.[62] The reaction is simple to perform, but puts high requirements of monomer purity and anhydrous conditions, since the stannyl compounds can easily degrade and monofunctional monomers result in an end capped polymer, limiting molecular weight. A large disadvantage of the reaction is the high toxicity of the tin-compounds used, especially trimethyltin chloride which is sometimes used to stannylate the monomer before polymerization.[63] They are highly environmentally hazardous as well, which means extra care needs to be taken when handling these compounds. The reaction should be avoided for upscaling and large scale production, and preferably for lab scale as well. It is hard to replace completely, however.

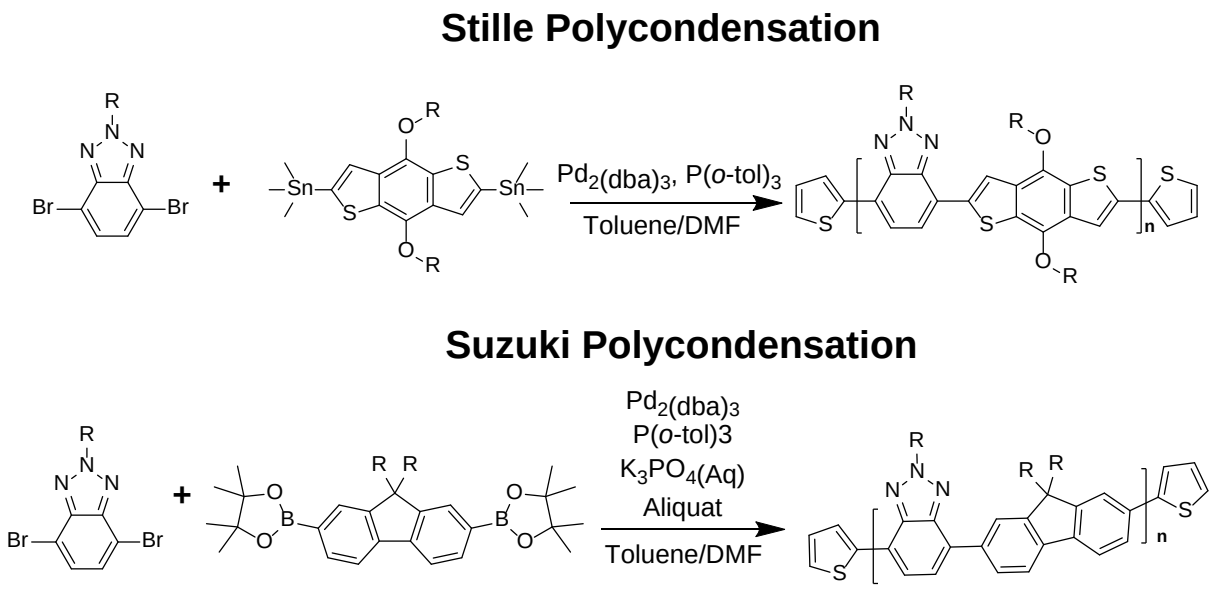

Scheme 1.3. Examples of Stille Polycondensation (upper) and Suzuki Polycondensation (lower) between benzotriazole and benzodithiophene or fluorene

Suzuki Polymerization

The Suzuki-Miyaura reaction (or Suzuki reaction) is an attractive alternative to Stille couplings, due to the far lower toxicity of the boron-based functional groups used in the reaction.[64] An illustration of this reaction is shown at the bottom of Scheme 1.3. It can often be used interchangeably with Stille reactions, but there are some limitations. The boron group can be used either in ester or acid form, and the reaction requires the presence of a base to activate the boron group. Since a base is required for the reaction, an additional step could be included into the catalytic cycle of Figure 1.3 b) before the transmetalation process, where the base activates the organoboron acid or ester. The presence of the base means that some structures with base-sensitive functional groups are better of using the base-free Stille reaction instead.

Direct Arylation Polymerization

A new and interesting development the last few years has been Direct Arylation polymerization (DArP). [65-66] This reaction is somewhat similar to the previous polymerization methods, using one dibrominated monomer but the other has aromatic hydrogens. These are activated to take part in the reaction, eliminating the need to create the organometallic compound and a reaction step and source of waste is removed. Furthermore, direct arylation polymerization can produce highly pure polymers, since metallic compounds can be difficult to completely remove in some cases. Direct arylation polymerization is still somewhat limiting when it comes to reaching high molecular weights.

Polymer Endcapping

When a polymerization reaction has been finished, the end of the polymer chain is left unreacted. It has long been unclear if this influences the properties of a polymer significantly, or if it is judicious to end-cap them with some aromatic group like a phenyl or thiophene. Some reports have shown improved polymer stacking upon endcapping the polymer, facilitating an improved charge transfer ability of the polymer.[67]

Degree of polymerization and molecular weight

Both Stille polymerization and Suzuki polymerization are step growth processes, which means the molecular weight is dependent on the degree of polymerization. This is described by the modified Carothers Equation[68-70]:

$$X_n = \frac{2}{(2 - p\bar{f})} \tag{1.1}$$

Where X_n is the number-average degree of polymerization, p degree of conversion and $\bar{f}$ the average degree of functionality of the monomers. This relation has important implications for the production of conjugated polymers. Since a high molecular weight is generally desirable to reach a large conjugation length, a very high degree of polymerization is required. This means the monomer ratios need to be highly equimolar and pure, any reaction solvent, catalyst and ligands added also need to be highly pure, dehydrated and in general well controlled with respect to reaction time, temperature and atmosphere. It also requires the inclusion of sufficient side chains to keep the growing polymer chain in solution until completion.

The molecular weight of a polymer can be measured either by number-average molecular weight (M_n) or by weight average molecular weight (M_w):

$$M_n = M_0 \frac{1}{1-p} \tag{1.2}$$

$$M_w = M_0 \frac{1+p}{1-p} \tag{1.3}$$

Where M_0 is the molecular weight of the monomer and p the degree of conversion.[70] Another highly influential value is the size distribution of the polymers, measured by polydispersity index (PDI, or Đ) is a relation between the two molecular weight values:

$$PDI = \frac{M_w}{M_n} = 1 + p \tag{1.4}$$

A small dispersity has proven to be important for the function of a conjugated polymer. Identical polymer structures with different PDIs have been compared in OPVs, where higher PDI was associated with performance loss in charge carrier mobility, more bimolecular recombination, more charge traps which ultimately led to dramatically worse performance.[71]

1.5. Characterization Methods

Due to the wide variety of properties conjugated polymers have that affect their use in downstream applications, plenty of characterization methods are used, depending on the property of interest. For this work, the most important factors studied were the optoelectronic properties and polymeric size distributions. Other important factors to study are the film morphology, thermal stability, surface energy and bulk properties of blends.

Optical properties

UV-Vis Spectroscopy (UV-Vis) is one of the most widely used characterization methods for conjugated materials, since it gives direct information about the critical E_g. The optical band gap E^{opt} is defined as the lowest optical transition for optical excitation. E^{opt} is related to the IP and EA, as presented in **Figure 1.1**. The energy required for the transition is given by the Planck-Einstein Relation:

$$E^{opt} = hv = \frac{hc}{\lambda} = \frac{1240}{\lambda_{onset}} \tag{1.5}$$

Where h is the Planck constant (6.626×10^{-34} J s), v is the frequency, c is the speed of light (2.998×10^{8} m s^{-1}) and λ the wavelength. By measuring the absorption of a molecule

experimentally, the E^{opt} can be calculated using the onset of absorption. The absorption is given from Beer-Lambert law:

$$A = log_{10}\frac{I_0}{I} = \varepsilon cl \tag{1.6}$$

Where A is the optical absorption, I_0 the incoming intensity, I the transmitted intensity, ε the molar absorptivity or absorption coefficient, c the concentration and l the length of the light path. With careful control of the concentration, the molar absorptivity can be calculated from solutions, which is a useful material property. Conjugated polymers tend to have very high absorption coefficients, which means very thin films can absorb the vast majority of incoming light.

Electrochemical properties

The concepts of the IP and EA and their relation to the Eg were introduced in chapter 1.3. Electrochemical measurements can be used to measure the IP and EA of a molecule by measuring the potentials required to oxidize and reduce it, *i.e.* the redox potentials. From the redox potentials, the HOMO and LUMO levels can be estimated. Since the measurement takes place in an electrolyte solution and not in vacuum, a reference is needed to convert the measurements to the vacuum energy scale.[72] This is done using a reference with a known energy level compared to the vacuum level, which is often the normal hydrogen electrode (4.5 V *vs.* vacuum),[73] which in turn needs to be compared with a second reference if the measurements take place in a different environment than water. Here the ferrocenium/ferrocene (Fc^+/Fc) redox couple is often used, due to its assumed insensitivity to environmental effects. Fc^+/Fc has a peak oxidation energy of 0.63 eV*vs.* vacuum, for a total of 5.13 eV.[74] Thus, the HOMO and LUMO values can be calculated as following:

$$HOMO = -(E_{ox} + 5.13)\ \text{eV} \tag{1.7}$$

$$LUMO = -(E_{red} + 5.13)\ \text{eV} \tag{1.8}$$

The difference between these two values is the electrochemical band gap (E^{ec}), which tends to be slightly different from E^{opt}. This is due in part to the solvation of the molecule and also the fact that the charge carrier is completely separated from the molecule, whereas in optical spectroscopy the excited species is not charge separated. This difference was described as E_B

in Figure 1.1. Thus the E^{ec} is often slightly larger than E^{opt} and cannot be expected to converge completely.

The most widely used electrochemical method for conjugated materials is cyclic voltammetry (CV), in which a linear potential sweep is applied in cycles between the maximum potential and minimum potential over the electrochemical cell and the analyte, covering the redox window of the molecule. A schematic view of this cycle is presented in Figure 1.4 a). Any faradic current generated between the working electrode and counter electrode is monitored. This can give information of both the energy levels of the molecule and the reversibility of the redox processes. The onset of oxidation or reduction is generally used for the determination of the energy band edges.

An electrochemical method used somewhat less is square wave voltammetry (SWV), which has been shown to have advantages when compared to CV for conjugated polymers.[75] This method is similar to CV but instead of a linear sweep potential, SWV applies pulses of square waves in a staircase shape, illustrated in Figure 1.4 b).[76] By increasing and decreasing the potentials successively, and recording the difference in current, only the reversible processes are recorded and a very simple voltammograms is produced. The purpose of this is to decrease the time dependence of the CV measurement which makes the sweep speed relevant. Instead of using onset potentials, the peak potential is used in SWV.

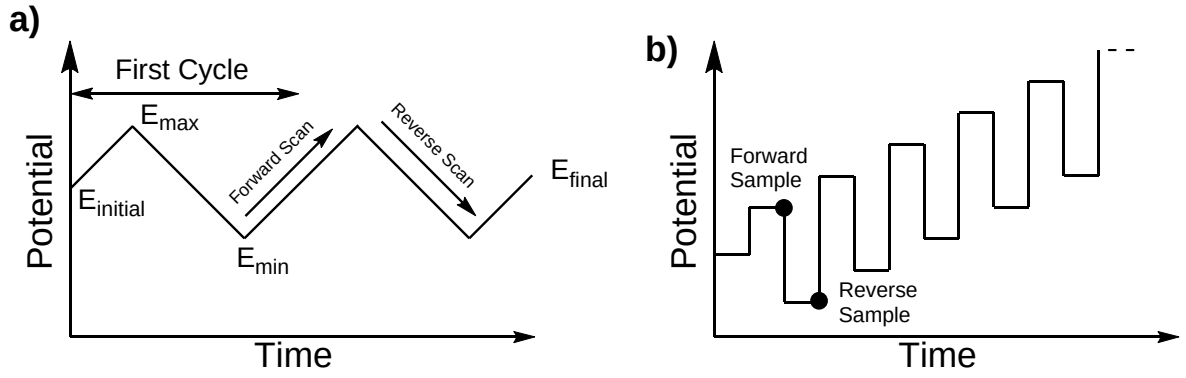

Figure 1.4. a) Scheme of CV potential sweep **b)** Scheme of SWV step potentials

Molecular weight and Size Distribution Determination

Due to the large impact on the material properties, the molecular weights of polymers require careful characterization. The size and rigidity can make this problematic, but one efficient way is to use high temperature gel permeation chromatography (GPC). This is a specialized type of weight characterization which utilizes a stationary phase, often crosslinked, porous polystyrene-beads. The weight separation is diffusion driven, where smaller molecules have a

higher diffusion coefficient, leading to a larger diffusion into the pores of the stationary phase. Thus larger molecules traverse the column faster and a size separation is achieved. The mobile phase vary depending on the system and the analyte, where a polar molecule can be analyzed using tetrahydrofuran (THF). In the case of long, stiff conjugated polymers, 1,2,4-trichlorobenzene at 150 °C can be used, which dissolves most polymers. The size distribution is compared to a reference sample calibration or with a universal calibration. The reference sample calibration makes the method a relative one, which means the results can vary quite widely depending on how different from the reference sample the analyte is. The universal calibration makes use of several detectors, often a refractive index detector and an intrinsic viscosity detector, to produce an absolute method of determining the molecular weight. It is a recent development, proposed as late as 1967,[77] and molecular weights are often still often reported in relative terms. This method can give information about M_n, M_w and PDI.

Another method to analyze the molecular weight of a polymer is matrix-assisted light desorption/ionization – time of flight (MALDI-TOF). Mass spectroscopy is quite modular and MALDI is the ionization method and TOF is the detector used to analyze the data. MALDI-TOF is a method suitable for soft matter and is often used for biomolecules, but is also useful for polymers. MALDI was developed to be an indirect method of ionization, to ionize molecules much more softly than direct ionization methods. In MALDI, it is also possible to apply the laser to a more stable analyte without the use of a matrix, directly ionizing it. This is achieved by embedding the molecule in a matrix of easily ionized molecules. The ion is transferred to the target molecule, which are accelerated with strong magnetic fields at a curvature. The time of flight and flight path are then used to calculate the mass of the molecule. This method is useful for small molecules, but also for shorter polymers, due to the relatively simple measurements. The information that can be gained by using MALDI-TOF is similar to GPC, but no standard is required.

2. Organic Photovoltaics

2.1. Background

The historical development of OPVs was treated briefly in chapter 1.2. Here, the background to why it is a beneficial development and why it further needs to be developed will be discussed. The quickly growing global population and rapid industrialization and modernization of most countries in the 20th century until today has created a vast and growing need for energy. However, the use of fossil fuel such as coal and oil, adds previously sequestered carbon into the atmosphere as carbon dioxide upon combustion. This acts as an insulating layer, keeping more of the heat radiation inside the Earth's atmosphere, increasing the temperature. The added CO_2 we have added to the atmosphere is in the hundreds of ppm, which is enough to significantly affect the heat retention of the planet. According to a report by the International Energy Agency released in 2015, the current rate of emissions mean we will pass a 2 degree increase in average temperature by 2040.[78] In October of 2018, a special report by the Intergovernmental Panel on Climate Change was released, where the consequences of passing 1.5 degrees increase are presented.[79] The report paints a bleak picture with severe effects of climate change the chance of staying below 1.5 degrees is presented as still possible, but only with drastic measures within the next decade.

A large part of the global energy production is still fossil based, and an important component in diversifying energy production to renewable sources will most likely be solar energy. The sun inundates the earth with massive amounts of energy every day, which can be captured and transformed into electrical energy. Silicon solar cells have become the commercial standard with power conversion efficiencies of around 22% for monocrystalline cells and 14-18% for polycrystalline.[80] These cells are very energy intensive to produce and have energy payback times around two to four years, but luckily with lifetimes of decades to match.[80] The crystalline silicon-wafer based solar cells are often referred to as first-generation photovoltaics. The second generation photovoltaics is the thin-film based technologies of amorphous silicon, II-VI semiconductors such as Cadmium-Telluride or Copper-Indium-Selenide.[80-81] The so-called third generation of solar cells includes Dye-sensitized solar cells, Perovskites, Quantum dot solar cells, and also organic solar cells.[82-84]

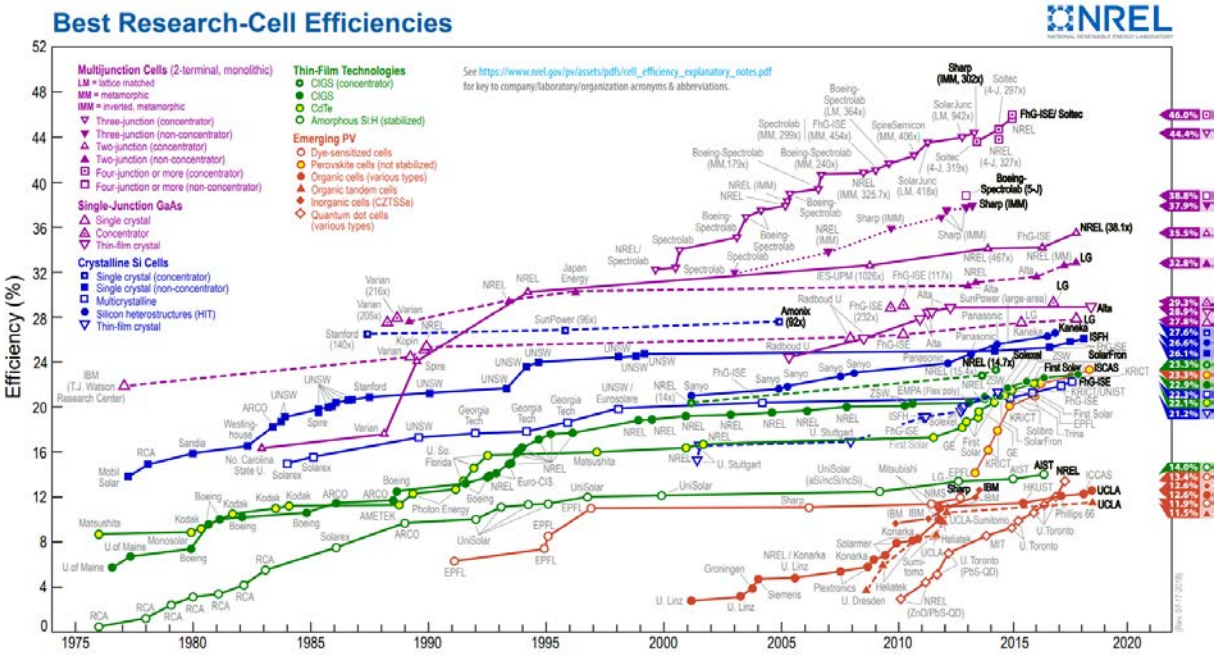

Figure 2.1. NREL Chart of best solar cell performance of various technologies. This plot is courtesy of the National Renewable Energy Laboratory, Golden, CO.[85]

It is possible to produce solar cells based on the semiconducting properties of conjugated molecules presented in chapter 1. Organic solar cells based on conjugated polymers or small organic molecular semiconductors have a few advantages when compared to silicon-based ones. The close-to-current best research-cell efficiencies are summarized in Figure 2.1, where organic solar cell technology can be found as a solid red dot close to the bottom right corner. With the recent world record of single junction organic solar cells with 14.2%, the technology has gained a few positions lately, but is still far below many other technologies.[19] OPVs have properties which might compensate for this major disadvantage, however. Due to the high molecular absorptivity of conjugated molecules, extremely thin layers of photoactive material in the order of a few hundred nanometers are needed to give good photon absorption. This means the weight of material needed is very small, leading to cheaper production and lighter panels. A major advantage is the possibility of solution processing and roll-to-roll printing, which enables cheap large-scale production. The thin layers in combination with the mechanical properties of the materials also enable flexible devices, such as rolls or on clothing. Furthermore the design flexibility of the molecules lead to significant customizability to different conditions. They also exhibit exceptional low-light properties, which is advantageous in Sweden or for indoors applications, compared to other photovoltaic systems.[86]

To evaluate a solar cell, a uniform standard of comparison is needed. A reference spectrum which simulates the sun light called the AM1.5G spectrum is used. This simulates the solar

irradiation on Earth's surface at 48.2° relative to the normal with the atmosphere's effect taken into account. An AM1.5G spectrum is shown in Figure 2.2. There is an energy-dependent upper limit to the possible efficiency a p-n single junction solar cell can deliver, called the Shockley-Queisser limit.[87] The Shockley-Queisser limit at different wavelengths is shown on top of the AM1.5G spectrum in Figure 2.2, and the maximum efficiencies are achievable around 800 nm to 1200 nm and unfortunately does not cover the maximum of solar energy indundation.

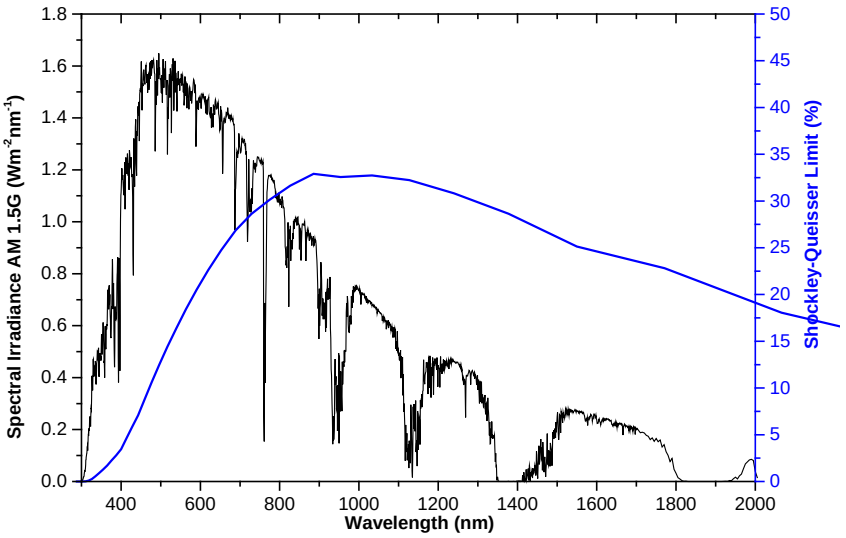

Figure 2.2. The black spectrum represents the simulated **s**olar spectrum at AM1.5G condition and the blue one the Shockley-Queisser limit at different wavelengths.

It is important to note that the Shockley-Queisser limit is based on several assumptions, which can be circumvented, meaning the limit can be surpassed.[88] Some examples of ways this is possible is the use of multiple junction solar cells, since the Shockley-Queisser limit is only valid for a single junctions, using light concentrators or photon upconversion or by splitting excited states into several excitons which has produced devices with external quantum efficiencies of over 100%.[89-90] To conclude, the Shockley-Queisser limit seems more like a suggestion than a rule.

2.2. Polymer Solar Cells

Working Principle

The working principle of polymer solar cells is divisible into several discreet steps. An illustration of these steps is shown to the left in Figure 2.3. The initial step **a)** is the absorption of a photon with energy of E_g or more by an active layer component. This process was discussed in chapter 1.3. The photon excites an electron from the HOMO-level of a molecule to the

LUMO level, leaving an electron hole behind, but the Coulombic interaction still binds them. Together they are called an exciton. The hole is not a physical particle as such, and can just as well be seen as a cascade of electron movements in the HOMO-level when it moves, but it is easier to imagine it as a charge carrying particle like the electron.

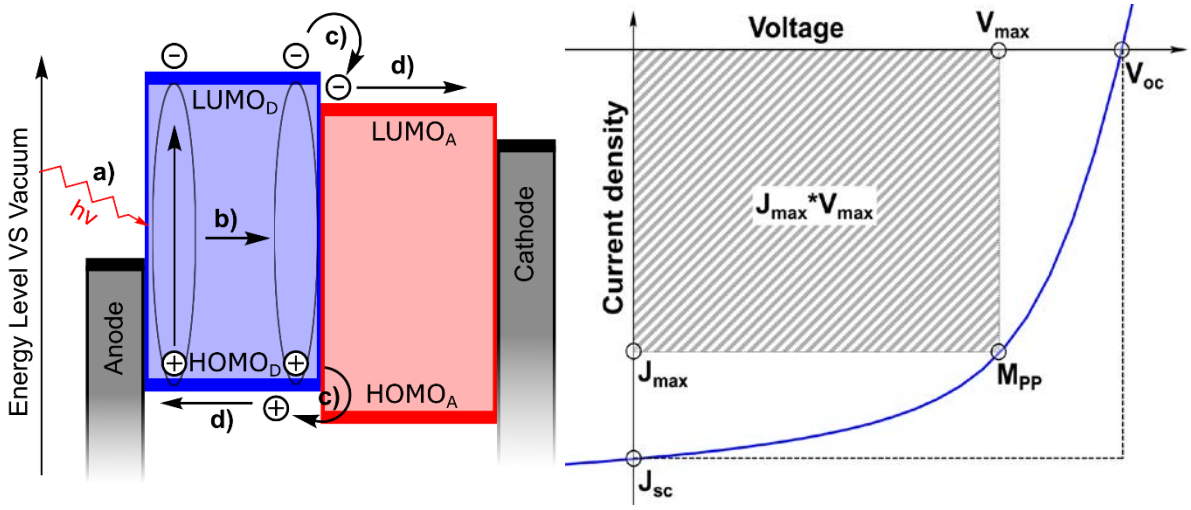

Figure 2.3. left) Illustration of the process of charge generation in OPVs. **right)** A schematic J-V curve in light condition.

The next process **b)** is the diffusion of the exciton to a donor-acceptor interface, which is needed to break the strong electrostatic interaction of the exciton. The exciton can recombine at any time, which limits the travel distance to what is called the exciton diffusion length. This length is typically around 10 nm, but varies mostly from 5 to 20 nm.[91] The thickness of the active layer is generally over 100 nm. Since the interface between the donor-phase and acceptor phase is required for charge separation, the bilayer structure is not very efficient for OPVs, when compared to silicon solar cells. The next step **c)** is the charge separation at the donor-acceptor-interface. It requires a slightly lower $LUMO_A$ compared to $LUMO_D$, often called the driving force, which leads to a transfer of the electron to the acceptor in an intermediate state called a charge transfer state. With the help of the driving force, the charges can then separate and start to move independently toward the respective electrodes in step **d)**. Recent reports have shown that it is possible to make well performing devices with very small driving force, which enables a higher open-circuit voltage (V_{oc}) of the final device.[92] The final step is the charge extraction from the device. The now free electrons will drift along the acceptor-rich regions of the BHJ toward the cathode while the holes drift along the donor-rich regions to the anode. The charges are extracted from the solar cell and a current is formed. This is a highly simplified description of the events taking place and every single process has been studied in depth. While the understanding is still not complete, it is far better now than a decade ago.

Figures of merit

The main figure of merit of polymer solar cells is the power conversion efficiency (PCE), which is the ratio of incoming energy to produced electrical energy.[81] The PCE depends on several factors and relation between them is shown in Equation 2.1.

$$\mathrm{PCE} = \frac{J_{max}V_{max}}{P_{inc}} = FF\frac{J_{SC}V_{OC}}{P_{inc}} \tag{2.1}$$

Where J_{max} is the maximum point of current density, V_{max} the maximum point of voltage and P_{inc} the energy. FF is the fill factor, J_{sc} the short-circuit current density, and the open-circuit voltage is represented by V_{oc}. The relation between these factors is best illustrated with the current density-voltage diagram (*J*-*V* diagram) shown to the right in Figure 2.3. The PCE is clearly dependent on many variables, which in turn depend on structure-property relationships both from the materials involved, but also from device architecture and morphology of the active layer. This leads to highly complex design problems where the versatility of conjugated polymers can be very useful.

The V_{oc} of an OPV is the potential at zero current and is a function of the band gap of the device. The transfer of electron from donor to acceptor means the relevant band gap is that between $HOMO_D$ to $LUMO_A$, called the charge-transfer energy (E_{CT}). Due to several loss-factors, the produced voltage of the device is far lower than the actual E_{CT} and typical single junction OPVs end up with V_{OC} of around 1 V. There have been no OPV system presented with potential loss below 0.5 eV and they often exhibit a total potential loss of around 0.7-1.0 V.[93-94] A common source of energy loss is recombination of the exciton, either in radiative or non-radiative decay.[95] Recombination can be reduced with a suitable $LUMO_A$-$LUMO_D$ offset, which encourages charge separation.[96] Since this offset also limits the maximum potential of the device, it should be kept as low as possible while still providing enough of a driving force to avoid recombination.

The J_{SC} is the current density of a device at zero bias. It is affected by the capability to generate charges and to extract them from the device.[97] The most important factor affecting the charge generation is spectral coverage, where the maximum values attainable according to the Shockley-Queisser limit are for materials with E_g in the region of 1.0-1.5 eV. Other factors affecting the J_{sc} are the absorption coefficient, active layer thickness and illumination level, which is not varied when testing with AM1.5G solar simulators.

The FF of the device can be described as the square-shape of the *J-V* curve. Equation (2.2 shows the relation between the fill factor and the other factors, and a graphical illustration is the proportion of the square outlined by $J_{sc}*V_{oc}$ (dashed line) that is covered by that of $J_{max}*V_{max}$ (filled square) shown in Figure 2.3. The ideal FF is unity (100%) but good OPVs often end up in the 60-70% region. It depends on the ability to extract the charges from the device and can be reduced by imbalanced charge carrier mobilities and the morphology of the blend.[98]

$$\mathrm{FF} = \frac{J_{max}V_{max}}{J_{SC}V_{OC}} \tag{2.2}$$

Another value to evaluate a solar cell is the external quantum efficiency (EQE), which is defined as the numbers of charges collected (N_{ph}^{out}) divided by the number of incident photons (N_{ph}^{in}) at a specific wavelength. EQE is sometimes referred to as incidence photon-to-electron conversion efficiency as well (IPES).

$$EQE(\lambda) = \frac{N_{el}^{out}(\lambda)}{N_{ph}^{in}(\lambda)} \tag{2.3}$$

Bulk Heterojunction

The BHJ was an important improvement on OPV device structures. Previous bilayer devices never achieved high PCE-values, mainly due to a low interfacial area between the phases. An illustrative schematic of a BHJ morphology is shown in Figure 2.4. It is important to note that this type of illustration is slightly misleading, since neither the donor-rich nor the acceptor-rich regions are pure. The formation of bicontinous pathways all the way to the electrodes is important, to avoid charge trapping which leads to recombination losses. Due to the exciton diffusion length of about 10 nm and the need for a DA interface for charge separation, the optimal performance is reached when the phase domains are about 20 nm big. Fine-tuning the BHJ morphology can be done with altering processing conditions such as spin-coating speed, concentration or solvents but also with heat annealing steps or solvent annealing steps. A widely used method is by incorporating high boiling point cosolvents such as 1,8-diiodooctane or 1,2-dichlorobenzene, which slows down the film-forming during spin coating.

Small molecular and fullerene based systems can have stability problems due to diffusion taking place over time. Fullerenes tend to crystallize or aggregate, which can significantly coarsen the morphology of the device, or in some cases even form crystals large enough to destroy the device.

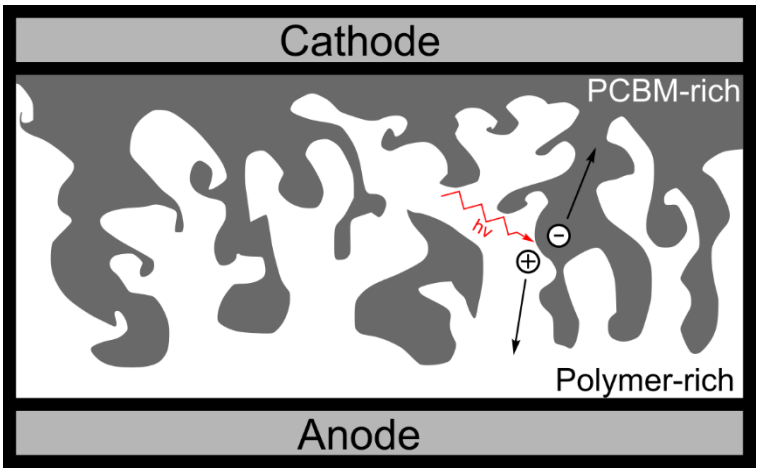

Figure 2.4. Schematic illustration of the BHJ-morphology of an OPV.

There are a few device architectures commonly used for OPVs, with significant differences in performance, stability and materials used. The two most common device structures are called conventional and inverted device structures, depending on which direction the anode and cathode are facing relative to the transparent electrode. A schematic depiction of the two device architectures depiction can be seen in Figure 2.5. All the individual components in the schematics are exchangeable for other alternatives, however.

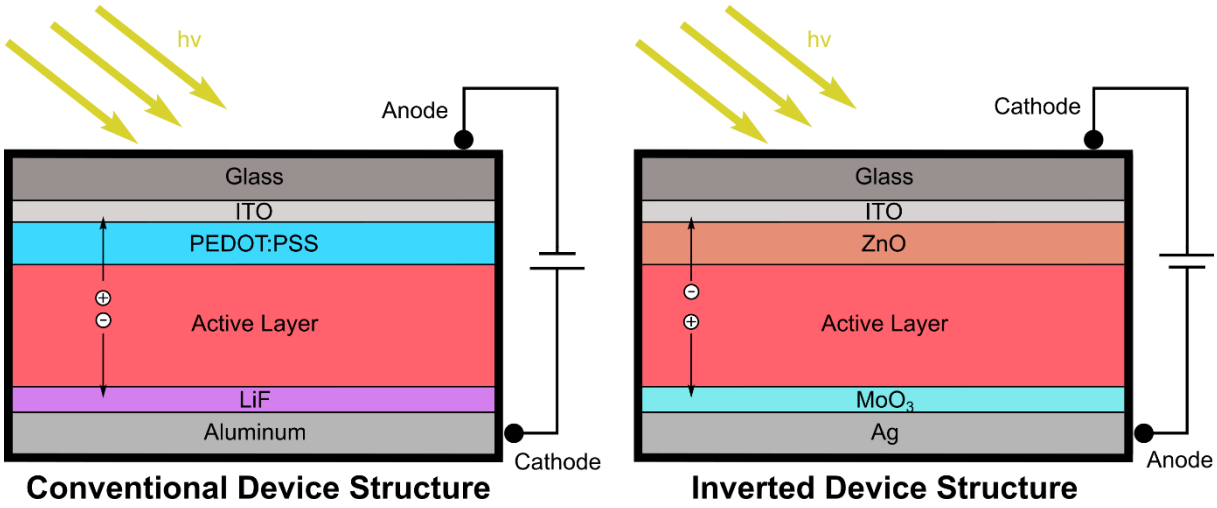

Figure 2.5. Conventional and inverted single junction device structures.

Conventional Device Structure

The first component to consider is the substrate, which is almost always glass in lab-scale solar cells. For printing, more flexible substrates are needed and PET-plastic is a common choice. Since the absorption takes place in the active layer, which is placed between the electrodes and behind the substrate, both the substrate and the electrode coating it needs to be transparent. This has led to the vast majority of devices make use glass of with a thin coating of indium tin oxide (ITO) as one of the electrodes, since it has exceptional optical transmittance and satisfactory

electrical conductivity. It is not without problems, however. It is not very flexible, so large scale production using it on PET is not a viable choice. It is also quite expensive and ITO sputtering is by far the most energy intensive part of the solar cell production.[24]

The work function of the electrodes play an important role in the performance of a solar cell. To not limit the V_{oc} of the device, two metals or metal oxides with a large difference in work function (WF) are used. The interface between electrodes and active layer is critical for device performance since the energy level alignment between them directly affect the charge extraction.[99-101] By using interfacial layers with polar side chains, the difference between the polymer energy levels and the metal/oxide electrode work functions. This is achieved by forming an interfacial dipole, and can be achieved with very thin layers of just a few nanometers. poly(3,4-ethylenedioxythiophene) polystyrene sulfonate (PEDOT:PSS) is a commonly used hole-transport layer (HTL) on the anode interface. The same problem arises on the opposite electrode where an electron-transport layer (ETL) is placed instead. While the HTL has been ubiquitously applied, since devices without them barely function at all, the use of ETLs has been slightly lower.

Cathode Interfacial Materials

The use of ETL, or cathode interfacial materials (CIM), has proven highly beneficial to improve both life-time and performance of OPVs. The primary function of them is to tune the WF of the cathode, but they also serve more functions such as improving wettability and acting as a metal ion diffusion barrier.[101-103] Commonly used cathode interfacial materials (CIM) are ZnO, LiF and compounds with aliphatic amine groups.[104-107] A few very successful polymeric materials with aliphatic amines are polyethyleneimine (PEI) and polyethyleneimine ethoxylated (PEIE) and polyfluorenes with side chains with tertiary amine pendant groups (PFN), but there are many more.[102,108-109] The metals or metal oxides used as electrodes are hydrophilic, while the active layers are hydrophobic, which means the wetting properties directly onto the electrodes is unsuitable.

Inverted Structures

One of the electrodes in this device configurations will have a low WF, which makes it reactive. This can damage the device performance and limit the lifetime of devices.[110] Conventional devices have a device stack which exposes the lower WF metal such as aluminum, calcium or barium, while protecting the higher WF such as ITO or fluorine doped tin oxide.[111] To circumvent this problem, the inverted device structure was introduced in which the transparent ITO acts as cathode instead, and the high WF metal acts as anode.[112] This way, the devices

turn out to have improved stability. This also eliminates the need for the commonly used interlayer PEDOT:PSS, which is somewhat corrosive and hygroscopic. While the improved life-times of devices are attractive, inverted devices tend to produce lower efficiencies still.

Tandem devices and ternary devices

The previously presented device structures are single junction device architectures. In order to cover a larger part of the solar spectra, it is also possible to use tandem devices, which have two active layers with complementary absorption. The layers need to be separated by interlayers and the manufacturing of them is more complicated, but higher efficiencies are achievable. Another device architecture that has recently begun to gain popularity is called ternary devices, in which the active layer contains three components. Often these are two donor polymers and one acceptor, but other combinations are possible. This is an intermediate way to gain some of the advantages of tandem devices while the device structure is as simple as single junction devices to manufacture.

2.3. Acceptor Molecules

The role of donor molecule in the donor-acceptor BHJ systems can be filled with conjugated polymers. Their energy levels and other properties are suitable for the application, but the role of acceptor has a few viable alternatives and it has varied over the years. Initially, attempts at using acceptor polymers were not very successful, but when soluble fullerene derivatives were introduced, they quickly became the standard acceptor molecule. The advent of high-performing acceptor polymers is fairly recent, and has mostly been present since 2013 and forward. Small molecular acceptors (SMA) has been even more recent, but are now very popular. An example of a PCBM, an acceptor polymer and a SMA are presented in Figure 2.6.

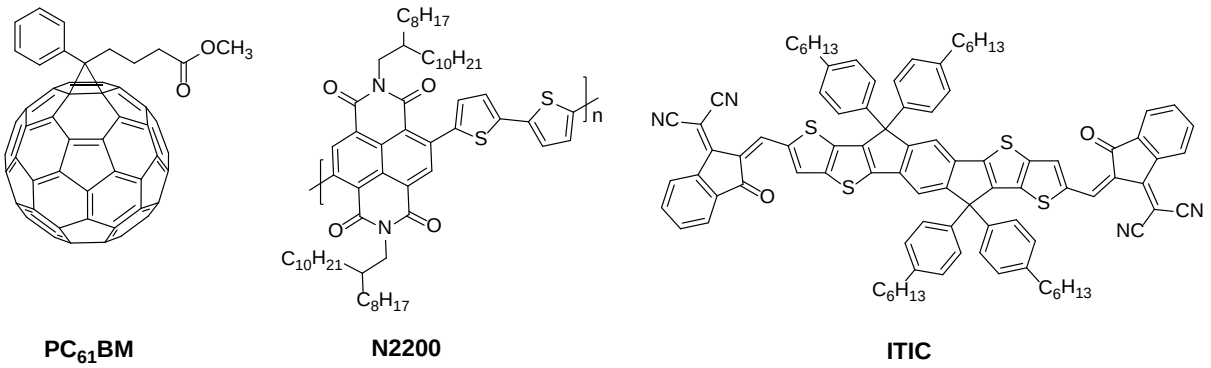

Figure 2.6. Example of the three acceptor molecule classes discussed here.

Fullerene Derivatives

As previously mentioned in section 1.2, PCBM, fullerene derivative with increased solubility was developed in 1995 and rapidly improved the whole PSC-field simply by being a solution-processable acceptor molecule with suitable energy levels.[14] A major limiting factor of PCBM, especially $PC_{71}BM$, is the production cost. $PC_{61}BM$ can cost around 300 USD/g and $PC_{71}BM$ around 900 USD/g. One of OPVs most important selling points is the production cost and to have a major component with costs of many hundreds of USD per gram is very counterproductive for large scale production. Further problems they have include very limited optical absorption, limiting their contribution to the photocurrent. The chemistry available to modify them is quite limited as well, so most of the design has been to tune donor-polymers around these factors instead of modifying the PCBM. They also tend to aggregate or crystallize over time, giving a source of device degradation when the sensitive morphology changes.[113] All these negative properties aside, they have been a centerpiece of the PSC field for around two decades and for good reason. The high electron affinity of the molecules give an efficient charge separation and the electron mobilities they exhibit is very high.

Polymeric Acceptors

Early in the developments of PSCs, attempts were made to use polymer acceptor molecules. In 1995, the same year as major breakthroughs in PCBM and BHJ structure solar cells were made, a study of blends of MEH-PPV and a cyano-containing PPV derivative developed the year before for OLEDs.[114-115] This material was also developed by Heeger's group at the same time.[116] Many different structures were used, but rarely performed well compared to those with PCBM, which led to most research being into polymer:PCBM systems. The early acceptor polymers often had respectable *V*oc values because of suitable LUMO levels, but the charge mobility was low and they had limited absorption in the visible region, limiting both *J*sc and FF. A few years ago, naphthalene-diimide and perylene-diimide structures started being used, which produced proficient acceptor polymers.[117] These polymers could satisfy the requirement of high electron mobility, while improving the light harvesting and yielding good *V*oc values. Further advantages acceptor polymers have over PCBM is improved flexibility and better compatibility with the donor polymer, giving higher stability.

Small Molecular Acceptors

The developments in SMAs has been rapid the last three years and is currently the best performing acceptor molecule with devices reaching 14.2%.[19] These molecules share some of

the advantages with acceptor polymers, such as improved absorption compared with fullerene acceptors and are generally easier to purify than polymers.[20] They are also more uniform, since there is no molecular weight distribution to take into consideration. The complementary absorption they enable greatly benefit the J_{sc} of devices, while the V_{oc} has been somewhat low. The design of SMAs is similar to that of conjugated polymers, including donor and acceptor segments with solubilizing side chains. They commonly apply a D-A-D or A-π-D-π-A structure, where π is a conjugated spacer like thiophene. The structure ITIC, shown in Figure 2.6, includes the indacenodithieno[3,2-*b*]thiophene (IDTT) unit as a central, planar electron rich donor unit with flanking electron deficient groups. The IDTT unit will be further discussed in chapter 6 where they are used for electrochromic purposes. Recent advances in polymer:SMA systems can be partially explained with improvements in molecular design, leading to complementary absorption spectra and increasing *J*sc significantly.[19] These systems still have quite low Voc of around 0.9 V however, which means there is still room to improve the already impressive results.

3. Cathode Interlayers for All-Polymer Solar Cells

The following chapter is based on the work presented in Paper II, which was published in *ACS Applied Energy Materials* in May, 2018.[118] The work covers the synthesis of four different conjugated polymers used as cathode interfacial layers in All-PSCs. The two active layer polymers along with the four CIMs are shown in Scheme 3.1. The four polymers had polar side chains with three different pendant group and two backbone configurations and were used in devices with the two conventional OPV polymers PBDB-T and PNDI-T10. The resulting devices performed well compared to devices with bare Al electrodes, improving the PCE from 2.7% to 5.3%, which is comparable to devices with Li/Al electrodes. The results prove that conventional interfacial polymers can be used in all-PSCs with comparable results to low work-function metals, which is very important for future roll-to-roll processing of large-scale solar cells.

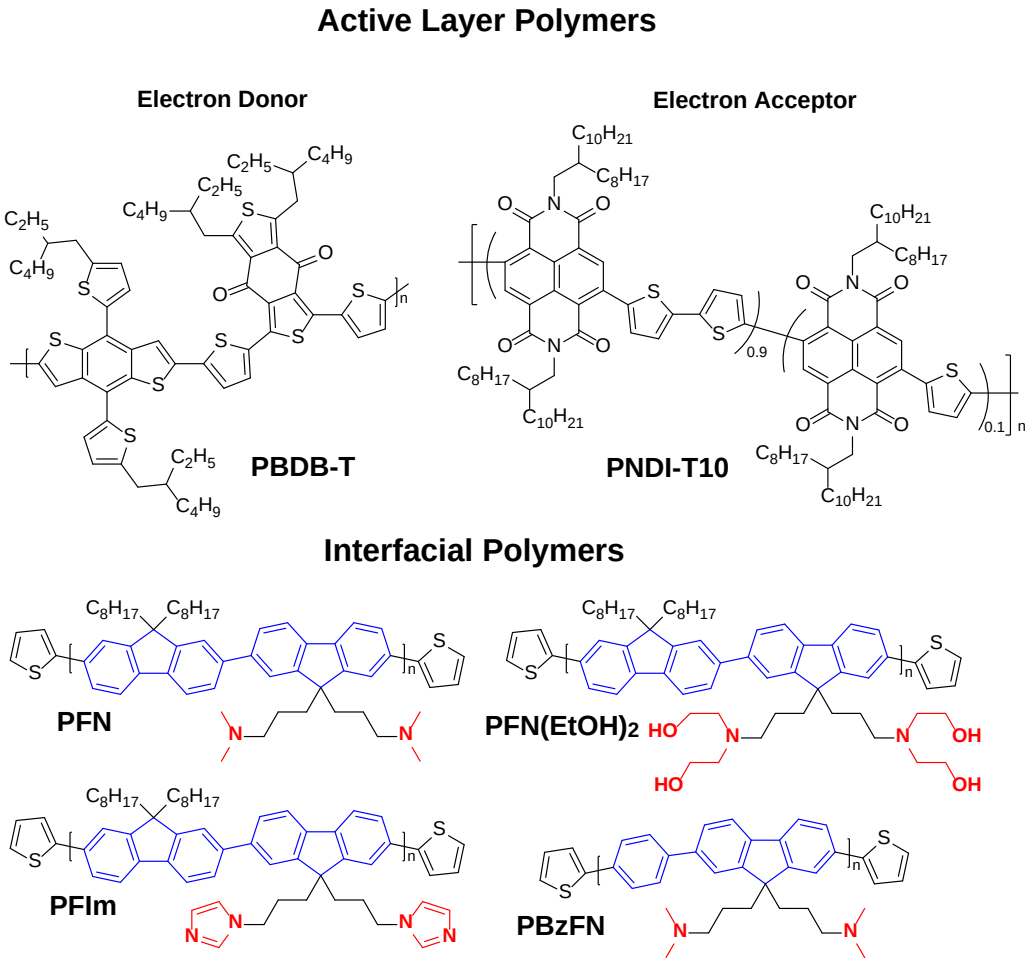

Scheme 3.1. Structures of the two active layer polymers and the four CIMs

3.1. Background and motivation

Since the advances in All-PSCs are still quite recent, details in their functionality have not been as well studied as polymer:PCBM solar cells. [119] One such detail is the interface between the active layer and the cathode which has been extensively studied, but mainly for conventional OPVs using PCBM. An important factor in improving the performance of PCBM-based solar cells with cathode interfacial polymers is using amine-containing interfacial polymers.[120] They have been shown to n-dope the fullerenes, leading to reduced interfacial resistance and increased conductivity, an effect mostly absent in All-PSCs with NDI-based acceptor polymers such as N2200.[121] Therefore, to study the effect of a few different polymers as CIMs, we synthesized four polymers with two backbone compositions and three different side chain pendant groups. These were dimethylamine, diethanolamine and imidazole. The two backbone configurations used were polyfluorene and poly(fluorene-*alt*-phenylene). The two components of the photoactive layer used in this study have previously been used together in two studies and reached a PCE of 7.1%.[122-123] The donor polymer has mainly been used in solar cells with the small molecule acceptor ITIC, which in combination reached over 11% PCE.[124-125] PNDI-T10 is a locally produced version of N2200 with 10% thiophene instead of bithiophene spacers unevenly distributed over the polymer chain.[126] This polymer has improved upon conventional N2200 by reducing crystallinity and increasing achievable molecular weights.

3.2. Synthesis

The synthesis of the CIMs was simple and achieved in just a few steps from commercial reagents. The only monomer synthesized was the alkylation of the fluorene unit, illustrated in Scheme 3.2. This synthesis was performed in anhydrous DMSO with an excess of KOH and 1,3-dibromopropane. The reaction took place at 80 °C overnight and the crude compound was purified by precipitation from methanol followed by recrystallization from methanol with a final yield of 35%. Two polymers were synthesized using Suzuki Cross Coupling polymerization. Three of the final polymers were produced from the precursor polymer PFBr by post-polymerization functionalization. These reactions were based on previously presented reactions.[104,109,127-128] The last polymer, PBzFN, was wholly made from commercial monomers.

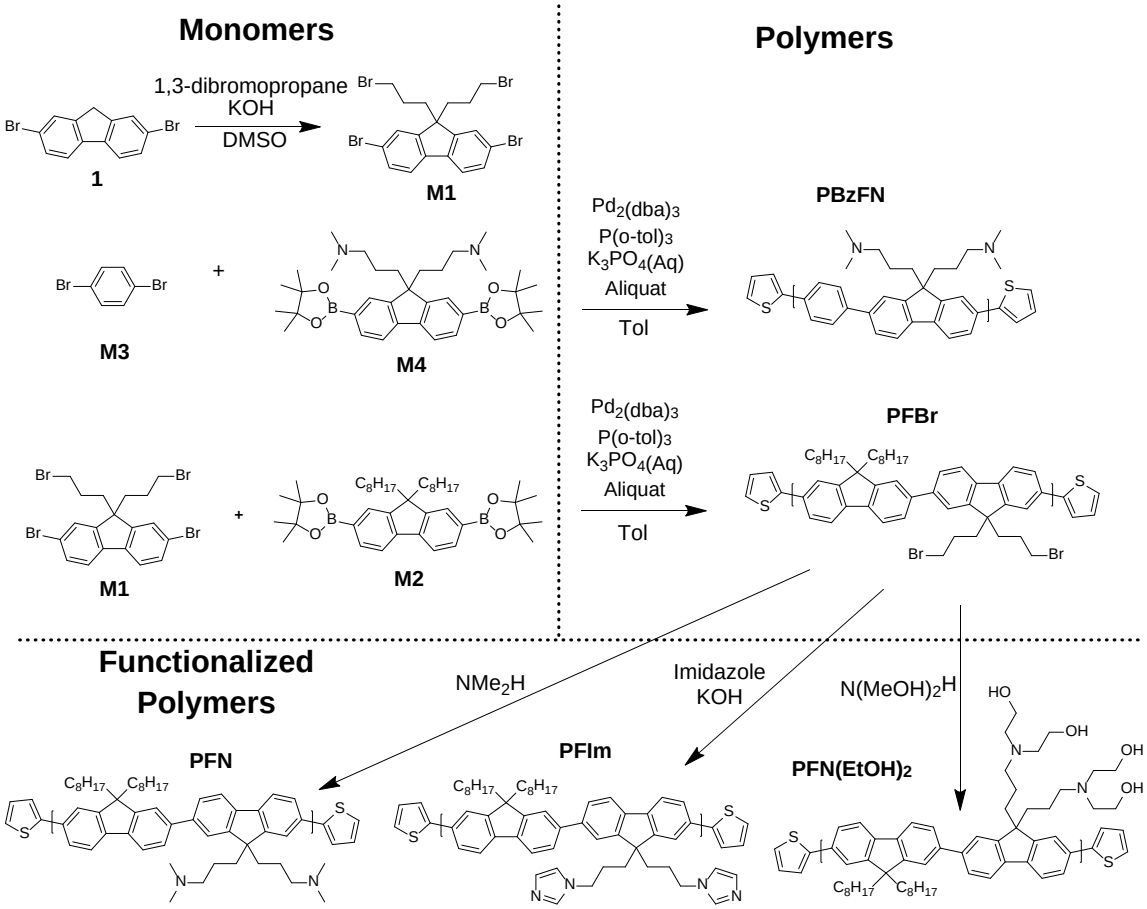

Scheme 3.2. Complete synthesis scheme for monomer and the five polymers presented

The reaction procedures for both polymerization reactions performed were identical. The reactions were performed in toluene with $Pd_2(dba)_3$ as catalyst and P(*o*-Tol)$_3$ as ligand. Since these reactions were Suzuki polymerizations, a base was needed as well, so 1 M K_3PO_4(Aq) was added to the solutions, together with a few drops of aliquat 336 as a phase transfer agent. The reactions proceeded for 72 hours at 80 °C under N_2 atmosphere. The polymers were then endcapped with 2-(trimethylstannyl)thiophene and 2-bromothiophene. The heating was removed and when the solution cooled down, the polymers were precipitated from methanol and filtered. The polymers were then purified by Soxhlet extraction with petroleum ether, diethyl ether, acetone and chloroform. The chloroform fractions were finally purified over a short silica plug, precipitated from methanol, filtered and dried. PFBr was produced in a final yield of 76% while PBzFN had a low yield of 38%. This is most likely due to the amine pendant groups interacting with the silica in the final purification step.

The post-polymerization functionalization of PFBr, yielding the three polymers PFN, PFIm and PFN(EtOH)$_2$ were performed in chloroform for PFN and THF for the latter two. For PFN a large excess of Me_2NH was added to the polymer solution, after which the mixture was heated

overnight. The polymer was purified over a neutral alumina plug and precipitated from hexane. The procedure for PFN(EtOH)$_2$ was almost identical, but with the addition of (EtOH)$_2$NH to the polymer solution. A higher temperature could also be used, due to the far higher boiling point of the added amine. The procedure for PFIm was quite different, however. A solution of 1*H*-imidazole, potassium hydroxide and tetrabutylammonium bromide was stirred vigorously for 30 min before addition to the polymer solution. The mixture was stirred and heated overnight. The purification was the same. The completeness of these reactions were hard to verify with conventional means, but the altered solubility and thermal stability suggests a high degree of conversion from the bromine groups.

3.3. Results and Discussion

The polymers were characterized independently with respect to electrochemical and optical properties, as well as thermal stability measurements. Since their application is to be used in extremely thin interfacial layers of around 3-5 nm, their optical properties are not highly influential on device performance. Due to the similar backbone structures, the energy levels were also very similar. The energy levels of the four CIMs, the precursor polymer, the two active layer polymers and PC$_{71}$BM are summarized in Figure 3.1. The CIMs have far wider band gaps due to the backbone structure with repeating fluorenes, and phenylenes in the case of PBzFN. This means they have now donor-acceptor structures which leads to larger band gaps. The repeating units also have high dihedral angles. This leads to short range conjugation over the long molecules, which leads to further increase the band gap. Many active layer polymers use five membered rings such as thiophene to reduce the dihedral angle.

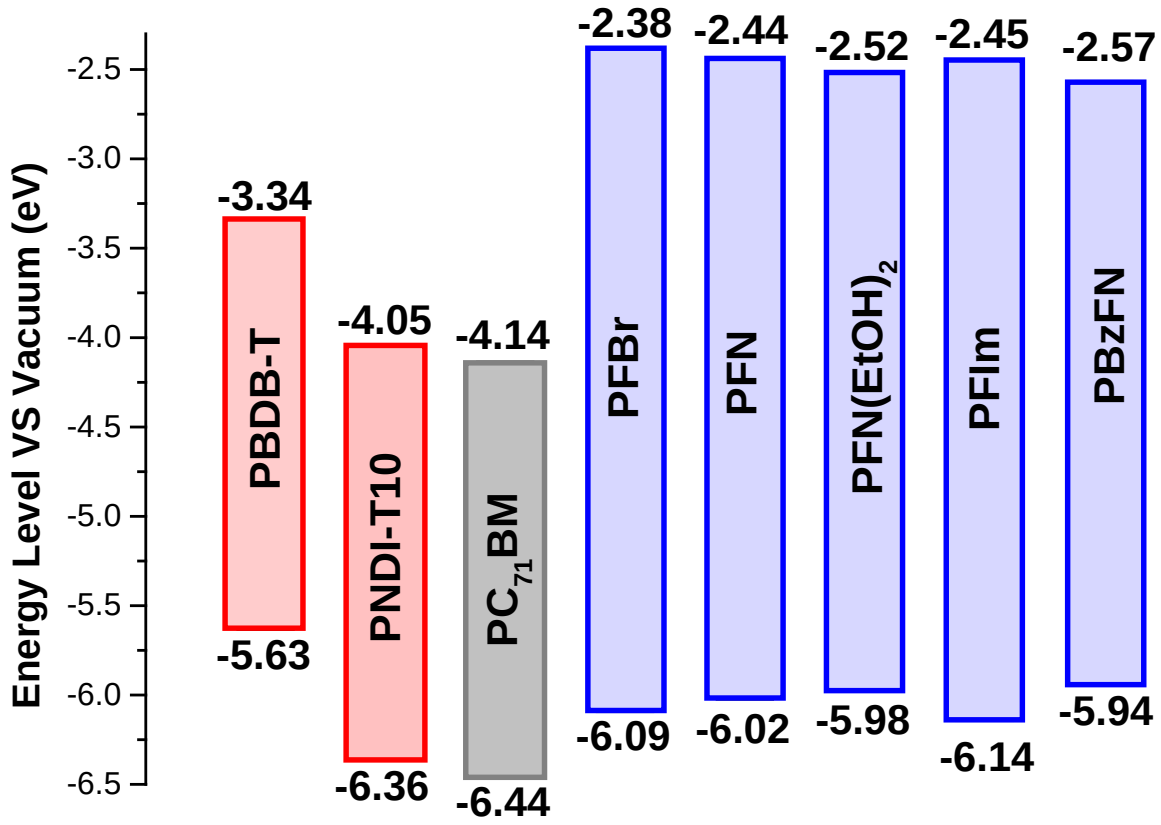

Figure 3.1. Energy levels for the active and interfacial polymers with $PC_{71}BM$ as a reference.

Solar cell devices were made with conventional device structure with the following layers: (ITO/PEDOT:PSS/Active Layer/CIM/Al). The solar cell devices were characterized under illumination of a simulated AM 1.5G solar light at 100 mW/cm^2. The *J-V* characteristics in light and dark conditions, EQE-curves and electron mobilities are shown in Figure 3.2.

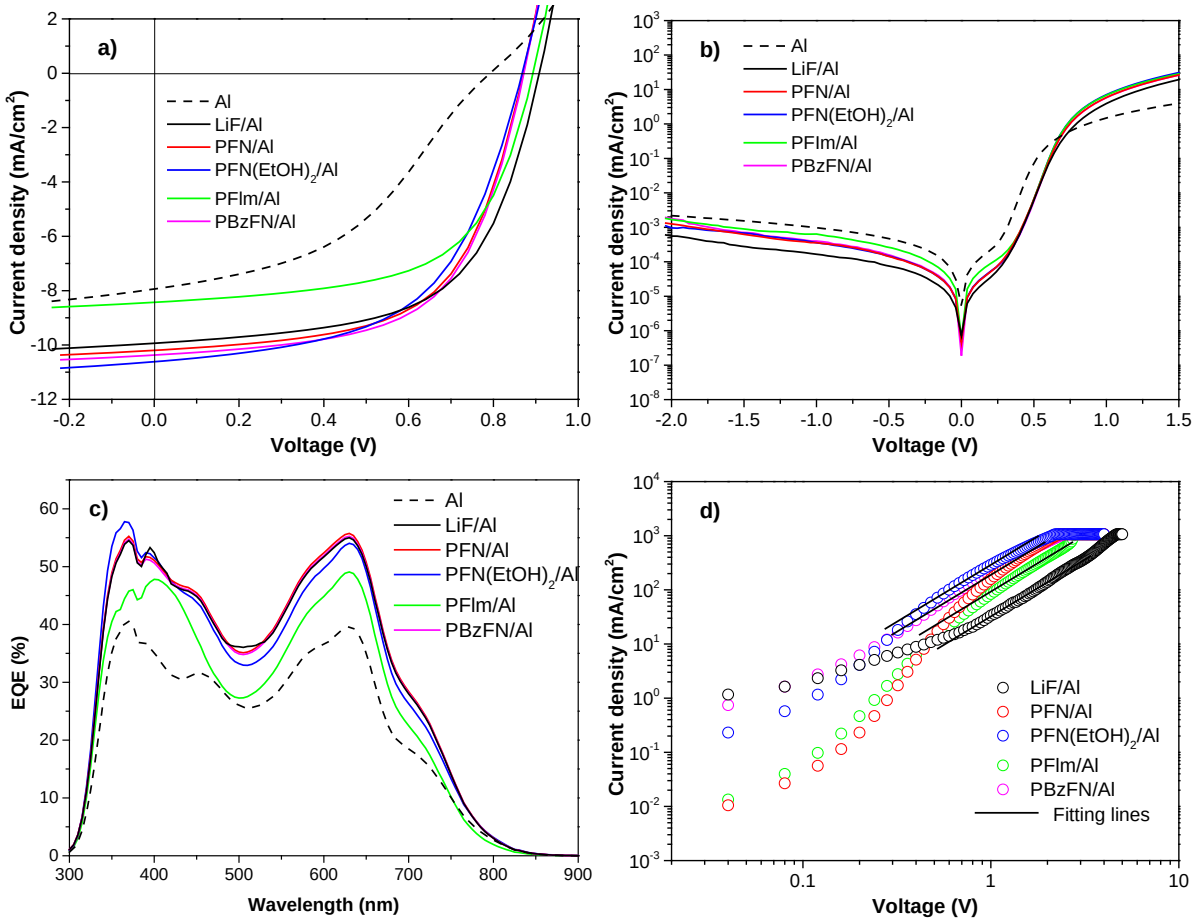

Figure 3.2. *J–V* characteristics **a)** under illumination and **b)** in dark **c)** EQE curves **d)** Electron mobility in electron-only devices.

The polymer performance is compared to devices without CIM and devices with LiF. The device performance is also summarized in Table 3.1. The devices without CIM performed poorly, with a final PCE of 2.7 %. This is to be expected and the reason CIMs are used in the first place. Both the V_{oc} and J_{sc} were increased with the addition of LiF to the cathodes. This led to a close to doubling of the PCE to 5.3%. Interestingly, three of the four polymer CIMs performed almost identically, where PFN, PFN(EtOH)2 and PBzFN gave 5.3%, 5.3% and 5.4% devices, respectively. The biggest deviation was PFIm, which was in-between with 4.5%, i.e. better than bare electrode but worse than the other devices.

Table 3.1. Device parameters of the all-PSCs.

Cathode	V_{oc} [V]	J_{sc} [mA/cm^2]	FF	PCE [%]	μ_e [cm^2 V^{-1} s^{-1}]
Al	0.79	7.9[a] (7.1)[b]	0.43	2.7	-
LiF/Al	0.90	9.9 (10.1)	0.60	5.3	7.94×10^{-5}
PFN/Al	0.87	10.2 (10.2)	0.60	5.3	7.45×10^{-5}
PFN(EtOH)$_2$/Al	0.86	10.6 (9.8)	0.58	5.3	7.50×10^{-5}
PFlm/Al	0.89	8.4 (8.5)	0.60	4.5	7.16×10^{-5}
PBzFN/Al	0.87	10.4 (10.1)	0.60	5.4	7.55×10^{-5}

[a]Average values from ten devices; [b]Photocurrents obtained by integrating the EQE with the AM1.5G spectrum

To further study the surface properties of the CIMs, films were prepared with the active layer, coated with the CIMs. These films were then studied in AFM and contact angle measurements, shown in Figure 3.3 and Figure 3.4 respectively. The surface topology measurements show that the extremely thin layers of CIMs on top barely have any effect when compared to coated and uncoated film. The root mean square measure of surface roughness was very close in all five treatments, varying from 1.27 nm for PFIm to 1.46 nm for PFN.

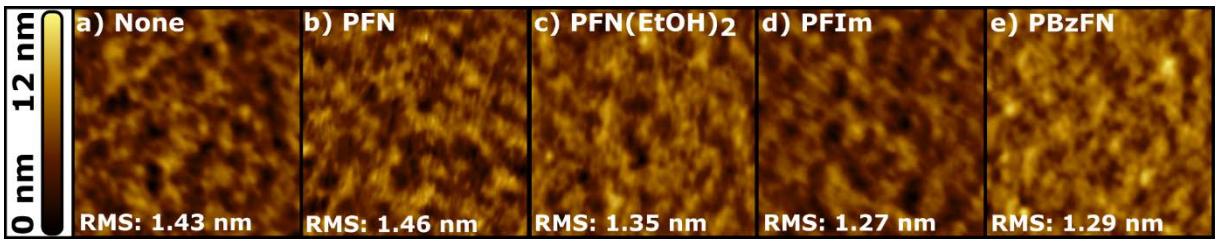

Figure 3.3. AFM images (2.5×2.5 µm) of **a)** the naked active layer and **b-e)** four interlayers on top of the active layer.

The contact angle measurements were similarly compared to a bare film and here a significant difference can be measured. The measurement was performed by dropping a single drop of deionized water on top of the film and optically measuring the drop from the side. This was repeated five times for each film and an average contact angle was calculated. The images shown were chosen as representative. The films were somewhat reflective, making the photos a bit hard to judge by eye. The bare film a) had an average contact angle of 105.4°, meaning a fairly hydrophobic surface. When the CIMs were applied, the average contact angles reduced by roughly 15°. While not a huge difference, this means the surface was significantly less hydrophobic for all four polymers.

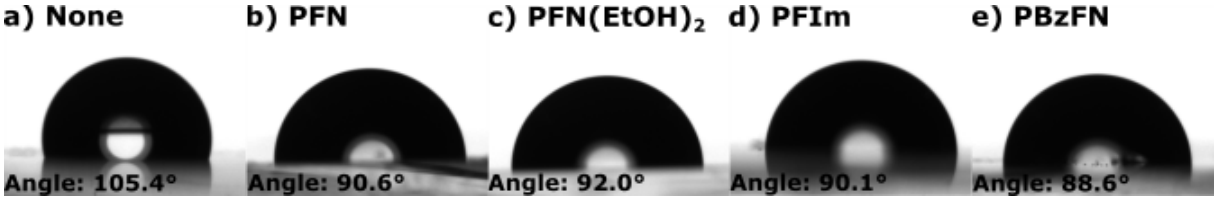

Figure 3.4 Contact angle measurements for **a)** the naked active layer and **b-e)** the four different interlayers.

The polymers presented in this work have been proven to be useful substitutes to the common LiF/Al cathodes. This is advantageous since LiF has to be vacuum deposited onto the active layers, which is an unsuitable processing method for large scale production, where roll-to-roll printing will most likely be dominant. LiF can also be a significant source of device degradation, so substituting it will be important. Therefore, these polymers are suggested as viable candidates for use in large scale production of All-PSCs.

4. Tertiary Amine Pendant Group Polymers

Chapter 4 will treat Paper III, which is a manuscript focusing on the synthesis and characterization of seven different polymers with tertiary amine pendant groups. The aim of these polymers was to use them as active layer donor polymers in organic photovoltaics. Earlier studies have shown that the presence of tertiary amines severely limiting the device performance due to hole trap formation. To study if the energy level of the polymer backbone in relation to that of the pendant groups would affect this performance drop, the seven polymers had varied energy levels. The electrochemical and optical properties were studied in depth and the polymers were used in BHJ PSCs with PCBM. Most of the polymers resulted in barely functioning devices, but one of them had a stable PCE of 1% which is one of the highest recorded results for a device with tertiary amine pendant groups in the active layer components. Further study is needed to understand why this polymer functioned, while the others did not.

4.1. Background

The processing of active layers for OPVs is currently completely dependent on toxic and environmentally unfriendly solvents such as toluene, chloroform or even *o*-dichlorobenzene. This might work on lab scale production of devices, but is a large downside when scaling up to large scale roll-to-roll printing of solar cells and much work is done to improve polymer solubility in green solvents.[129-140] The ideal would be to have polymers processable with aqueous alcohol mixtures and a powerful tool to achieve this would be the inclusion of tertiary amines in the sidechains.[141] These polar groups could be made very hydrophilic with trace amounts of volatile acids like acetic- or formic acid and then turned back to just less hydrophilic with their evaporation. Since the sidechain does not directly influence the energy level of the polymer, they are more customizable without affecting the main function of a material.[46] There are many examples of interfacial polymers with tertiary amines, presented in Chapter 3, but few examples of the successful inclusion of *t*-amines in active layer polymers.[102]

In 2013, Duan *et al*. published a paper in which a carbazole unit used in a donor polymer and a fullerene derivative bearing *t*-amine pendant groups was presented.[141] The polymer and fullerene worked well as thin interfacial layers, which was expected, but resulted in severe hole-trapping and no photovoltaic output when used as active layer. Furthermore, they showed that the amines negatively impacted the electron mobility of the fullerene. The following year,

however, two papers were published somewhat contradicting those results. One paper presented a different fullerene derivative with amine functionalities, which was successfully used with P3HT in the active layer.[142] They noticed significant vertical phase separation, which led to inverted device architectures performing well even without the use of a cathode interfacial layer, since the fullerene modified the ITO cathode. This was corroborated by another study using the same fullerene derivative and later with other fullerene derivatives.[143-144] In 2015, Cai *et al.* presented the theory that the hole trapping problem could be circumvented by using a donor polymer with a HOMO above that of the ionization energy of the amino group.[145] They compare two polymers, one with HOMO above and one below that of the *t*-amine group and used them in devices with amine containing fullerene derivatives. The higher HOMO-level polymer P3HT had a significant photovoltaic effect, while the other polymer did not, confirming their theory. Recent studies further corroborate this theory.[146]

In order to study this effect and further confirm this effect, and also to study if the device configuration could be a key in understanding if the HOMO level is the only relevant factor, Paper III present a series of donor polymers with varied backbone energy levels bearing *t*-amine pendant groups.

4.2. Synthesis

The synthesis of the seven polymers included the production of thee conventional acceptor segments with the added diethylamine pendant group. The three monomers, called **M1**, **M2** and **M3** in Scheme 4.1 were benzotriazole (BTz), diketopyrrolopyrrole (DPP) and isoindigo (II) respectively. The synthesis of **M1** started from another commonly used component benzothiadiazole (BT), which was reductively ring opened with metallic zinc in acetic acid. The zinc was filtered off and the ring was closed with sodium nitrite, giving benzotriazole (**3**). This compound was alkylated with 1,6-dibromohexane, sodium hydroxide and potassium iodine in anhydrous dimethyl sulfoxide (DMSO). The purification of the produced **4** is important, to remove the significant byproduct produced where one of the side nitrogens are alkylated. The ratio between them is roughly 2:1 of product to byproduct. Luckily, the compounds can be separated over a silica column. The final step is an amination, using diethylamine (Et_2NH) in a bi-molecular nucleophilic substitution reaction (S_N2). The second monomer **M2** started from the DPP-core unit, which can be produced in one step from thiophene-3-carbonitrile and diisopropyl succinate, but was already available. The core unit has limited solubility so the initial step is introducing the alkyl chain in an alkylation reaction

similar to the previous one, but with the weaker base potassium carbonate, yielding compound **6**. The final monomer needs to be brominated to be used in Suzuki- or Stille polymerizations, and the purification is easier before the amine is introduced, so NBS was used to brominate **6**. The final amination was identical for all three monomers **M1**, **M2** and **M3** with slight differences in purification. The final monomer **M3** was even simpler, since the starting material was already brominated. It was both alkylated and aminated in identical fashion to **M2**.

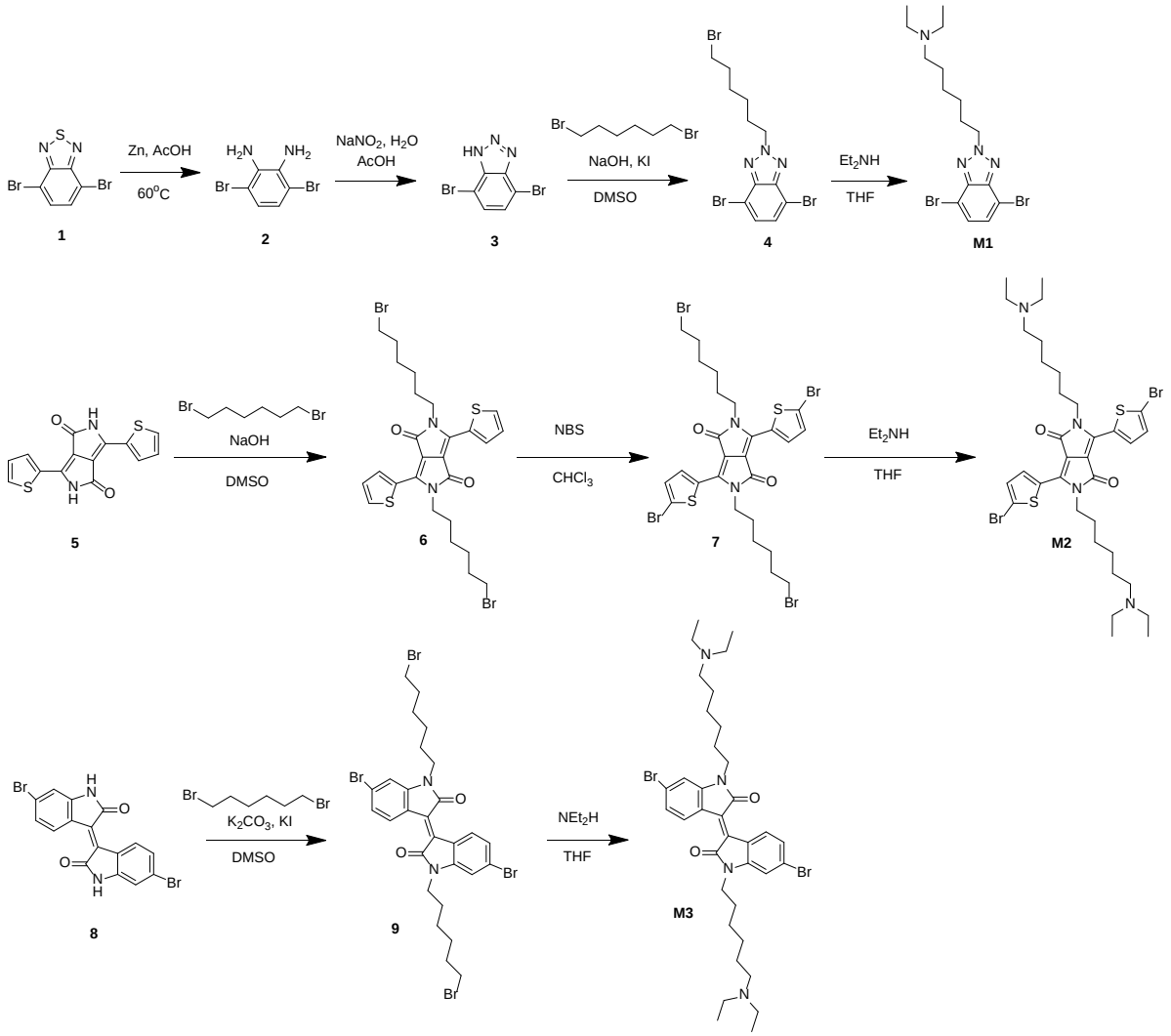

Scheme 4.1. Synthesis of tertiary amine pendant group monomers **M1**, **M2** and **M3.**

All the polymerizations illustrated in Scheme 4.2 were performed with commercially available electron rich donor segments. These were benzodithiophene (BDT) (**M4**), thiophene (**M5**) and fluorene (**M6**). The polymerization reactions were either Suzuki- or Stille polymerizations. Due to the similarity to the polymerization reactions presented in the previous chapter, the Suzuki reactions used for PIIFl-N and PBTzFl-N are not described in detail here. The five polymers

synthesized with Stille polymerizations were PBTzBDT-N, PDPPBDT-N, PIIBDT-N, PDPPT-N and PBTzT-N.

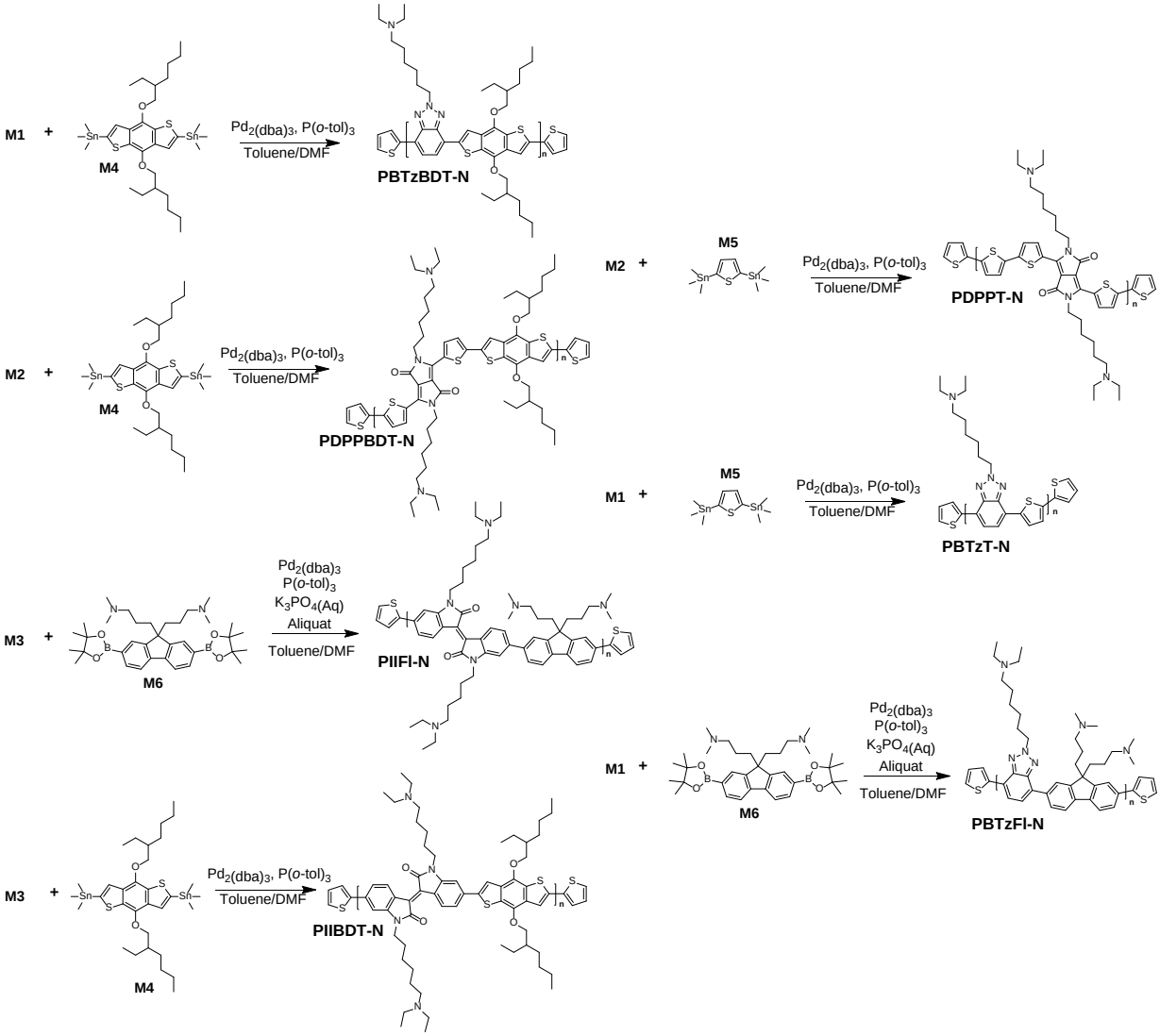

Scheme 4.2. Polymerization reactions for the seven copolymers, PBTzBDT-N, PDPPT-N, PDPPBDT-N, PBTzT-N, PIIFl-N, PBTzFl-N and PIIBDT-N.

The reactions were performed by very careful weighing of the two monomers, the catalyst and the ligand. These were then placed in the reaction vessel which was repeatedly purged with nitrogen and vacuum to remove any trace of air. Anhydrous toluene:DMF at a 9:1 ratio was degassed, added to the reaction vessel and then degassed again. The reaction vessel was heated to 80 °C and vigorous stirring was used. The solutions were closely monitored in the beginning, in case they quickly turn to very viscous. They were then protected from light and kept stirring for up to 72 hours. 2-(Trimethylstannyl)thiophene followed by 2-bromothiophene were then added to endcap the polymers. After the solutions had cooled down, the polymers were precipitated from petroleum ether and collected in Soxhlet thimbles and purified by Soxhlet

extraction with petroleum ether, diethyl ether, acetone and chloroform. The chloroform fractions was purified over a short neutral alumina plug and the polymer were once again precipitated from petroleum ether and the polymers filtered and dried. Some minor deviations might have taken place, but generally the polymerizations were performed very similarly. These reactions tend to give very high yields, which is reduced by the purification steps where low molecular fractions might be removed during the Soxhlet extraction.

4.3. Results and Discussion

An important part in the design of the polymers was to vary the backbone energy levels enough to see if their relation to the tertiary amine pendant group would affect their performance in solar cells. To this end, their energy levels were studied in detail with both electrochemical and optical methods. Triethylamine was used as a reference molecule which should have similar properties to the diethylamine pendant groups. In Figure 4.1 the electrochemical properties, measured by both SWV and CV are shown. In **a**), the SWV clearly shows highly variable levels of both oxidation and reduction potentials. This is also reflected in the cyclic voltammograms shown in **b**), however the amount of peaks make it far less clear.The optical properties of the polymers, studied with UV-Vis absorption spectroscopy in both solution and film have a similar spread. The curves shown in Figure 4.2 a) show the absorption in film and b) in chloroform solution.

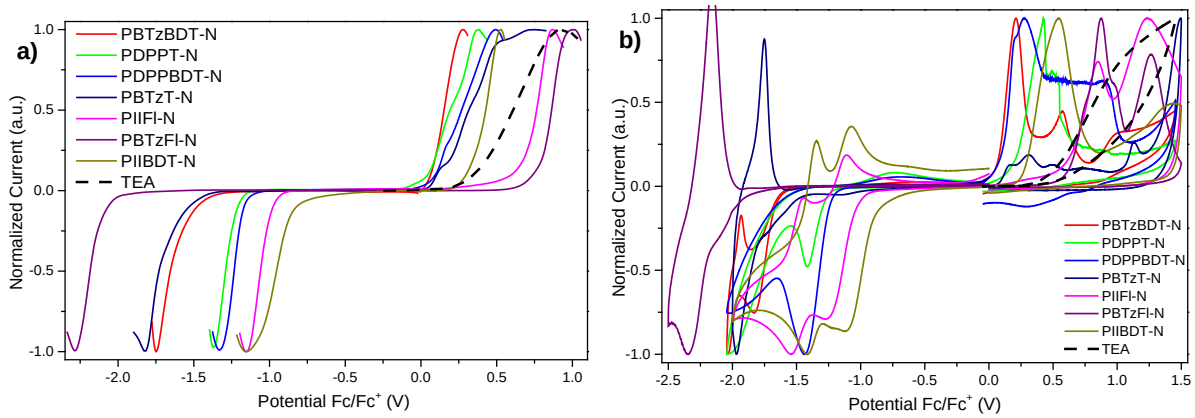

Figure 4.1. a) SWV and **b)** CV for the seven polymers.

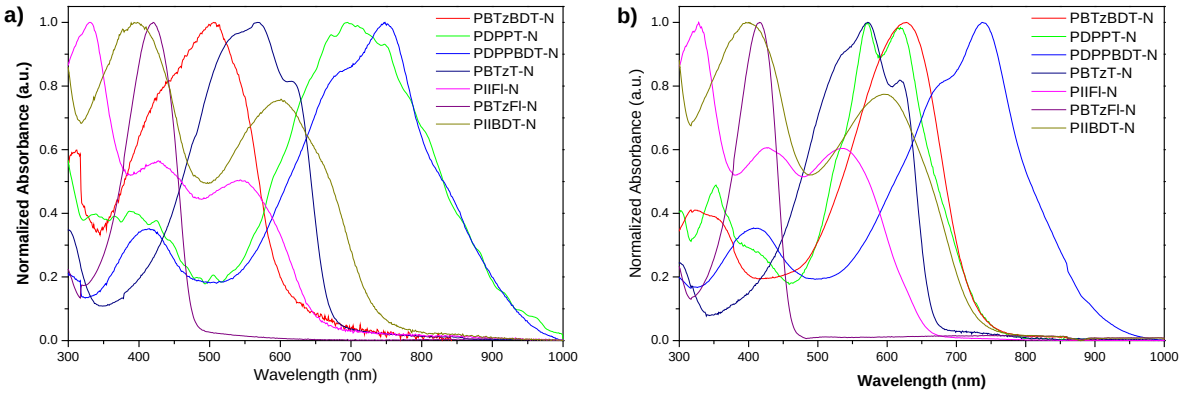

Figure 4.2. a) Normalized UV-Vis absorption spectra of polymers in film. **b)** Normalized UV-Vis absorption spectra of polymers in solution.

To present the energy levels in a clear way for comparison, an energy level diagram was compiled from the SWV data and is shown in Figure 4.3. The polymers are compared with both TEA and $PC_{71}BM$. Only one polymer had a deeper HOMO than TEA, which is BTzFl-N. This polymer backbone contains linked six-membered rings with II bonded to Fl. These bonds create a large dihedral angle between the two rings, leading to a short conjugation and thus a high band gap.[147] The polymer therefore also has the widest band gap and the highest LUMO.

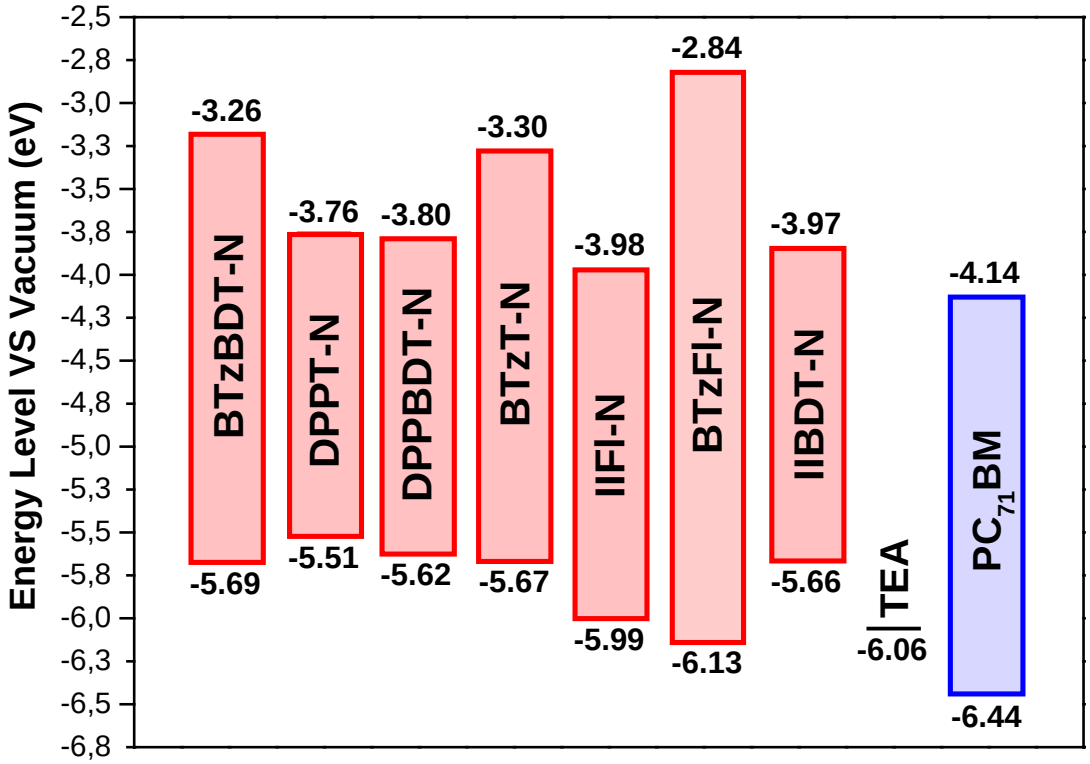

Figure 4.3. Energy level of the seven donor polymers measured by square wave voltammetry.

The values of the SWV and UV-Vis absorption was compiled into Table 4.1. The comparison between the E^{opt} and the E^{ec} often deviates quite a bit. This deviation was described in chapter

1.5, and mainly attributed to the charge separation taking place in electrochemical measurements and not optical ones.

Table 4.1. Optical and electrochemical properties of the copolymers.

	UV−Vis absorption				SWV		
	Solution	Film					
Polymer	λ_{max}[a] (nm)	λ_{max}[b] (nm)	λ_{onset} (nm)	E_g^{opt} (eV)[c]	HOMO (eV)	LUMO (eV)	E_g^{ec} (eV)[d]
PBTzBDT-N	625	504	601	2.07	–5.40	–3.49	1.91
PDPPT-N	571	697	934	1.32	–5.51	–3.76	1.75
PDPPBDT-N	738	751	940	1.32	–5.62	–3.80	1.82
PBTzT-N	569	569	671	1.85	–5.67	–3.30	2.37
PIIFl-N	328	330	644	1.92	–5.99	–3.98	2.01
PBTzFl-N	415	425	482	2.58	–6.13	–2.84	3.29
PIIBDT-N	396	400	727	1.71	–5.66	–3.97	1.69

[a]Absorption maximum in chloroform solution; [b]Absorption maximum in film; [c]Optical band gap; [d]Electrochemical band gap.

Another reason to analyze the electrochemical measurements in detail was to see if the oxidation of the pendant group. In previous studies, this has been observed in some polymers and not in others.[141,145] To this end, the oxidation of each polymer from both SWV and CV compared to those of TEA are presented individually in Figure 4.4. When performing CV measurements on conjugated polymers, the common method is to oxidize it to just past the first oxidation peak. Here the polymers were instead oxidized far past the first peak and in some cases a second or third oxidation peak closely matches that of TEA.

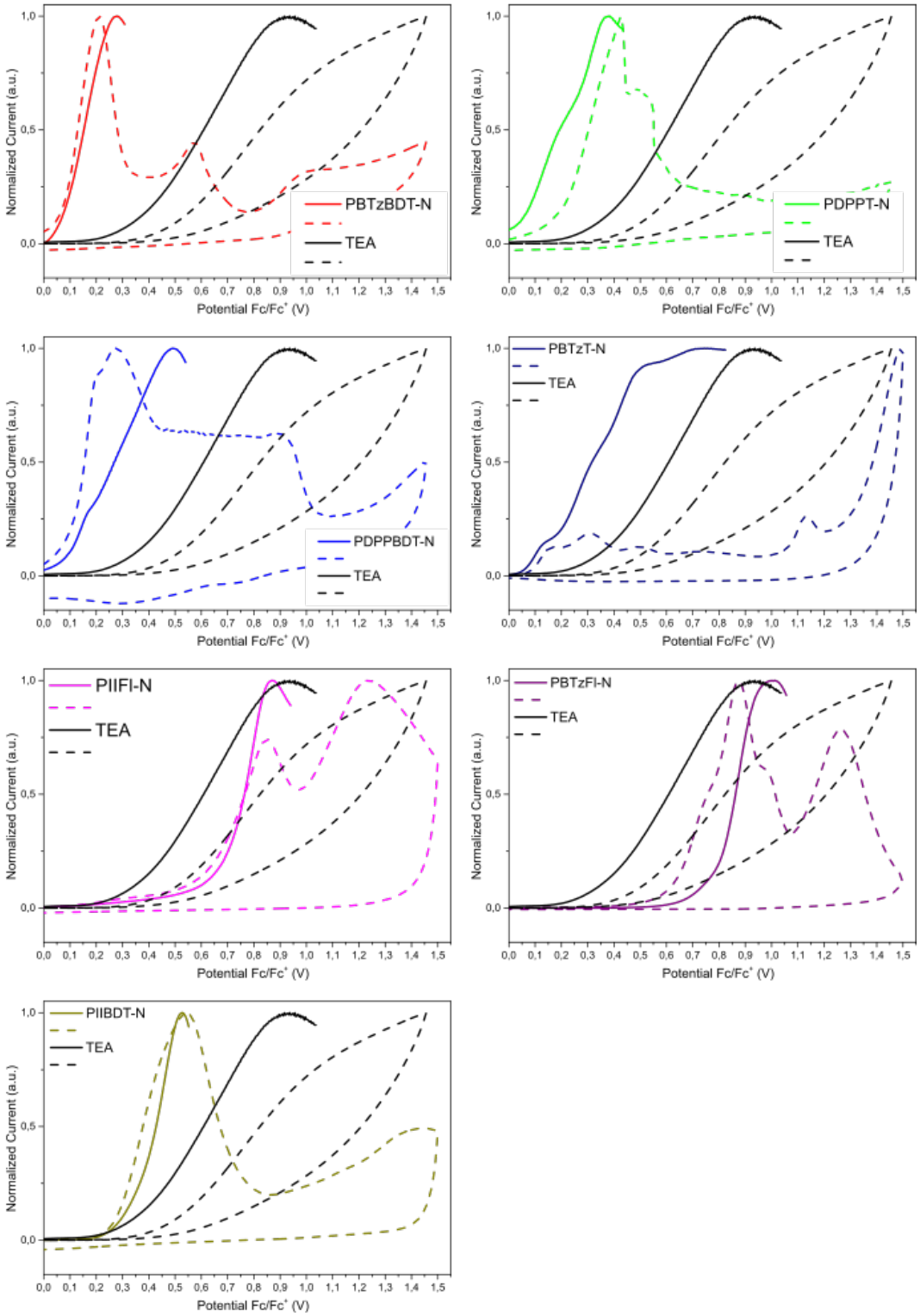

Figure 4.4. Comparison of oxidation measured by SWV (solid lines) and CV (dashed lines) for all seven polymers with TEA as a reference.

The polymers were used as active layer components in PSCs together with $PC_{71}BM$ as acceptor molecule. The polymers were initially tested in solar cells with conventional device structures of ITO/ZnO/Polymer:$PC_{71}BM$/C_{60}/LiF/Ag, where C_{60} was used as a passivating electron transport layer, to separate the amine-containing polymers from the LiF/Ag cathode. From these

devices, all but two polymers performed abysmally with barely measurable currents. The two outliers were PBTzBDT-N and PDPPBDT-N. A second batch of the first polymer named PBTzBDT-Nb was synthesized and a more detailed study with other device configurations was carried out. The device structures used were for conventional devices (ITO/ZnO/Polymer:$PC_{71}BM$ (1:2.5) /MoO_x/Ag) and for inverted structures with and without a TPD interfacial layer (ITO/ZnO/Polymer:$PC_{71}BM$ (1:2.5) /(TPD)/MoO_x/Ag). In another case, the conventional structure device had the anode interfacial layer ZnO replaced with PEDOT:PSS. The results from these are shown in Table 4.2.

Table 4.2. Photovoltaic parameters of devices fabricated using Polymer:$PC_{71}BM$ (1:2.5) bulk heterojunction. The average is from six identical devices.

Polymer	J_{SC} (mA cm^{-2})	FF (%)	V_{OC} (V)	PCE (%)
PBTzBDT-N:$PC_{71}BM$[a]	3.1 (2.98 ± 0.13)	42 (41 ± 1)	0.83 (0.82 ± 0.01)	1.01 (1 ± 0.02)
PBTzBDT-N:$PC_{71}BM$[b]	2.72 (2.57 ± 0.1)	40 (40 ± 0.5)	0.88 (0.86 ± 0.02)	0.94 (0.87 ± 0.04)
PBTzBDT-N:$PC_{71}BM$[c]	2.15 (1.85 ± 0.5)	38 (36 ± 1)	0.82 (0.79 ± 0.03)	0.61 (0.53 ± 0.04)
PBTzBDT-Nb:$PC_{71}BM$[a]	2.4 (2.25 ± 0.1)	43 (41 ± 2)	0.37 (0.34 ± 0.02)	0.34 (0.31± 0.02)
PBTzBDT-Nb:$PC_{71}BM$[b]	2.25 (2.57 ± 0.1)	37 (36 ± 0.5)	0.51 (0.50 ± 0.01)	0.41 (0.38 ± 0.03)
PBTzBDT-Nb:$PC_{71}BM$[d]	1.24 (1± 0.14)	27 (26± 0.4)	0.45 (0.44± 0.02)	0.14 (0.11± 0.01)
PDPPBDT-N:$PC_{71}BM$[a]	1.08 (1 ± 0.05)	34 (32 ± 1)	0.13 (0.12 ± 0.01)	0.04 (0.04± 0.00)
PDPPBDT-N:$PC_{71}BM$[b]	1.64 (1.52 ± 0.06)	35 (34 ± 0.5)	0.34 (0.33 ± 0.01)	0.18 (0.17 ± 0.07)
PDPPBDT-N:$PC_{71}BM$[c]	1.65 (1.38± 0.13)	38 (36± 3)	0.34 (0.32± 0.03)	0.21 (0.16± 0.03)

[a]Inverted device without TPD; [b]Inverted device with TPD; [c]Conventional device with MoO_x; [d]Conventional device with PEDOT:PSS

A few conclusions can be drawn from the device results. Primarily that the polymers do not perform well, but they give measurable currents. There was no obvious trend between conventional or inverted structure devices, but the devices with PEDOT:PSS performed well below all others for both PBTzBDT-N and PBTzBDT-Nb. The TPD passivating layer did not seem to consistently improve the devices performance either. In the end, the only solar cells

that gave relatively acceptable performance was the inverted solar cells using PBTzBDT-N. The reason why the first batch of the same structure polymer performed so much better has not yet been determined.

A possible explanation could be the incomplete functionalization of the benzotriazole monomer with diethylamine. NMR-measurements of the monomer proves no residual 6-bromohexyl residues, however. The polymer could possibly have degraded, but the tertiary amine structure is fairly stable and the polymer was stored at room temperature in the dark. Another possibility could be a contaminant, which could interact with the free electron pair of the amine. This would explain the batch-to-batch-variation, but no such contaminant has been found. In any case, these results indicate that the application of amino-containing polymers as active layers for solar cells is not so promising. Further study is needed to fully understand the reasons for their poor performance.

5. Organic Electrochromics

5.1. Background

Electrochromic properties signify the ability of a material to change color when it gains or loses one or more electrons. The name electrochromism was first coined by John R. Platt in 1961 when it was theorized that strong electric fields could shift the absorption of a dye.[148] Early studies found the property in the dye Prussian Blue in 1978.[149] Since then, the property has been found in a vast array of molecules, often with transition metals or viologens.[150-151] Electrochromism is also fairly common in the polymers commonly used for other organic electronics applications. Conjugated polymers can be used for electrochromic devices in which they have similar benefits as for other applications, such as solution processability, customizable molecular design, and flexible mechanical properties.[152-153] Conjugated polymers, with their high absorption coefficients, require a very thin layer of materials to absorb much of the incoming light. This means a small current can be used for oxidation/reduction of the thin layer, leading to energy efficient devices.

A polymer called PITN, previously mentioned in chapter 1.3, was used to investigate the quinoidal structure and its influence on narrowing the band gap. The same polymer was also influential in developing the understanding of electrochromism in conjugated materials, so called electrochromic polymers (ECP).[154] It was also the first report of a transparent conducting polymer, since it turned almost completely transparent upon oxidation. This study had a detailed structural analysis of the PITN films using TEM, from which they drew the conclusion that the rate limiting factor of electrochromic switching was the diffusion of dopant counter ions into the polymer structure.

Since most conjugated polymers serve as electron rich materials which can be easily oxidized for an electrochromic transition, this will be the focus of this section. Over the last decade, the amount of publications on conjugated polymers used for electrochromic applications have increased dramatically, and the DA structure commonly used in OPV polymers has proven to be useful for electrochromics as well.[155-159] The mechanism behind the color change comes from the formation of radical cations and dications, called polarons and bipolarons, which lead to conformational changes in the polymer and the formation of polaron and bipolaron states in the band gap decrease the π-π^* absorption energy.[160] This effect is illustrated in Figure 5.1. As

with OPVs, most polymers used are electron rich, meaning they work best as p-doped materials. There are few examples of n-doped conjugated polymers for organic electrochromics (OEC), but it is not unheard of.[161]

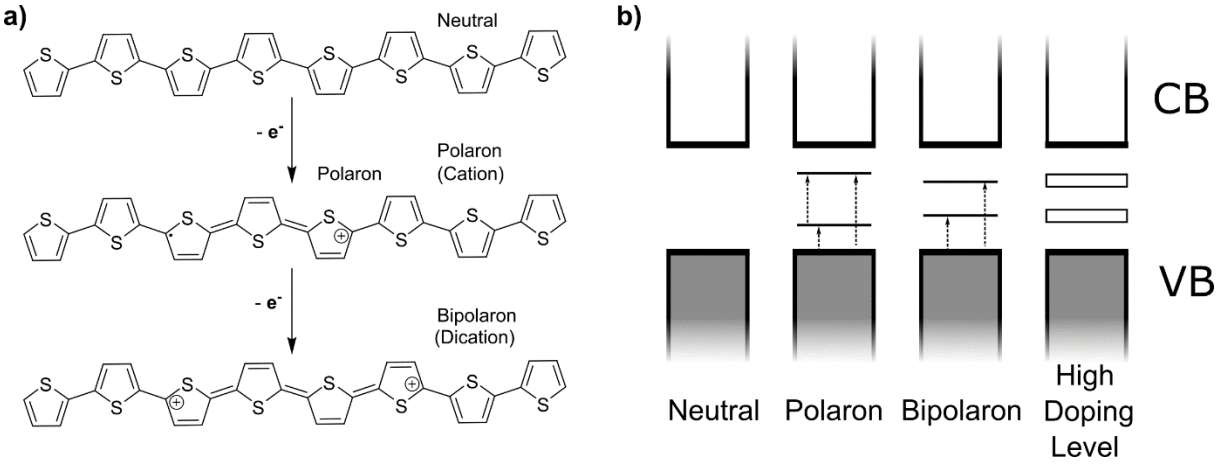

Figure 5.1. a) Schematic formation of polarons and bipolarons in poly(thiophene) **b)** Suggested new band structures formed by the polarons and bipolarons.

If the neutral polymer absorbs light in the visible region, the new low energy absorption bands formed upon n-doping or p-doping is often shifted into the near-IR or IR-region and thus much more optically transparent. For many applications the goal is to go from colored to transparent. Therefore, polymers with large band gaps with absorption in the blue region need a large redshift from around 400 nm to over 700 nm. A common consequence of this is that residual absorption in the visible region give blue-tinted transparent transparency, which is especially common for yellow polymers. The first polymer exhibiting orange color to transparent was published in 2010 and was a major step towards completing the electrochromic colored to transparent spectrum.[162] The year after, the palette was completed with the addition of yellow to clear, also by the Reynolds group.[163-164] Due to the relatively high potential of 1.1 V for complete switching, the polymer is unsuitable for use in blends with other polymers since overoxidation significantly decreases the lifetime. For this reason, more work needs to be done to reduce yellow polymers' oxidation potential, while keeping the coloration before and after oxidation intact.[165]

The term spectral engineering has become more important with the advent of OECs.[166] While the shape of an absorption spectrum is relevant for OPVs, the main goal is a high absorption coefficient in the correct region for the device structure. This is not the case for OECs, however, where the visual color is often the desired property. Therefore the term spectral engineering

was coined, to describe the tuning of the absorption spectra for a desired coloration. This has become more relevant for OPVs as well, with the rise in popularity of all-PSCs and SMAs, where it is important to minimize the spectral overlap between the two components. Conjugated polymers have a characteristic double peak absorption where a short wavelength absorption often ends up in the UV-region and the longer wavelength one in the middle of the visible region.[166]

Overlap between organic electrochromics and photovoltaics

There seems to be a significant overlap in the design of conjugated molecules for applications of electrochromics and organic photovoltaics. In part, that depends on the suitable energies needed to place a chromophore in the visible part of the spectrum. The small band gap polymers often require fairly low potentials for oxidation with the associated color change. The rich library of available materials, combined with the relative ease of characterizing the polymers for electrochromic properties give a favorable situation where plenty of materials can be screened. There are also obvious similarities when it comes to the other components used in electrochromic devices, such as ITO and substrates, due to the transparency requirements. These factors, as well as the shared molecular design elements give a significant overlap with the field of organic photovoltaics. This is also reflected in the same influential research groups publishing in both fields, as well as other neighboring ones like OLED, OEC and OPD.

5.2. Spectroelectrochemistry

The term spectroelectrochemistry refers to the use of spectroscopy *in situ* inside an electrochemical cell. This method can be applied in many potential setups to measure a wide variety of material properties.[167] The study of the kinetics in optical switching is called chronoabsorptometry. This is usually performed by identifying the position of maximum optical contrast between neutral and charged states, which is commonly found at an absorbance maximum and applying cyclic or square waves. A polymer presented in chapter 6 has overlapping absorption in neutral and oxidized states, which led to a new absorption band at 705 nm being chosen instead. The measurement is then done by monitoring the specified wavelength over time, while performing cycles or square waves of electrochemical transitions. Longer cycles of tens of seconds are often used initially, to verify complete optical transition. The cycles are then shortened until the polymer does not have time to properly transition for each cycle and the proportion of transmittance reached in faster cycles is compared to slower cycles. A schematic representation of the response of a polymeric material can be seen in Figure

5.2, in which a square wave potential is applied (a)). The electrochemical response (b)) is very fast upon switching, gradually approaching no faradic current produced as more of the polymer has been oxidized or reduced. The optical response (**c)**)is similar but approaches the maximum or minimum optical density as more polymer is oxidized or reduced.

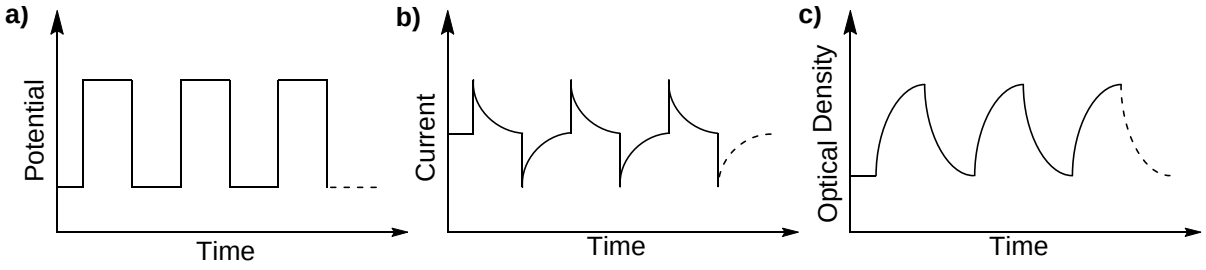

Figure 5.2. Schematic representation of the **a)** applied potential square waves and resulting **b)** electrochemical and **c)** optical response

An important factor to consider when performing spectroelectrochemistry is the film thickness. It has been shown that film thickness directly affects optical contrast, and for a quinoxaline polymer the maximum contrast was found when the absorbance was around 0.7-0.9.[168] A common aim is around 1 absorbance.[165] The most important material properties of an ECP is the color, electrochromic contrast, electrochromic switching rate and the stability of the material. There are several more important factors that can be measured, which include coloration efficiency, reflectance and the optical memory of the material.

Coloration

The band gap is not the main focus of electrochromic materials, but instead the coloration. This means an aesthetically pleasing combination of hue, saturation and intensity is the target. A way to measure the coloration has been developed which is not dependent on subjective analysis by eye. This method is the colorimetric analysis, introduced by Reynolds *et al.* in 2000.[169] Due to the need for both quick color comparison and information of color change, a coordinate system where before and after color transition can be marked was developed. The *L*a*b* system is very commonly used in fields with color focus, in which the values are where *L* is the luminance and a*b the color coordinates. These values can be calculated from the CIE 1931 color space diagram, exemplified in Figure 5.3, which instead uses the trimulus value *Yxy,* where *Y* is a percentage of luminance compared to the background luminance Y_0:

$$Y(\%) = 100 \times \frac{Y}{Y_0} \tag{5.1}$$

The x and y values signify the coordinates on the diagram. The relative luminance of a material affects in how bright a material is experienced, which affects the color experience. Compared to the *L*a*b* system, the *Yxy* has the advantage that the color of mixtures can be directly calculated from it. The use of a simple coordinate system is very beneficial for descriptive power and a color change following an oxidation or reduction can be readily described.

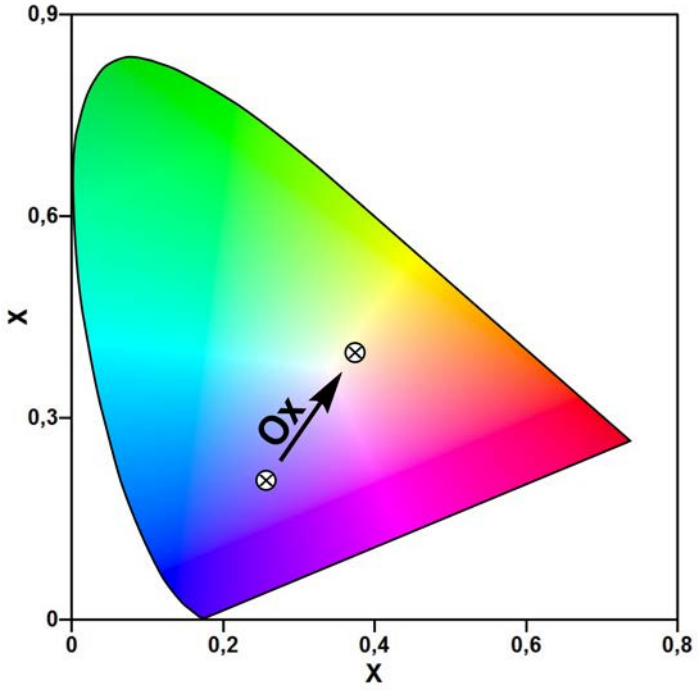

Figure 5.3. CIE 1931 color diagram with a hypothetical color change following an oxidation.

The *Yxy* values can be measured using a colorimeter. The colorimeter eliminates some error sources as compared to an ordinary spectrophotometer, since it can vary illumination conditions and is calibrated to take the eyesight into account when measuring a color change.

Electrochromic Contrast

The electrochromic contrast is another primary figure of merit of an OEC. The electrochromic contrast is generally reported as the difference in transmittance (ΔT%) at a specific wavelength. The wavelength chosen is often the point of maximum contrast, which is generally, but not always, the absorption maximum. The transmittance T is defined as the light transmitted through the material divided by the incident light:

$$T = \frac{I}{I_0} \tag{5.2}$$

Which is related to the absorbance, according to the Beer-Lambert law (Eq. (1.6) as:

$$A = log_{10}\frac{I_0}{I} = log_{10}(T) \tag{5.3}$$

Switching Rate

The electrochromic contrast is important, but the switching rate is also an important property. Not all applications require very fast switching, such as eyewear or switchable windows, but it is critical for display-purposes. The switching rate can be defined as the time it takes for an electrochrome to switch from one redox state to another.[170] The switching rate is far less straight forward to compare than other figures of merits of OECs, due to diffusion dependence and differences in setups used to measure it. Since the film morphology and thickness is influential, the exact preparation of the film affects the measurement and factors such as solution concentrations, deposition method, temperature used and substrate can affect the measurement. This means measurements with different experimental setups might produce widely variable results, so literature values are not completely reliable in all cases.

Stability

The electrochemical stability of the polymers used for electrochromic applications is of critical importance. Measuring the electrochemical stability can be done by repeated square waves or cyclical waves to a completed redox transition and back again. Preferably over 10 000 cycles, which requires an inert atmosphere and anhydrous electrolyte solutions. One mode of long-term degradation that has been found is unsubstituted phenylene and thiophene groups that cause crosslinking over redox-cycles, which reduces contrast.[165] The use of overpotential is a source of degradation which can be problematic in polymer blends with different oxidation potentials.[171-172]

Optical Memory

The ability to retain a redox state after the external field is switched off is called the optical memory. This factor is important for applications such as nonemissive displays, where a high optical memory can enable very low power consumption. Though it might not completely remove the power consumption at a set color since a refreshing pulse can be required to keep coloration, it will still require far less energy than an emissive display.

5.3. Electrochromic devices

Organic Electrochromic Devices (OED) come in several device structures and shapes for a wide variety of applications where non-emissive coloration is desirable. They have been applied to the passenger-controlled dimmable windows in the new Boeing 787 Dreamliner, in tunable sunglasses and various other applications.[152,173-174] Another application which relies on low-power consumption might be sun-powered calculators, passive screens or other simple displays.[175] Conjugated molecules share some of the same advantages for electrochromic devices as they do for OPVs. They are light-weight, cheap to produce, solution processable etc. Early iterations of inorganic electrochromic materials relied on passive light switching from sunlight or other light sources, which is a quite slow process and can take minutes. By contrast, most OECs can switch coloration within seconds. They also have a relatively high optical contrast. Due to the solution processability of OEC polymers, electrochromic devices can be made with several methods, such as slot-die coating, bar coating, spray coating, inkjet printing, screen printing and rotary screen printing.[153]

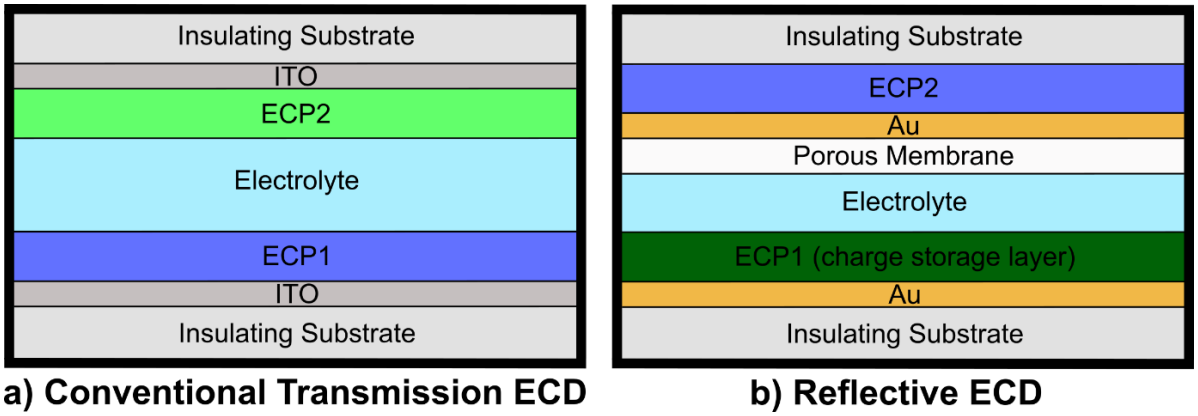

Figure 5.4. **a)** Generic device architecture of an absorption/transmission ECD and **b)** a reflective ECD

The device architecture varies depending on the application, for obvious reasons. The simplest case is an absorption/transmission ECD, often consisting of two polymers for complementary absorption.[170] Another example is a reflective ECD, which has slightly more complex device structures. When producing absorption/transmission ECDs, a critical component is the transmittance of all components in the device stack. Often, this is achieved by flanking the absorbing layer with ITO as both anode and cathode, due to its exceptional transmittance, which is hard to match with other metal oxides. The entire device needs to be well sealed as well, to prevent moisture or oxygen migrating into the device, which drastically decrease the lifetime of the device.[175] The dual ECP setup is used to maximize the optical contrast by having one

cathodically coloring polymer and one anodically coloring coloring polymer, where they complement each other's absorption. Another important reason is that a balanced redox pair is required for long-term stability of the device.[176] This poses additional material design problems, however, since they need to be electrochromically active in the same potential window.

Another use of ECPs is in reflective devices. This makes use of the high wavelength broad absorption of ECPs in the oxidized states, which extend far into the IR-region. One report states absorption between 2.5 μm to 45 μm.[177] These unique properties enable very efficient reflective screens for temperature control applications and has been suggested to fill a previously unfilled material property niche for use in spacecraft applications.[177] The device stack is similar, but has some differences. One difference is that the bottom ECP does not necessarily need to be strongly colored in the potential region, but can instead act as an electrochemical charge storage. This is significantly easier to find suitable candidates for, when the optical properties are not critical. In the device stack shown in Figure 5.4, which was first presented in a patent by Chandrasekhar in 1999, the top electrode was gold coated mylar which was patterned to allow ion transport.[178] This highly flexible device reached reflectance of 55% in the visible region and over 80% in the NIR region, while losing less than 20% contrast after 10 000 cycles.

The advances in PECs the last few years has led to increasing research into device fabrication for display applications as well. The possibility of using masks for patterning and solvent deposition of the polymer using spray coating or other methods enable fast production of devices. One successful example of a functional device produced was published in 2015, where a simple display with a digital and temperature, as well as logo of the company sponsoring partnering with the researchers.[175] The devices proved highly stable after sealing and tens of thousands of oxidation cycles yielded low loss of transparency. An interesting detail noticed was that the finer details of the logos degraded faster, while the larger elements of the display was stable even above 200 000 cycles. They also saw that the long-term stability was improved by using a lower potential with slower switching speeds.

6. Synthesis and characterization of Electrochromic Polymers

The following chapter is based on Paper IV and Paper V, which both treat polymers made for electrochromic devices. One set of polymers shared the IDTT donor unit, which has previously been used in polymers for both OPVs and organic light-emitting cells.[93,179-181] The last polymer presented was an anthraquinone-based polymer. All polymers turned out to have favorable properties for electrochromics, where the IDTT set exhibited high stability and fast kinetics, coupled with respectable optical contrast. The anthraquinone-polymer, on the other hand, was fairly unstable but with exceptional initial contrast which quickly reduced. Several of the IDTT polymers would likely be viable for OEC applications without further improvements, while the anthraquinone polymer requires further study to see if other subunits could stabilize it. The chemical composition of all five polymers presented in the chapter are shown in Scheme 6.1.

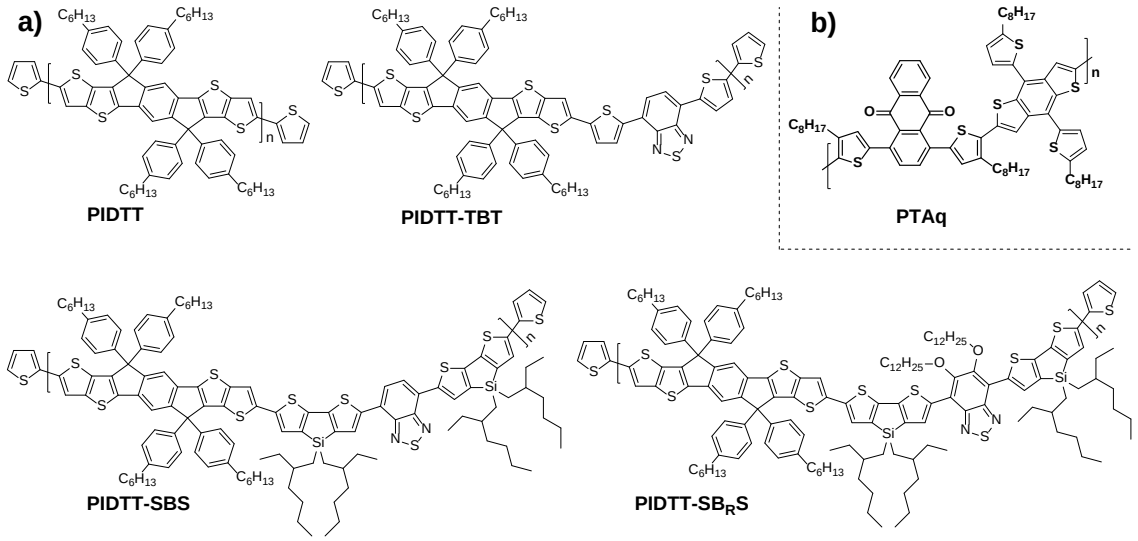

Scheme 6.1. Chemical composition of **a)** the four IDTT based polymers and **b)** the Anthraquinone-based polymers.

6.1. Background

The electron rich IDTT-block has become popular within the fields of OPV and OLED due to its suitable energy levels, high degree of chemical stability and fairly simple synthesis. It has been used in SMAs for OPV with great success, where some of the best performances has been with an A-D-A motif molecule called ITIC, shown in Figure 2.6. In chapter 5, the concept of absorption/transmission electrochromic devices, which require wide absorption covering the whole visible spectra or electrochemical compatibility with a complementary absorbing

polymer. The homopolymer PIDTT shown in Scheme 6.1 has a narrow band absorption, so to use the toolbox of spectral engineering, the IDTT unit was combined with three different electron deficient units. One was conventional TBT-block (PIDTT-TBT) and the other two had the thiophenes replaced with silolo[3,2-*b*:4,5-*b*']dithiophene (PIDTT-SBS) instead, with the last polymer bearing dodecyloxy side chains on the BT unit (PIDTT-SB_RS). The final polymer shown in Scheme 6.1 b) is based on anthraquinone and benzodithiophene and is named PTAq. The anthraquinone is an acceptor unit which has been reported rarely in other organic semiconductor applications, but is relatively common in dye preparation both for its stability and ease of synthesis.[182] The benzodithiophene combined with the anthraquinone is a very common electron rich unit.

6.2. Synthesis

Most of the monomers used for the IDTT polymers were bought from commercial vendors and SBS and SB_RS were synthesized in our laboratory for a separate publication in 2018.[181] Thus the only synthesis performed for this work was the polymerization reactions summarized in Scheme 6.2. All four of the copolymers use Stille couplings as polymerization reaction, with the IDTT-Sn block and a brominated D-A-D monomer. In the case of the homopolymer PIDTT, the brominated monomer was also an IDTT-unit.

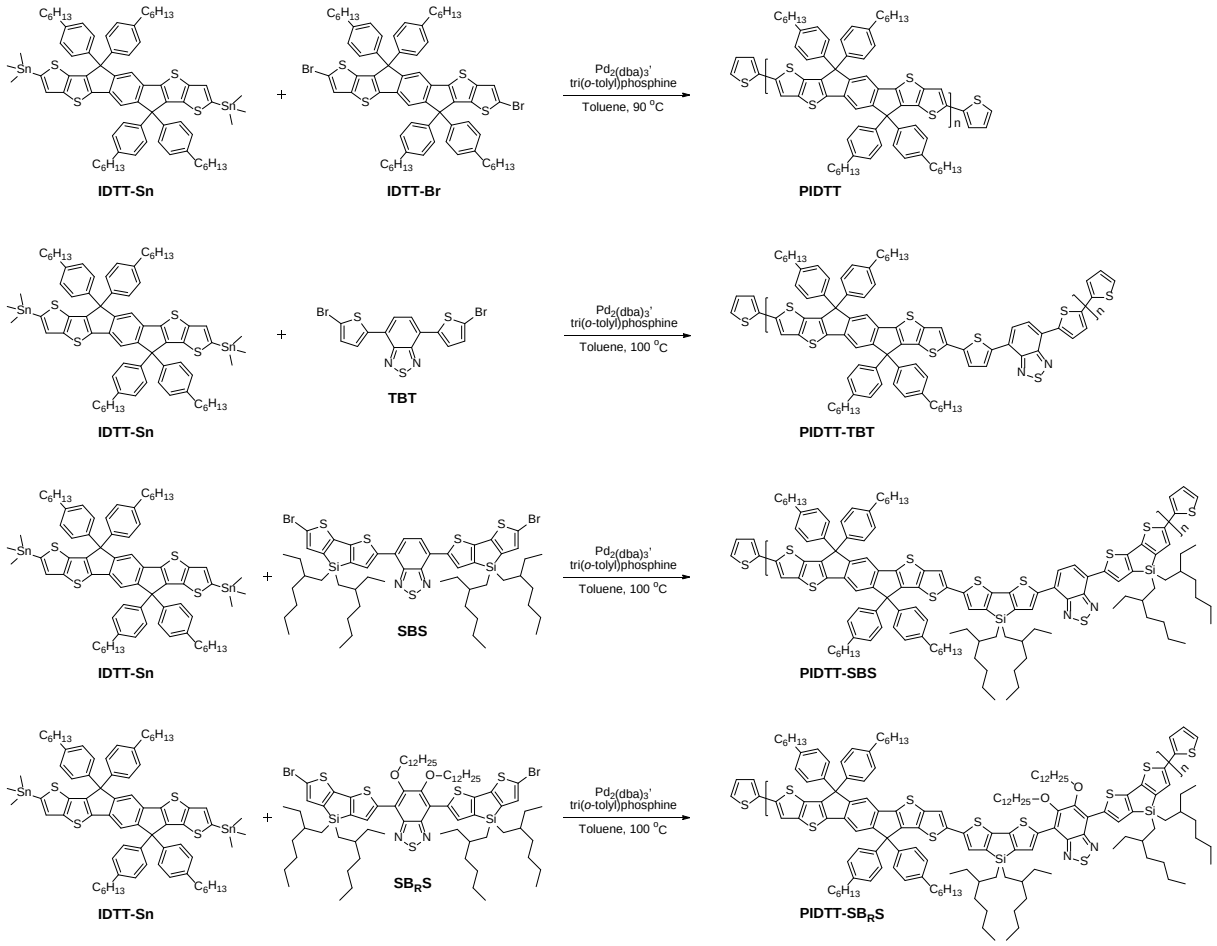

Scheme 6.2. Synthesis of the four polymers PIDTT, PIDTT-TBT, PIDTT-SBS and PIDTT-SB_RS.

The complete synthesis of PTAq is shown in Scheme 6.3. PTAq was synthesized from the commercial stannylated BDT monomer **5** with the locally produced brominated monomer **4**. The complete synthesis path is illustrated in Scheme 6.3**.** Monomer **4** was made from the commercial compound 1 which was diazotized and then quenched with $CuBr_2$. The dibrominated compound was then coupled with an alkylated, stannylated thiophene using a Stille coupling. The resulting compound was brominated using NBS to yield monomer **4** at a total yield of 8.1%. Since the limiting step was the first one, with a low yield of 19%.

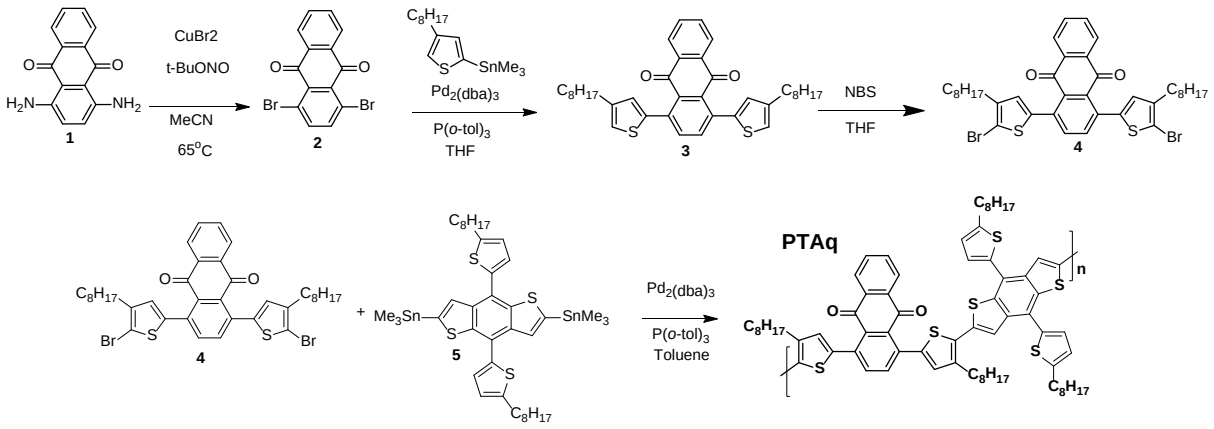

Scheme 6.3. Synthesis of compound **4** and the polymer PTAq

The polymerization with the two monomers was a Stille Cross Coupling polymerization. The reaction took place in anhydrous toluene, with Pd_2dba_3 as catalyst and P(*o*-tolyl)$_3$ as ligand. The reaction was heated to 90 °C for 5 hours, when the solution was viscous. The polymer was precipitated from methanol, redissolved in chloroform and stirred in an aqueous complexing agent solution overnight. The chloroform solution was then thoroughly washed with distilled water and the polymer was once again precipitated from methanol. Soxhlet extraction was used to purify the polymer using methanol, hexane, diethyl ether and chloroform. The polymer was finally precipitated from methanol a third time, filtered and dried. The yield was 96.5% and the polymer was a brick red solid.

6.3. Results and Discussion

The absorption spectra associated with the four IDTT polymers' electrochromic transitions are shown in Figure 6.1 with small inserts of the actual colors of the films. All four polymers show a double peak absorption pattern in the visible region when neutral. In the case of PIDTT, the absorption pattern is far narrower compared to the other three polymers. This is due to the homopolymer structure giving a wider E^{opt} and thus a higher excitation energy barrier and narrower absorption.[51,183] Generally, the commonly observed double peak pattern in donor-acceptor systems is attributed to two different modes of charge transfer. The high energy, short wavelength absorption band corresponds to the π-π* excitation. The lower energy, longer wavelength absorption band corresponds to the intrachain charge transfer between. The difference in absorption is also observed in the photos. PIDTT has a bright red color when neutral but the other three has purple to brown or even black colors, depending on the film thickness when the photos were taken. When external potential is applied to the film, the absorption peaks in the visible region quickly starts reducing in intensity and is more or less

extinguished at a potential of around 0.8 V for all four polymers. Instead, new even lower energy absorption bands form in the near infrared region between 700 nm and 1000 nm. The same trend as before between PIDTT and the other three polymers was observed where PIDTT had a higher energy peak, with a maximum just above 700 nm while the others peak at above 800 nm. A commonly sought after feature in electrochromic materials is a colored to transparent color change, which means four of these polymers show suitable absorption spectra both before and after oxidation. PIDTT has a well-defined red to transparent coloration, which could be suitable for display applications. The other three polymers with their broad absorbance covered most of the visible spectra. With absorption/transparent-applications in mind, the PIDTT-SBS might be too purple in the neutral state, but the other two copolymers could be suitable without the need for a complementary polymer.

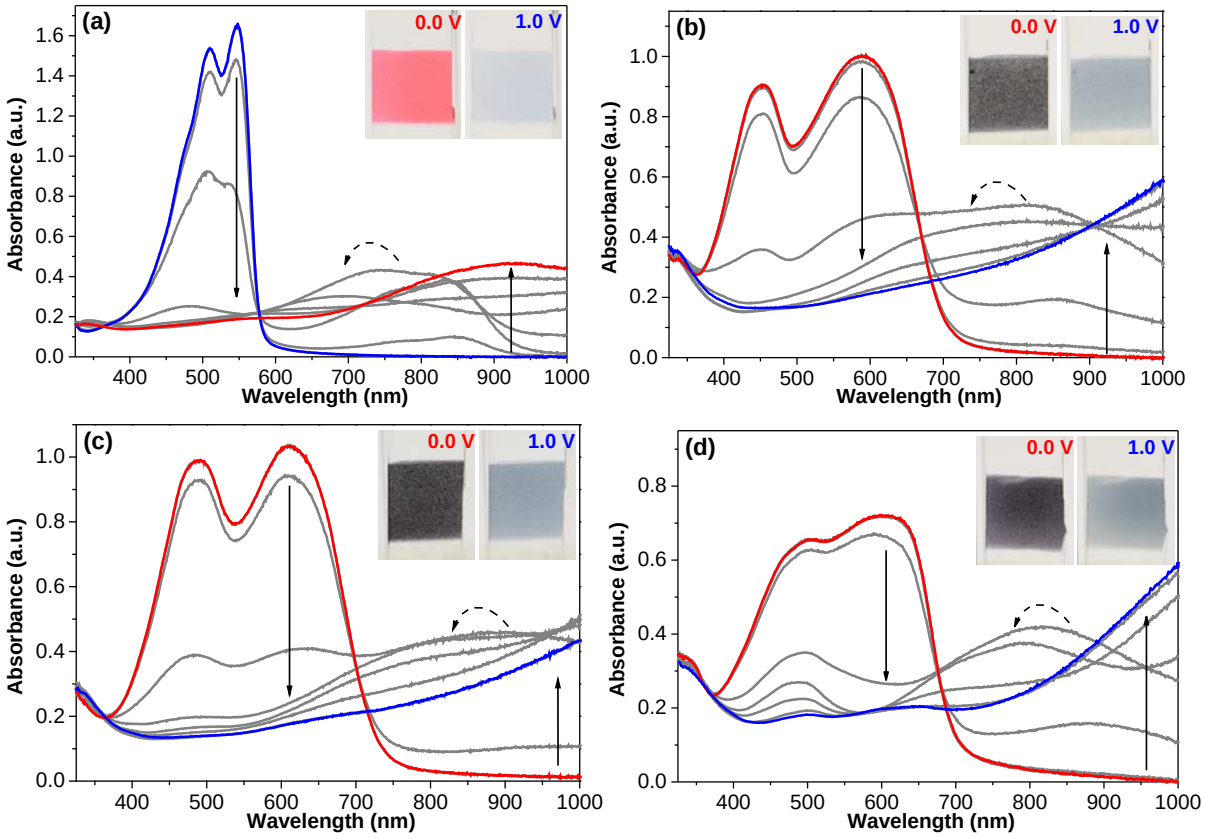

Figure 6.1. Electrochromic spectra of **a)** PIDTT **b)** PIDTT-TBT **c)** PIDTT-SBS and **d)** PIDTT-SB$_R$S with photo cut-out at 0 V and 0.8 V.

The absorption spectra of PTAq, shown in Figure 6.2 is significantly more blue-shifted than the IDTT-series, with neutral absorption maxima at 345 nm and 435 nm. Part of this might be explained by the relatively weak electron acceptor anthraquinone not narrowing the band gap very much, resulting in an E^{ec} of 2.26 eV. The significant absorption in the UV and blue region yielded a bright, fluorescent yellow color which was very aesthetically pleasing. When

oxidized, this turned into a deep green color. The commonly seen pattern for ECPs is that the absorption maximum red-shifts several hundred nanometers which was also observed, with a new local maximum at 705 nm. In this case, however, a new absorption maximum formed at 473 nm as well. Without this new absorption maximum the polymer would be blue-tinted transmissive, but instead it turned dark green.

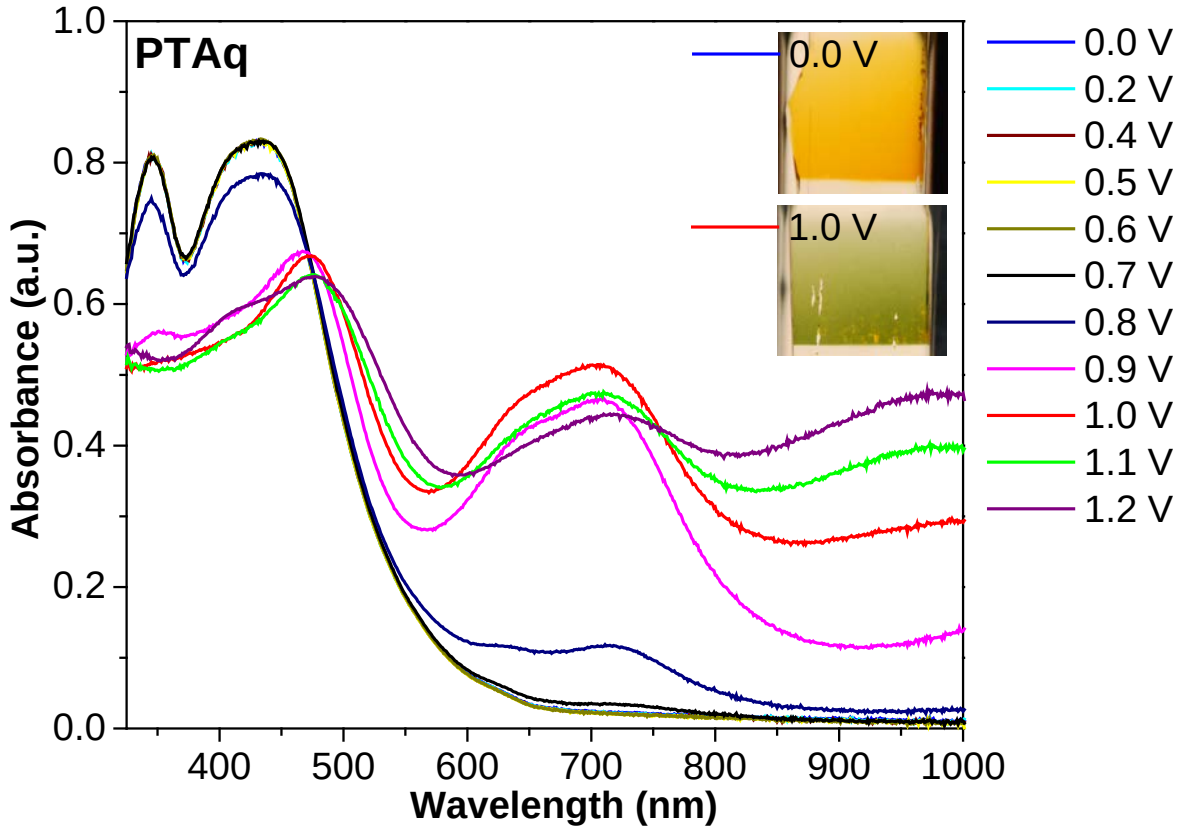

Figure 6.2. UV-Vis absorption spectra at potentials ranging from 0 V to 1.2 V and inset with the visual color change from 0 V to 1 V.

The kinetic properties of the polymers were measured by square wave potentials of 0.6-0.8 V for the IDTT polymers and up to 1.0 V for PTAq. The steps were 10 s, 2.5 s, 1 s and 0.5 s long alternating with 0 V steps of the same length. This measurement is designed to show several factors, such as the stability of the transmission level both in neutral and oxidized states, the speed of transmission, shown by the shape of the steps and also by how much of the $\Delta T\%$ is retained in the faster step cycles. The results for the IDTT polymers are shown in Figure 6.3.

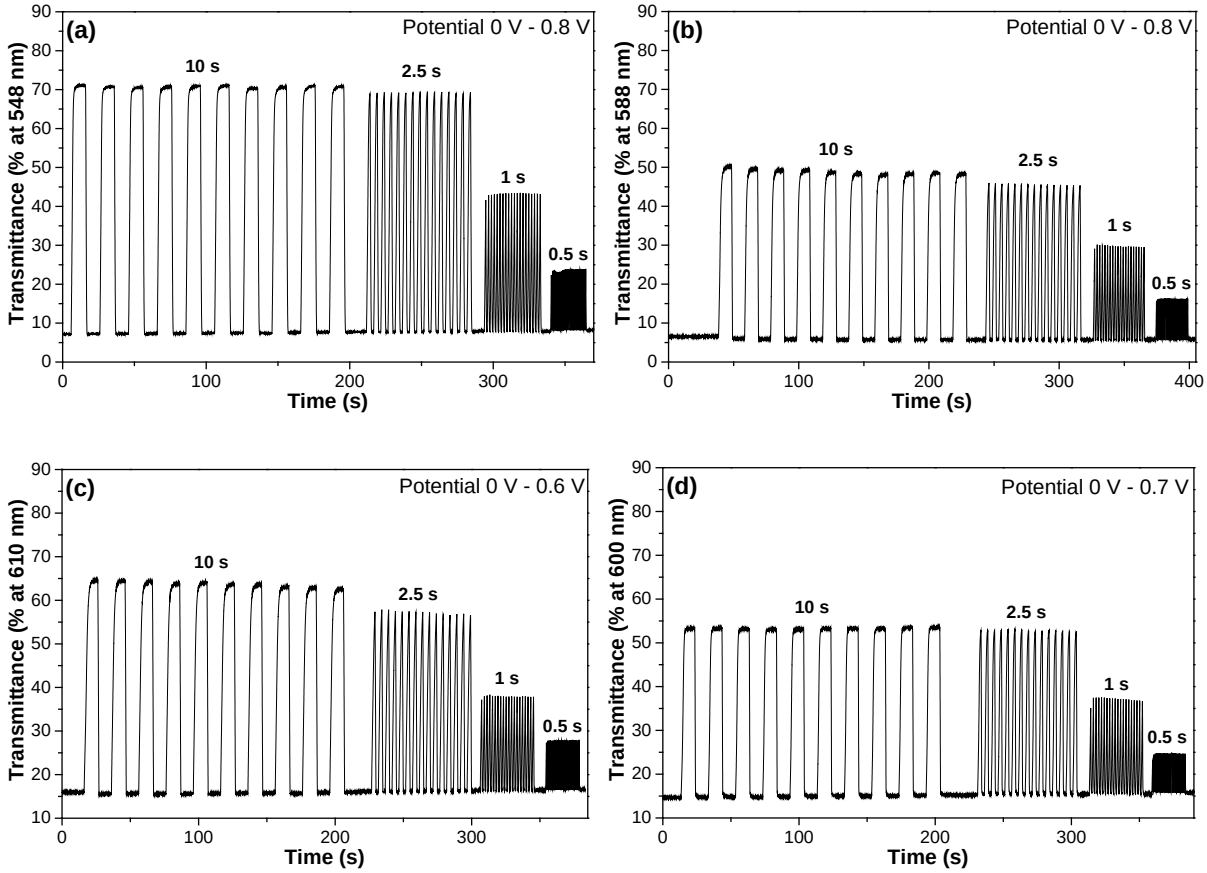

Figure 6.3. Kinetic measurement at maximum transmittance difference in absorption spectra for **a)** PIDTT **b)** PIDTT-TBT **c)** PIDTT-SBS and **d)** PIDTT-SB_RS

Generally, the homopolymer PIDTT performed better in the kinetic measurements, compared to the three IDTT-copolymers. The 10 s cycles showed large electrochromic contrast with fast switching and could reach the characteristic plateau within a few seconds of oxidation, yielding satisfactory 'squareness' without any noticeable loss in contrast over the measurements. The loss in ΔT% in the 2.5 s cycles was minimal, and the one-second cycles kept more than half of the transmittance. PIDTT-SBS was balanced with decent squareness in the 10 s cycles, with ΔT% of roughly 50%. The 2.5 s cycles retained 40%, 1 s cycles 20% and 0.5 s cycles 10%. Far above that of PIDTT. PIDTT-SB_RS had interesting kinetic performance. The initial ΔT% was lower than PIDTT-SBS and PIDTT-TBT, with only about 38%, but the 2.5 s cycles showed no reduction at all. The reduction first came with the 1 s cycles which gave 20% and 0.5 around 10%. For the last polymer, PIDTT-TBT, the initial ΔT% was 45%, going down to 40%, 22% and 10% for the faster cycles. Well worth noting is that all three IDTT-based copolymers PIDTT-SBS, PIDTT-TBT and PIDTT-SB_RS show very stable levels after the measurements with a total of over 60 oxidation cycles.

Since the absorption maximum is generally the point of maximum electrochromic contrast as well, this is generally the wavelength chosen for switching speed measurements. Due to the overlapping high energy absorption before and after oxidation of PTAQ, the new low energy absorption peak that forms upon oxidation was chosen instead. The wavelength of this peak is 705 nm. The switching speed measurements are shown in Figure 6.4. The initial cycle showed a massive ΔT% of 75%, going from very transmissive to almost completely nontransmissive very quickly. Unfortunately, the initial transmittance degraded over every cycle and seemed to stabilize at around 50% after several cycles. Still, this means a ΔT% of around 45% with fast switching speed. A large portion of the contrast can be reached over the 2.5 s cycles, but the 1 s cycles were fast enough to reduce the ΔT% to around 35%. This dropped even further in the fastest cycles down to around 25%. It has to be noted that not all applications require sub-second transitions, but instead a large electrochromic contrast.

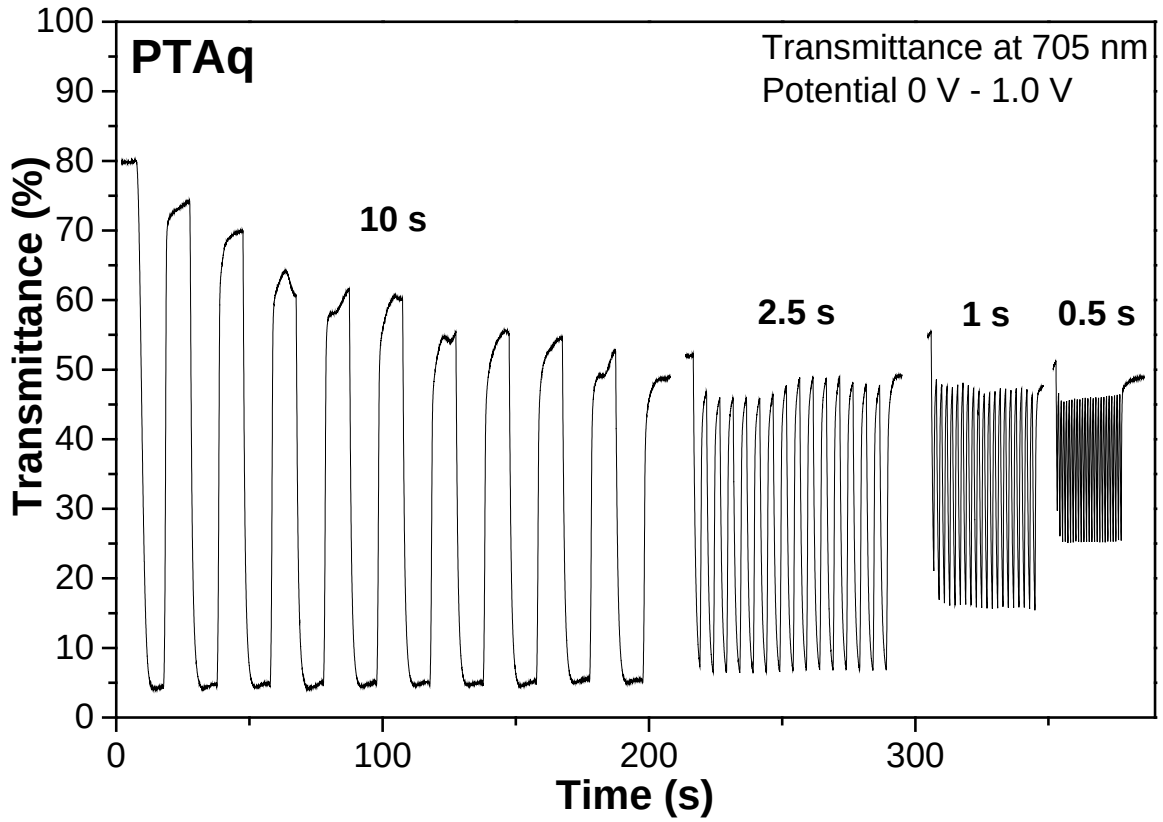

Figure 6.4. Transmittance kinetics at 705 nm with step potentials from 0 V to 1.0 V with step durations of 10 s, 2.5 s, 1 s and 0.5 s.

To summarize, five polymers were synthesized and characterized for their electrochromic properties. The IDTT series contained four polymer with previously unreported structures for OEC applications. The IDTT unit is interesting since it has performed very well in OPVs. This gives rise to the question how many other well-performing OPV, OLED and OFET polymers

could be used in other, neighboring areas like OEC. As for applications, especially PIDTT-SB_RS might be suitable for absorption/transmission applications with an absorption spectra with coalesced absorption maxima covering more or less the whole visible region (400 nm to 700 nm), which is mostly eliminated upon oxidation. On the other hand, PIDTT had exceptionally strong absorption and a very narrow absorption before oxidation which almost completely disappeares. This in combination with impressive kinetic properties and stability make it a suitable red-colored ECP.

While the IDTT polymers showed great promise for use as ECPs, PTAq was far more limited. The polymer showed that the use of the anthraquinone conjugated polymers can give materials with large optical band gap properties and fast switching speeds. Unfortunately, the limited stability makes it unsuitable for any practical use. This leads to the conclusion that further study on this line of material development needs to be considered, with a focus on improving stability, due to the promise it holds.

7. Thermocleavable polymers

In this chapter Paper I will be treated. This paper, titled *Synthesis and Characterization of Isoindigo-Based Polymers with Thermocleavable Side Chains* was published in January 2018 in *Macromolecular Chemistry and Physics*. A common theme Paper I shares with Paper II and Paper III is the focus on side chain alteration of conventional backbone polymers. Many properties can be tuned simply by altering the side chains and in this paper, a series of isoindigo-based polymers with thermocleavable side chains were synthesized and are illustrated in Scheme 7.1.

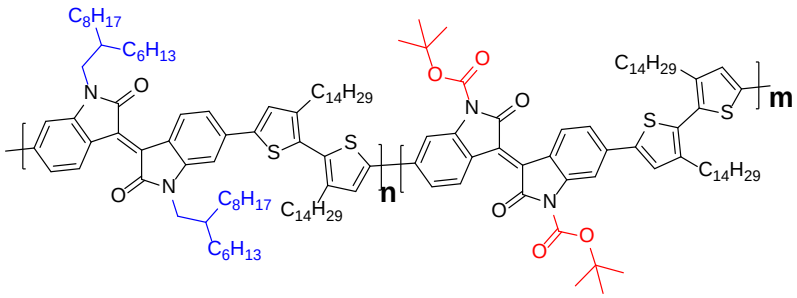

Scheme 7.1. Chemical composition of the five polymers.

They were never applied in either OPVs or OECs, but the design principle has previously been used in OPVs elsewhere and the structures could be relevant for OECs as well. The polymers were characterized in depth to study the effect on thin films before and after cleaving of the side chains and the polymer with pure thermocleavable side chains was shown to effectively improve the thermal stability with regards to crystal growth and face separation when combined with PCBM.

7.1. Background

A critical component in organic semiconductor polymers is the side chains, as has been shown in previous chapters of this thesis. Extensive work on fine-tuning side chains on well performing polymers has been reported.[130-139,184] A general method that has been used is incorporating unstable side chains that can be removed using acid, UV-light or heat.[48,131,185-194]. Tertiary esters such as *tert*-butyloxycarbonyl (*t*-BOC) has been used as such kind of side chains, which are quite unstable in either acidic conditions or when exposed to heat. BOC-protection was developed for synthesis of monosubstituted diimidium salt, as an alteration of the classic benzyloxycarbonyl from early 20:th century.[195-196] It cannot solve the problem it was developed for, but it proved useful in peptide synthesis. The structure can be used to

produce materials with switchable properties, depending on what the functionality outside of the cleavable group is. The simplest case could be the inclusion of a longer alkyl chain, which upon removal renders the polymer less soluble or insoluble. Since it is simple to both add and remove from an amine, it serves the purpose well. The reaction uses di-*tert*-butyl dicarbonate and a catalytic base and adds the *t*-BOC group to two amines per molecule of the dicarbonate.

In this work, we chose to utilize *t*-BOC on isoindigo as the electron poor unit in a DA polymer. Two monomers based on isoindigo were synthesized, one with the thermocleavable *t*-BOC group and one with conventional alkyl side chains. The synthesis of the monomers used for the five polymers in the P2TI-BOC-series presented in this paper was fairly simple. Both of the produced monomers were made in one step from the isoindigo core unit which has been widely used in OPV research for around a decade, since introduced by the Reynolds' group and further popularized by Wang *et al.*[44,197] It is less used in OPV applications recently due to other structures outperforming it, but is still an attractive choice due to the facile synthesis, cheap starting material and abundant available research on it.

7.2. Synthesis and Characterization

The first monomer, **M1**, was made by a simple alkylation reaction with potassium carbonate and 1-bromo-2-hexyldecane. This long and branched side chain gives a high degree of solubility to the otherwise fairly insoluble isoindigo unit. This sidechain has been used with isoindigo in several papers and seems to be a suitable choice.[198] The reaction was performed in anhydrous DMF under inert atmosphere and overnight heating. The isoindigo core unit is weakly soluble in DMF before alkylation and due to the drastically increased solubility of the product, the main byproduct that needs to be removed is mono-alkylated isoindigo if the reaction has not gone to completion. This can easily be achieved over a silica column.

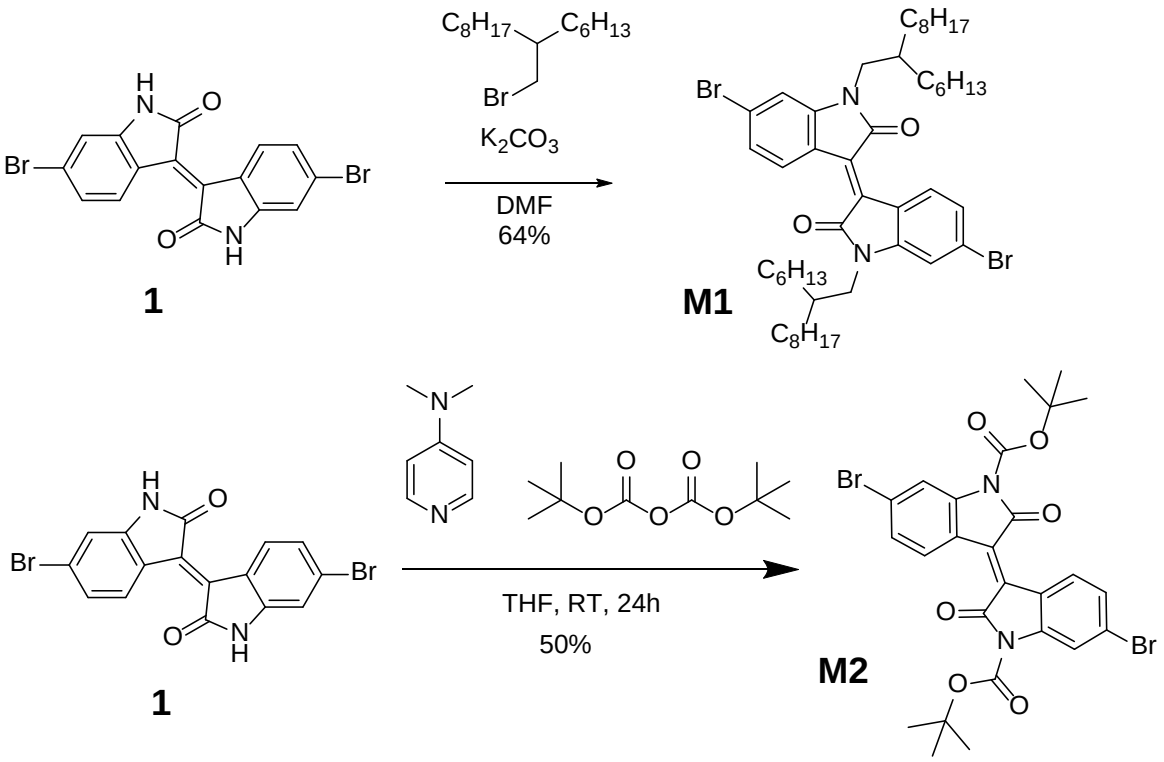

Scheme 7.2. Synthesis of the two isoindigo monomers used, where **M1** is conventional and **M2** bears the thermocleavable BOC-side chains.

The second monomer, **M2**, was made by BOC-protection the amine. The reaction is simple, but care needs to be taken with the reagent di-*tert*-butyl dicarbonate, since it is very toxic by inhalation. The isoindigo core unit **1** was placed in a carefully cleaned and dried flask together with dimethylamino pyridine and di-*tert*-butyl dicarbonate. The solids were put under vacuum for half an hour, after which anhydrous THF was added. No heating was required, but careful heating could probably have increased the low yield, since the reaction can give very high yields. The product was not stable in acid and was accidentally destroyed on weakly acidic silica, and thus had to be purified over neutral alumina instead.

The polymerization reactions used various ratios of **M1** and **M2** together with the commercial monomer **M3**. The reactions are summarized in Scheme 7.3. The reactions performed were Stille polycondensations, which have been described earlier in this thesis. The temperature used for the polymerization was 100 °C, which the monomer had been shown to be stable at.

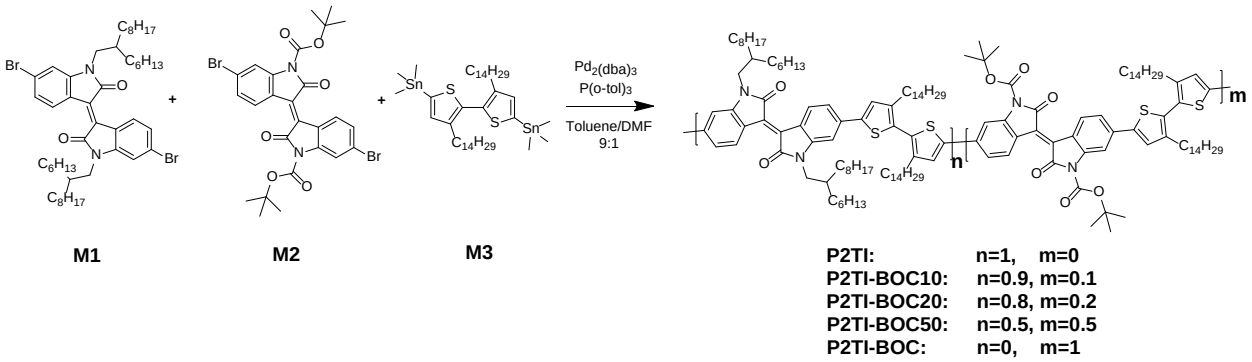

Scheme 7.3. Synthesis of thermocleavable sidechain containing polymers.

The polymers synthesized are named after the components they contain. P2TI is made only from **M1** and **M3** and thus contains no thermocleavable *t*-BOC. P2TI-BOC on the other hand is made purely out of **M2** and **M3** and thus contains only thermocleavable sidechains on the isoindigo moiety. The three intermediate polymers P2TI-BOC10, P2TI-BOC20 and P2TI-BOC50 contain 10%, 20% and 50% of **M1** to **M2**. This means the first and last polymers are alternating copolymers while the other three are random copolymers.

7.3. Results and Discussion

The polymers were characterized by a wide variety of methods, including UV-Vis, temperature dependent UV-Vis, FTIR, CV, TGA and DSC. The effect on film morphology when thermally cleaved was studied in blends with $PC_{71}BM$ and analyzed using solubility testing, TEM and AFM.

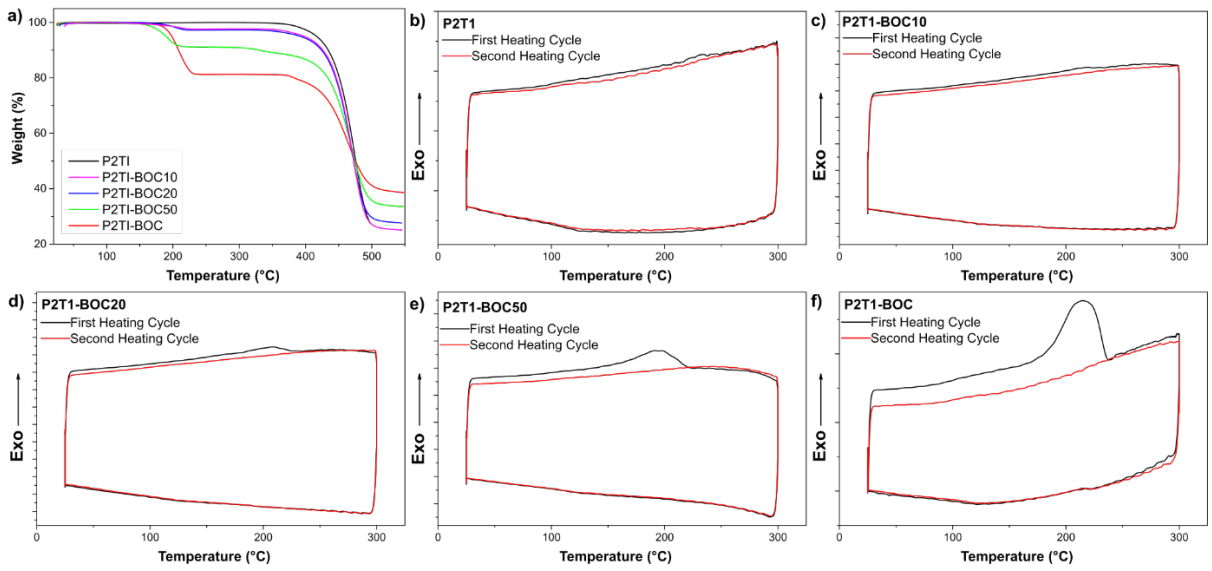

Figure 7.1. a) TGA analysis of the five polymers. **b-f)** DSC measurements of the five polymers.

Since the purpose of the polymers was to investigate the influence of the thermal cleavage of the side chain, both TGA and DSC was used to study the thermal properties of the polymers. The curves from both TGA and DSC is shown in Figure 7.1. The thermal degradation looks like expected, with two step degradations for the four polymers with *t*-BOC. The first degradation seems proportional, with P2TI-BOC50 losing roughly half the weight compared to P2TI-BOC. Both P2TI-BOC10 and P2TI-BOC20 lose just a few percent initially, which is reasonable. As seen in Table 7.1 the calculated theoretical weight loss corresponds quite well to the experimental values. The DSC curves confirm this trend with an increasing peak of heat flow around 200 °C which is not repeated on the second cycle. The molecular weights, also presented in Table 7.1, can tell the careful reader a few things. Since the ratio of monomers needs to be very precise to produce high molecular weight polymers, the random copolymers all have reduced molecular weights compared to the alternating copolymers due to the three monomers weighed up compared to two for the others. It is generous to call P2TI-BOC50 a polymer at all, since the molecular weight is closer to an oligomer. This means the monomers were most likely improperly weighed up, which was later confirmed.

Table 7.1. Molecular weights and thermal degradation of copolymers

	molecular weight			thermal degradation			
polymer	M_n (kDa)	M_w (kDa)	PDI	T_d^{1a} (°C)	T_d^{2a} (°C)	weight loss[b] (%)	weight loss[c] (%)
P2TI	42	108	2.6	-	434	-	-
P2TI-BOC10	30	70	2.3	183	434	1.6	2.4
P2TI-BOC20	22	51	2.3	182	434	3.3	2.8
P2TI-BOC50	6	13	2.0	170	427	8.8	8.8
P2TI-BOC	41	108	2.7	189	422	19.6	18.7

[a]T_d^1 = Temperature of the first decomposition; T_d^2 = Temperature of the second decomposition; [b]Theoretical weight loss of the t-BOC side chain; [c]Experimental weight loss observed

Optical properties of the polymers were studied using common UV-Vis absorption spectroscopy as well as temperature dependent UV-Vis absorption spectroscopy. The results are shown in Figure 7.2.

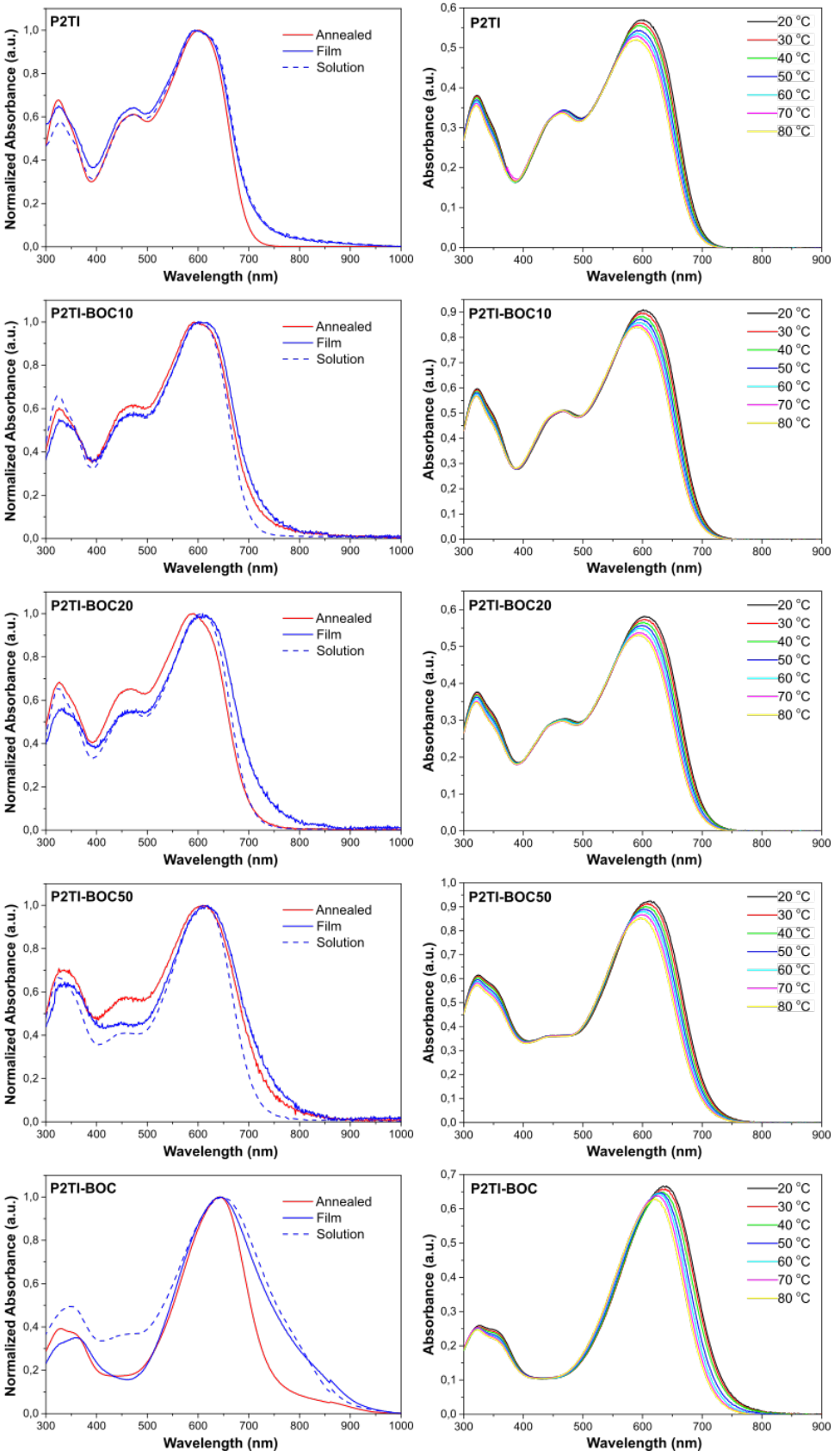

Figure 7.2. left) UV-Vis spectra of the five polymers in solution, film and annealed films. **right)** Temperature Dependent UV-Vis spectra of the polymers in chloroform solution at temperatures between 20 °C and 80 °C.

Due to the similarity of the structures, the absorption spectra of the polymers look generally very similar. Some minor differences such as red shift may be due to the deviation of the molecular weights of the polymers. A larger molecular weight leads to longer conjugation lengths, smaller band gap and thus a wider absorption spectrum. In this case, the electron withdrawing *t*-BOC side chains seem to be more influential, however. The polymer with pure *t*-BOC side chains P2TI-BOC has a far higher absorption maximum of 642 nm in film, compared to the 596 to 610 nm for the other four polymers. This led to P2TI-BOC having the only significant deviation in optical band gap, with around 0.25 eV lower band gap compared to the other polymers. A similar pattern was observed in cyclic voltammetry measurements. The polymers show a common double peak pattern, with a short wavelength peak corresponding to the π-π* transition of the polymer backbone and the longer wavelength peak to the intramolecular interaction between the electron rich bithiophene spacers and the electron deficient isoindigo units.[198]

Furthermore, a shoulder in the absorption can be observed in between the two maxima. The intensity of this shoulder decreases with increasing BOC-content before thermal treatment but increases after thermal treatment. This suggests the removal of the bulky *t*-BOC group enables increased aggregation and thus intermolecular interaction between the polymer chains. The temperature dependent UV-Vis absorption was performed to study the effect of aggregation on the absorption in solution. The measurements were performed from 20 °C to 80 °C. All the polymers exhibited slight blue shifts of around 5-10 nm over the temperature span, suggesting significant aggregation is present in solutions of the polymers at room temperature.[199]

The electrochemical properties, measured by CV, was mostly similar between the five polymers. The voltammograms are presented in Figure 7.3. The largest deviation, as with the optical properties, was exhibited by P2TI-BOC. The reduction peak of this polymer was significantly earlier than the other polymers, indicating a deeper LUMO level and thus a narrower band gap.

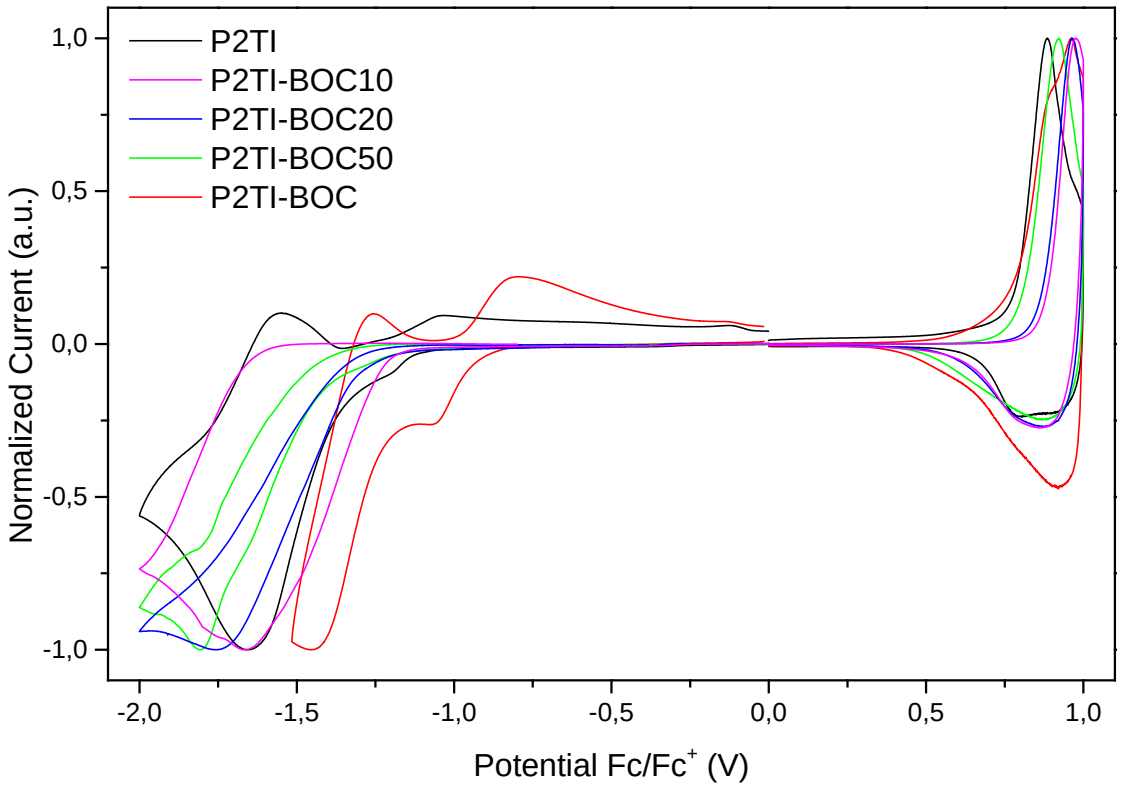

Figure 7.3. Cyclic voltammograms for the five polymers showing oxidation and reduction peaks for the two polymers.

The purpose of this study was to see how the thermal cleavage would affect the film morphology in blends with PCBM. To study this, both TEM and AFM were applied to films with 1:1 mass ratio between the polymers and $PC_{61}BM$. The sample preparations for the two methods have some differences. For TEM, the films need to be transferred to thin TEM-compatible copper grids. To achieve this, the blends were dissolved in *o*-DCB and spin coated on top of PEDOT:PSS films. After drying, the films could then be cut into suitable squares, dipped into deionized water and fished up with copper grids. These could then be directly inserted into the TEM instrument. Since the AFM measurement is applied only on the surface of the samples, the same films for TEM could be used before the water transfer. Figure 7.4 shows representative images obtained from TEM (upper, in gray) and AFM (lower, black and gold) measurements for the films from the five polymer blends before and after thermal annealing. The films were thermally annealed for 10 minutes at 200 °C under nitrogen, which was enough to completely cleave the *t*-BOC side chains in films. As can be seen for P2TI, which has purely conventional side chains, the aggregates observed before annealing completely disappear out of frame after annealing in the TEM. The PCBM molecules likely created large microscale crystals and what is seen in **f)** is mostly polymer. While the effect is

not as extreme in the AFM, severe coarsening takes place. The same trend can be seen for all three of the intermediate copolymers P2TI-BOC10, P2TI-BOC20 and P2TI-BOC50, but the large aggregates or crystals stay in the frame in the TEM micrographs. In AFM, the annealed films were quite similar to those of P2TI, with similar degrees of roughness on the surfaces. The most interesting thing happens in P2TI-BOC. Here, instead of severe coarsening, the aggregates seem to be stabilized. This could be an effect of the polymer turning insoluble, but hydrogen bonding likely has an important role as well, as shown by the FTIR measurements.

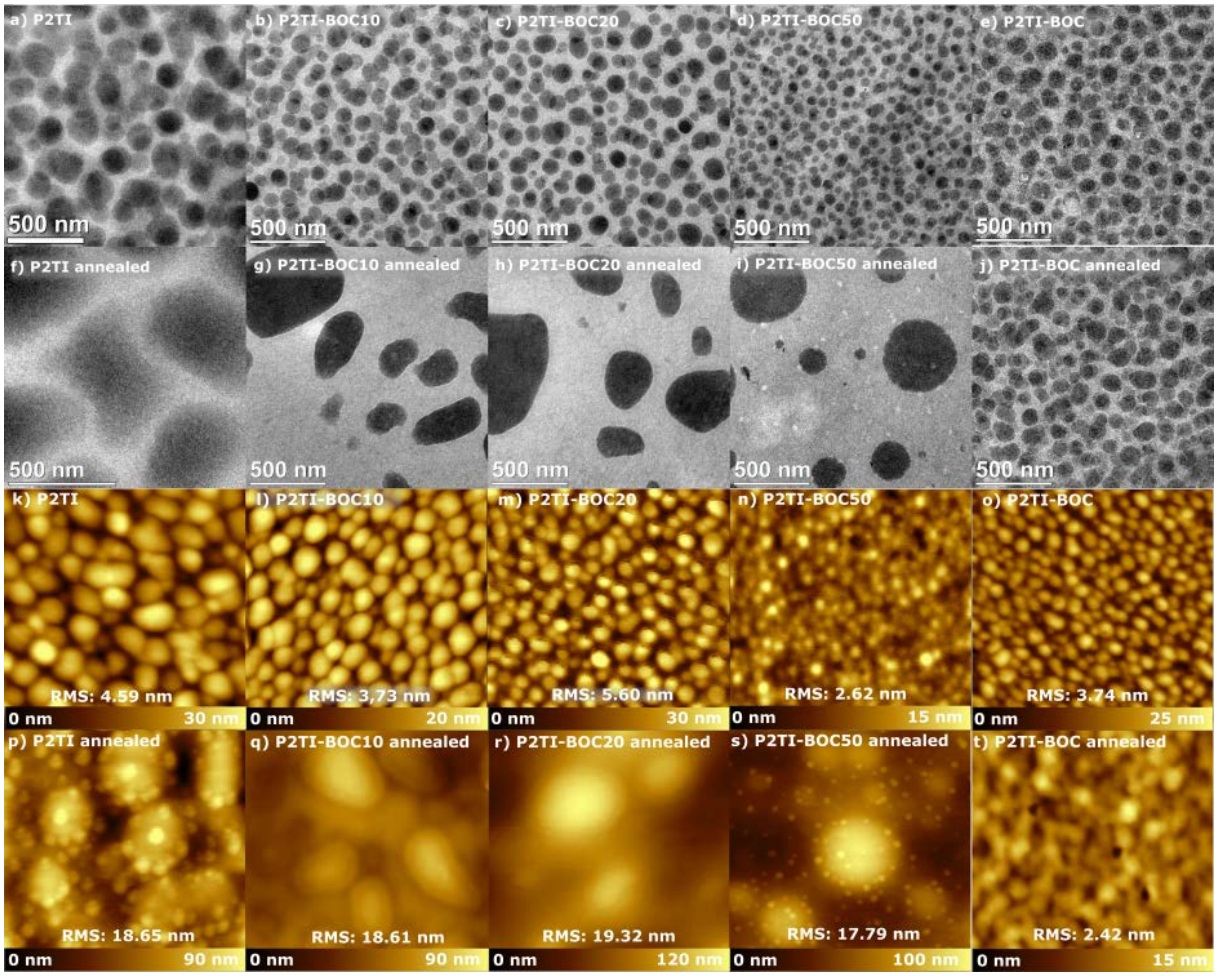

Figure 7.4. a-j) TEM bright-field micrographs of the five polymers. **a-e)** Films without thermal annealing and **f-j)** with 200 °C annealing for 10 min. **k-t)** Tapping mode AFM of 2x2 µm for the five polymer blends. k-o) show the polymer blends before annealing and **p-t)** after annealing at 200 °C for 10 min.

The results presented in this study suggests that BOC-protection can be used as a form of *in situ* crosslinking via hydrogen bonding, which should stabilize the films significantly at the very least from thermal changes over time. This result is encouraging, since PCBM aggregation and crystallization is a significant contributor to device degradation. The results for the random copolymers suggest that a large content of BOC-protection needs to be present to efficiently

stabilize the films. This study provided a useful strategy to develop polymers for morphologically stable films with the potential application in solar cells.

8. Conclusion and Outlook

In this thesis, the work from five articles and manuscripts have been presented with a focus on solar cells, electrochromics and design of conjugated polymers with functional side chains. While the applications have varied from photovoltaic charge generation, work function tuning of metal:organic interfaces to passive coloration, the materials have all been fairly similar structurally. Superficially, the chemical structures look different, but are based on the few design rules discussed in the introductory chapters of this thesis. The polymers were also all synthesized with just a couple of polymerization reactions with the same catalysis system. This proves the incredible versatility of organic electronics and promise a bright future of the class of semiconducting materials.

The field of organic photovoltaics has made massive advancements in the last decade, where the record performances have just about doubled. At this rate of improvement, the technology is reaching maturity quickly but there are still challenges to overcome which do not involve the top-line performances, but instead to minimize the environmental impacts of the technology. This is critical if the selling point of a cheap, easily replaced solar cell is supposed to be considered a “green energy source”. To this end, we wanted to make green solvent processable solar cells, where the active layer could be processed with water/alcohol mixtures. The resulting polymers included tertiary amine side chains which enabled solubility in weakly acidic methanol/water mixtures. They were characterized and one was found to produce a stable current with a final PCE of around 1%. The reason why has yet to be discovered, but could be an important piece in the way to produce well performing solar cells.

Due to the relatively immature field of all-PSCs, we wanted to make a series of cathode interfacial layers to study if the old design rules for polymer:fullerene solar cells were still valid for all-PSCs. Using similar synthesis and molecular units from the tertiary amine pendant group polymers, four polymers aimed at the cathode interlayer were produced and tried in all-PSCs. The produced devices showed a striking similarity in performance with the conventional inorganic counterparts they were compared to. The conclusion drawn from this paper was that the same design rules could be used for all-PSCs as well. This is encouraging since organic solar cells have proven quite complex and many factors are codependent on others, so changing one component might sometimes require significant changes in others as well.

With the recent advances in the field of organic photovoltaics in mind, it seems that previous assumptions about the efficiency limits of the systems were incorrect and we might soon pass 18% efficiencies. This level of efficiency is above what is strictly needed for commercial prospects for OPVs, since the selling points of OPVs are mainly other factors than efficiency such as flexibility and cheap large scale production with a low energy payback time. When it comes to mass production of large-area OPVs, there are technical bottlenecks to be overcome. The OPV field need to be able to translate lab-scale, clean room produced, 1×1 mm devices into roll-to-roll printing (or equivalent scale) of large-area solar cells without drastic loss of performance.

In parallel with the field of OPVs, the electrochromic properties of conjugated materials have been studied. Many of the same molecular designs used for OPVs has turned out to produce ECPs with favorable properties as well, with regards to coloration, electrochromic contrast, switching speeds and electrochemical stability. The IDTT polymers presented in this thesis, with the possible exception of PIDTT, could perform reasonably well in OPVs with their broad absorption and stable structure if a suitable acceptor molecule could be matched with them. Their electrochromic properties were very favorable with large electrochromic contrasts, fast switching speeds and high stability. These results were very encouraging, since the stability of the material is a critical property for future commercialization. This leads to the conclusion that the IDTT-block is very suitable for developing ECPs and further studies could attempt to develop new ECPs by combining IDTT with other electron deficient units in order to produce polymers with more defined coloration.

In the case of electrochromic polymers, it seems like the main hurdles in engineering suitable materials covering the whole color spectrum has been solved already. This leaves the field open for further, iterative research improving the materials in other ways needed for commercialization. As mentioned in chapter 5.1, there are already commercial OEC devices, but they are generally for black/gray to transparent applications like windows or eyewear, which is achieved with blends with complementary absorption. Future applications making use of the full spectrum could be exciting vibrantly colored passive coloration displays, using just a fraction of the energy required to drive OLED-screens. Using ECPs as display-materials has been proposed, but not as much used. Conventional non-emissive displays use completely different technologies and are mostly grayscale. With the large recent advances in OECs, non-emissive displays are getting within reach and commercialization is getting closer. Further research into producing vibrantly colored, highly stable devices is needed.

Overall, the flexibility of these organic semiconductors, particularly conjugated polymers, has proven to be immense. In some markets they might fill niches, they can be a cheap, flexible and light-weight alternative but will not likely have the high-end performance compared to other established technologies. In other markets they have unique, so far unmatched properties, such as switchable IR-reflector panels. There will likely be more applications for conjugated polymers in the future, since the molecular design rules developed are somewhat transferrable between different purposes. They might serve as polymer electrolytes in liquid flow batteries. They might serve as biocompatible sensors implanted in the skin. The possibilities are endless!

Acknowledgements

First and foremost I would like to acknowledge the Swedish Research Council (VR) for funding my research project. Without the public funding organizations much of the basic research taking place would never be possible and we should be glad they exist!

I am grateful to Ergang and Mats for giving me the opportunity to do my PhD studies! This has been five of the most developing, challenging, interesting, terrifying and enjoyable years of my life. The opportunity to come as a newbie to a field, spend time as a student and researcher and become an expert is quite unique and everyone who gets the chance should take it!

Prof. Xiaofeng Xu, who was with us from the start and was very important to teach me the necessary skills in the lab, as well as in the office, to complete my PhD studies. Though he left Sweden for China, I will always consider him a good friend. Petri Murto & Zhaojun Li, we started this thing together and while Zhaojun finished it slightly earlier, Petri and I will soon follow. I will always cherish the memories of our times together in the lab, at conferences and especially group meetings! Thank you Petri for all your help with my thesis! It is a far better document with all your helpful ideas and detailed corrections.

What makes or breaks a workplace is almost always the colleagues and in my case I am very happy. Without my great colleagues and friends in our group, I don't know if I would have made it through, so I would also like to thank Mariza Mone, Cedrik Wiberg, Lidia Marin, David James, Josué Ayuso and all the many guest researchers and visiting PhDs who came and went.

I would also like to acknowledge my collaborators Desta Gedefaw, Anirudh Sharma, Sait Elmas, Jonas Bjuggren, Caroline Pan, and Olof Bäcke without whom much of my work would still be unpublished. Collaboration is a corner stone in scientific work and it deeply enriches and enhances the work experience! Anders Mårtensson for endless amounts of GPC-characterization. A special thank you to my roommate Renee Kroon! In my licentiate thesis I thanked him for allowing me to turn the office into a greenhouse. It later turned into a jungle. For a year we lived with banana trees and other exotic plants. A huge thank you for the help and scientific discussions. They really helped when I needed them!

Without my parents, Dag & Görel, and all their help taking care of my daughter, I am not sure there would have been a thesis finished by now. I will always be grateful for all they have done for me! My daughter Vera deserves a special note for being such a good sleeper, which is a very useful trait when writing a thesis! Maria, my lovely wife, has been very patient with me

when we mainly met in the hallway, since I had to leave for the office as soon as she came home. I could not have done this without you. I love you with all my heart! A special thank you my good friend Patrik, who inspired me to get a child to delay my defense. Great idea!

Bibliography

[1] A. J. Heeger, A. G. MacDiarmid and H. Shirakawa, *The Nobel Prize in chemistry, 2000: conductive polymers.*, Royal Swedish Academy of Sciences, Stockholm, Sweden, **2000**

[2] H. Shirakawa, E. J. Louis, A. G. Macdiarmid, C. K. Chiang and A. J. Heeger, *J.C.S. Chem. Comm.* **1977**, 578-580.

[3] C. K. Chiang, M. A. Druy, S. C. Gau, A. J. Heeger, E. J. Louis, A. G. MacDiarmid, Y. W. Park and H. Shirakawa, *J. Am. Chem. Soc.* **1978**, *100*, 1013-1015.

[4] F. Wudl, M. Kobayashi and A. J. Heeger, *J. Org. Chem.* **1984**, *49*, 3382-3384.

[5] J. Brédas, A. Heeger and F. Wudl, *J. Chem. Phys.* **1986**, *85*, 4673-4678.

[6] J. Kuerti, P. R. Surjan and M. Kertesz, *J. Am. Chem. Soc.* **1991**, *113*, 9865-9867.

[7] Z.-H. Zhou, T. Maruyama, T. Kanbara, T. Ikeda, K. Ichimura, T. Yamamoto and K. Tokuda, *J.C.S. Chem. Comm.* **1991**, 1210-1212.

[8] E. Havinga, W. Ten Hoeve and H. Wynberg, *Synth. Met.* **1993**, *55*, 299-306.

[9] E. Havinga, W. Ten Hoeve and H. Wynberg, *Polym. Bull.* **1992**, *29*, 119-126.

[10] C. Kitamura, S. Tanaka and Y. Yamashita, *Chem. Mater.* **1996**, *8*, 570-578.

[11] T. Yamamoto, Z.-h. Zhou, T. Kanbara, M. Shimura, K. Kizu, T. Maruyama, Y. Nakamura, T. Fukuda, B.-L. Lee and N. Ooba, *J. Am. Chem. Soc.* **1996**, *118*, 10389-10399.

[12] C. W. Tang, *Appl. Phys. Lett.* **1986**, *48*, 183-185.

[13] N. S. Sariciftci, L. Smilowitz, A. J. Heeger and F. Wudl, *Science* **1992**, *258*, 1474-1476.

[14] J. C. Hummelen, B. W. Knight, F. LePeq, F. Wudl, J. Yao and C. L. Wilkins, *J. Org. Chem.* **1995**, *60*, 532-538.

[15] G. Yu, J. Gao, J. C. Hummelen, F. Wudl and A. J. Heeger, *Science* **1995**, *270*, 1789-1791.

[16] G. Li, V. Shrotriya, J. Huang, Y. Yao, T. Moriarty, K. Emery and Y. Yang, *Nat. Mater.* **2005**, *4*, 864.

[17] W. Ma, C. Yang, X. Gong, K. Lee and A. J. Heeger, *Adv. Funct. Mater.* **2005**, *15*, 1617-1622.

[18] W. Zhao, S. Li, H. Yao, S. Zhang, Y. Zhang, B. Yang and J. Hou, *J. Am. Chem. Soc.* **2017**, *139*, 7148-7151.

[19] S. Li, L. Ye, W. Zhao, H. Yan, B. Yang, D. Liu, W. Li, H. Ade and J. Hou, *J. Am. Chem. Soc.* **2018**, *140*, 7159-7167.

[20] P. Cheng, G. Li, X. Zhan and Y. Yang, *Nat. Photon.* **2018**, *12*, 131-142.

[21] Q. Burlingame, C. Coburn, X. Che, A. Panda, Y. Qu and S. R. Forrest, *Nature* **2018**, *554*, 77-80.

[22] R. Xue, J. Zhang, Y. Li and Y. Li, *Small* **2018**, e1801793.

[23] S. B. Darling and F. Q. You, *RSC Adv.* **2013**, *3*, 17633-17648.

[24] S. Lizin, S. Van Passel, E. De Schepper, W. Maes, L. Lutsen, J. Manca and D. Vanderzande, *Energy Environ. Sci.* **2013**, *6*, 3136.

[25] M. C. Scharber and N. S. Sariciftci, *Prog. Polym. Sci.* **2013**, *38*, 1929-1940.

[26] M. Pope, H. Kallmann and P. Magnante, *J. Chem. Phys.* **1963**, *38*, 2042-2043.

[27] W. Helfrich and W. Schneider, *Phys. Rev. Lett.* **1965**, *14*, 229.

[28] R. H. Friend, R. W. Gymer, A. B. Holmes, J. H. Burroughes, R. N. Marks, C. Taliani, D. D. C. Bradley, D. A. D. Santos, J. L. Brédas, M. Lögdlund and W. R. Salaneck, *Nature* **1999**, *397*, 121.

[29] C. W. Tang and S. A. VanSlyke, *Appl. Phys. Lett.* **1987**, *51*, 913-915.

[30] C. Adachi, T. Tsutsui and S. Saito, *Appl. Phys. Lett.* **1989**, *55*, 1489-1491.

[31] J. Burroughes, D. Bradley, A. Brown, R. Marks, K. Mackay, R. Friend, P. Burns and A. Holmes, *Nature* **1990**, *347*, 539.

[32] F. Garnier, R. Hajlaoui, A. Yassar and P. Srivastava, *Science* **1994**, *265*, 1684-1686.

[33] Y. Yang and A. Heeger, *Nature* **1994**, *372*, 344.

[34] A. Brown, A. Pomp, C. Hart and D. De Leeuw, *Science* **1995**, *270*, 972-974.

[35] H. Sirringhaus, N. Tessler and R. H. Friend, *Science* **1998**, *280*, 1741-1744.

[36] M. Granström, K. Petritsch, A. Arias, A. Lux, M. Andersson and R. Friend, *Nature* **1998**, *395*, 257.

[37] J.-L. Bredas, *Mater. Horizons* **2014**, *1*, 17-19.

[38] Y.-J. Cheng, S.-H. Yang and C.-S. Hsu, *Chem. Rev.* **2009**, *109*, 5868-5923.

[39] J.-L. Brédas, *J. Chem. Phys.* **1985**, *82*, 3808-3811.

[40] G. L. Gibson, T. M. McCormick and D. S. Seferos, *J. Am. Chem. Soc.* **2011**, *134*, 539-547.

[41] D. Mühlbacher, M. Scharber, M. Morana, Z. Zhu, D. Waller, R. Gaudiana and C. Brabec, *Adv. Mater.* **2006**, *18*, 2884-2889.

[42] J. C. Bijleveld, A. P. Zoombelt, S. G. Mathijssen, M. M. Wienk, M. Turbiez, D. M. de Leeuw and R. A. Janssen, *J. Am. Chem. Soc.* **2009**, *131*, 16616-16617.

[43] R. Stalder, J. Mei, J. Subbiah, C. Grand, L. A. Estrada, F. So and J. R. Reynolds, *Macromolecules* **2011**, *44*, 6303-6310.

[44] E. Wang, Z. Ma, Z. Zhang, K. Vandewal, P. Henriksson, O. Inganas, F. Zhang and M. R. Andersson, *J. Am. Chem. Soc.* **2011**, *133*, 14244-14247.

[45] K. Kawashima, T. Fukuhara, Y. Suda, Y. Suzuki, T. Koganezawa, H. Yoshida, H. Ohkita, I. Osaka and K. Takimiya, *J. Am. Chem. Soc.* **2016**, *138*, 10265-10275.

[46] J. Mei and Z. Bao, *Chem. Mater.* **2014**, *26*, 604-615.

[47] W. Lee, J. H. Seo and H. Y. Woo, *Polymer* **2013**, *54*, 5104-5121.

[48] M. Bjerring, J. S. Nielsen, N. C. Nielsen and F. C. Krebs, *Macromolecules* **2007**, *40*, 6012-6013.

[49] G. Wantz, L. Derue, O. Dautel, A. Rivaton, P. Hudhomme and C. Dagron-Lartigau, *Polym. Int.* **2014**, *63*, 1346-1361.

[50] H. Meier, U. Stalmach and H. Kolshorn, *Acta Polymer.* **1997**, *48*, 379-384.

[51] H. A. M. Van Mullekom, J. A. J. M. Vekemans, E. E. Havinga and E. W. Meijer, *Mater. Sci. Eng.* **2001**, *32*, 1-40.

[52] T. Yamamoto, A. Morita, Y. Miyazaki, T. Maruyama, H. Wakayama, Z. H. Zhou, Y. Nakamura, T. Kanbara, S. Sasaki and K. Kubota, *Macromolecules* **1992**, *25*, 1214-1223.

[53] S. Ludwigs, *P3HT Revisited-From Molecular Scale to Solar Cell Devices*, Springer, Berlin, **2014**.

[54] R. D. McCullough, *Adv. Mater.* **1998**, *10*, 93-116.

[55] J. Liu and R. D. McCullough, *Macromolecules* **2002**, *35*, 9882-9889.

[56] M. Jeffries-El, G. Sauvé and R. D. McCullough, *Adv. Mater.* **2004**, *16*, 1017-1019.

[57] Y.-J. Cheng and T.-Y. Luh, *J. Organomet. Chem.* **2004**, *689*, 4137-4148.

[58] K. H. Hendriks, W. Li, G. H. L. Heintges, G. W. P. van Pruissen, M. M. Wienk and R. A. J. Janssen, *J. Am. Chem. Soc.* **2014**, *136*, 11128-11133.

[59] F. Lombeck, H. Komber, D. Fazzi, D. Nava, J. Kuhlmann, D. Stegerer, K. Strassel, J. Brandt, A. D. de Zerio Mendaza, C. Müller, W. Thiel, M. Caironi, R. Friend and M. Sommer, *Adv. Energy Mater.* **2016**, *6*, 1601232.

[60] G. Pirotte, J. Kesters, T. Cardeynaels, P. Verstappen, J. D'Haen, L. Lutsen, B. Champagne, D. Vanderzande and W. Maes, *Macromol. Rapid Commun.* **2018**, *39*, 1800086.

[61] J. K. Stille, *Angew. Chem. Int. Ed. Engl.* **1986**, *25*, 508-524.

[62] Z. Bao, W. K. Chan and L. Yu, *J. Am. Chem. Soc.* **1995**, *117*, 12426-12435.

[63] I. J. Boyer, *Toxicology* **1989**, *55*, 253-298.

[64] N. Miyaura and A. Suzuki, *Chem. Rev.* **1995**, *95*, 2457-2483.

[65] L. Ackermann, *Chem. Rev.* **2011**, *111*, 1315-1345.

[66] M. Lafrance and K. Fagnou, *J. Am. Chem. Soc.* **2006**, *128*, 16496-16497.

[67] U. Koldemir, S. R. Puniredd, M. Wagner, S. Tongay, T. D. McCarley, G. D. Kamenov, K. Müllen, W. Pisula and J. R. Reynolds, *Macromolecules* **2015**, *48*, 6369-6377.

[68] W. H. Carothers, *Chem. Rev.* **1931**, *8*, 353-426.

[69] P. J. Flory, *Chem. Rev.* **1946**, *39*, 137-197.

[70] J. M. G. Cowie and V. Arrighi, *Polymers: Chemistry and Physics of Modern Materials*, CRC Press, **2007**.

[71] L. Lu, T. Zheng, T. Xu, D. Zhao and L. Yu, *Chem. Mater.* **2015**, *27*, 537-543.

[72] C. M. Cardona, W. Li, A. E. Kaifer, D. Stockdale and G. C. Bazan, *Adv. Mater.* **2011**, *23*, 2367-2371.

[73] A. J. Bard and L. R. Faulkner, *Electrochemical Methods: Fundamentals and Applications*, Wiley, **2000**.

[74] V. V. Pavlishchuk and A. W. Addison, *Inorganica Chim. Acta* **2000**, *298*, 97-102.

[75] R. Lomoth and S. Ott, *Dalton Trans.* **2009**, 9952-9959.

[76] F. Z. S. Hellström, O. Inganäs, M. R. Andersson, *Dalton Trans.* **2009**, *45*, 10032-10039.

[77] Z. Grubisic, P. Rempp and H. Benoit, *Journal of Polymer Science Part B: Polymer Letters* **1967**, *5*, 753-759.

[78] I. E. Agency, *World Energy Outlook Special Report*, **2015**

[79] IPCC, *Special Report on Global Warming of 1.5ºC*, Intergovernmental Panel on Climate Change (IPCC), Incheon, Republic of Korea, **2018**

[80] M. Tripathy, P. K. Sadhu and S. K. Panda, *Renew. Sust. Energy. Rev.* **2016**, *61*, 451-465.

[81] B. Kippelen and J.-L. Brédas, *Energy Environ. Sci.* **2009**, *2*, 251.

[82] N.-G. Park, *Mater. Today* **2015**, *18*, 65-72.

[83] A. Hagfeldt and M. Grätzel, *Acc. Chem. Res.* **2000**, *33*, 269-277.

[84] M. Yuan, M. Liu and E. H. Sargent, *Nat. Energy* **2016**, *1*, 16016.

[85] NREL, *Best Research-Cell Efficiencies*, Golden, Colorado, USA, **2018**

[86] R. Steim, T. Ameri, P. Schilinsky, C. Waldauf, G. Dennler, M. Scharber and C. J. Brabec, *Sol. Energy Mater. Sol. Cells* **2011**, *95*, 3256-3261.

[87] W. Shockley and H. J. Queisser, *J. Appl. Phys.* **1961**, *32*, 510-519.

[88] M. A. Green and S. P. Bremner, *Nat. Mater.* **2016**, *16*, 23.

[89] G. Li, W.-H. Chang and Y. Yang, *Nat. Rev. Mater.* **2017**, *2*, 17043.

[90] D. N. Congreve, J. Lee, N. J. Thompson, E. Hontz, S. R. Yost, P. D. Reusswig, M. E. Bahlke, S. Reineke, T. Van Voorhis and M. A. Baldo, *Science* **2013**, *340*, 334-337.

[91] P. W. Blom, V. D. Mihailetchi, L. J. A. Koster and D. E. Markov, *Adv. Mater.* **2007**, *19*, 1551-1566.

[92] J. Liu, S. Chen, D. Qian, B. Gautam, G. Yang, J. Zhao, J. Bergqvist, F. Zhang, W. Ma, H. Ade, O. Inganäs, K. Gundogdu, F. Gao and H. Yan, *Nat. Energy* **2016**, *1*, 16089.

[93] C. Wang, X. Xu, W. Zhang, J. Bergqvist, Y. Xia, X. Meng, K. Bini, W. Ma, A. Yartsev, K. Vandewal, M. R. Andersson, O. Inganäs, M. Fahlman and E. Wang, *Adv. Energy Mater.* **2016**, *6*, 1600148.

[94] S. M. Menke, N. A. Ran, G. C. Bazan and R. H. Friend, *Joule* **2018**, *2*, 25-35.

[95] C. M. Proctor, M. Kuik and T.-Q. Nguyen, *Prog. Polym. Sci.* **2013**, *38*, 1941-1960.

[96] T. M. Clarke and J. R. Durrant, *Chem. Rev.* **2010**, *110*, 6736-6767.

[97] H.-L. Yip and A. K. Y. Jen, *Energy Environ. Sci.* **2012**, *5*, 5994.

[98] B. Qi and J. Wang, *Phys. Chem. Chem. Phys.* **2013**, *15*, 8972-8982.

[99] S. Braun, W. R. Salaneck and M. Fahlman, *Adv. Mater.* **2009**, *21*, 1450-1472.

[100] T.-H. Lai, S.-W. Tsang, J. R. Manders, S. Chen and F. So, *Mater. Today* **2013**, *16*, 424-432.

[101] Z. H. Hu, Z. M. Zhong, Y. W. Chen, C. Sun, F. Huang, J. B. Peng, J. Wang and Y. Cao, *Adv. Funct. Mater.* **2016**, *26*, 129-136.

[102] Z. Hu, K. Zhang, F. Huang and Y. Cao, *Chem Commun (Camb)* **2015**, *51*, 5572-5585.

[103] Z. Yin, J. Wei and Q. Zheng, *Adv. Sci.* **2016**, *3*, 1500362.

[104] X. Xu, W. Cai, J. Chen and Y. Cao, *J. Polym. Sci. A Polym. Chem.* **2011**, *49*, 1263-1272.

[105] X. Xu, B. Han, J. Chen, J. Peng, H. Wu and Y. Cao, *Macromolecules* **2011**, *44*, 4204-4212.

[106] X. Xu, Y. Zhu, L. Zhang, J. Sun, J. Huang, J. Chen and Y. Cao, *J. Mater. Chem.* **2012**, *22*, 4329-4336.

[107] Z. George, E. Voroshazi, C. Lindqvist, R. Kroon, W. L. Zhuang, E. G. Wang, P. Henriksson, A. Hadipour and M. R. Andersson, *Sol. Energy Mater. Sol. Cells* **2015**, *133*, 99-104.

[108] Y. Zhou, C. Fuentes-Hernandez, J. Shim, J. Meyer, A. J. Giordano, H. Li, P. Winget, T. Papadopoulos, H. Cheun, J. Kim, M. Fenoll, A. Dindar, W. Haske, E. Najafabadi, T. M. Khan, H. Sojoudi, S. Barlow, S. Graham, J.-L. Brédas, S. R. Marder, A. Kahn and B. Kippelen, *Science* **2012**, *336*, 327-332.

[109] F. Huang, H. Wu, D. Wang, W. Yang and Y. Cao, *Chem. Mater.* **2004**, *16*, 708-716.

[110] M. Jorgensen, K. Norrman, S. A. Gevorgyan, T. Tromholt, B. Andreasen and F. C. Krebs, *Adv. Mater.* **2012**, *24*, 580-612.

[111] K. Wang, C. Liu, T. Meng, C. Yi and X. Gong, *Chem. Soc. Rev.* **2016**, *45*, 2937-2975.

[112] Z. C. He, C. M. Zhong, S. J. Su, M. Xu, H. B. Wu and Y. Cao, *Nat. Photon.* **2012**, *6*, 591-595.

[113] Xiaoniu Yang, Jeroen K. J. van Duren, René A. J. Janssen, Matthias A. J. Michels and J. Loos, *Macromolecules* **2004**, *37*, 2151-2158.

[114] J. Halls, C. Walsh, N. C. Greenham, E. Marseglia, R. H. Friend, S. Moratti and A. Holmes, *Nature* **1995**, *376*, 498.

[115] S. C. Moratti, D. D. Bradley, R. Cervini, R. H. Friend, N. C. Greenham and A. B. Holmes, *Adv. Photon. Mater. Inf. Tech.* **1994**, pp. 108-115.

[116] G. Yu and A. J. Heeger, *J. Appl. Phys.* **1995**, *78*, 4510-4515.

[117] T. Kim, J. H. Kim, T. E. Kang, C. Lee, H. Kang, M. Shin, C. Wang, B. Ma, U. Jeong, T. S. Kim and B. J. Kim, *Nat. Commun.* **2015**, *6*, 8547.

[118] K. Bini, X. Xu, M. R. Andersson and E. Wang, *ACS Appl. Energy Mater.* **2018**, *1*, 2176-2182.

[119] A. Facchetti, *Mater. Today* **2013**, *16*, 123-132.

[120] C. Z. Li, C. C. Chueh, F. Ding, H. L. Yip, P. W. Liang, X. Li and A. K. Jen, *Adv. Mater.* **2013**, *25*, 4425-4430.

[121] C. Sun, Z. Wu, Z. Hu, J. Xiao, W. Zhao, H.-W. Li, Q.-Y. Li, S.-W. Tsang, Y.-X. Xu, K. Zhang, H.-L. Yip, J. Hou, F. Huang and Y. Cao, *Energy Environ. Sci.* **2017**, *10*, 1784-1791.

[122] L. Ye, X. Jiao, M. Zhou, S. Zhang, H. Yao, W. Zhao, A. Xia, H. Ade and J. Hou, *Adv. Mater.* **2015**, *27*, 6046-6054.

[123] L. Ye, X. Jiao, W. Zhao, S. Zhang, H. Yao, S. Li, H. Ade and J. Hou, *Chem. Mater.* **2016**, *28*, 6178-6185.

[124] H. Bin, Z. G. Zhang, L. Gao, S. Chen, L. Zhong, L. Xue, C. Yang and Y. Li, *J. Am. Chem. Soc.* **2016**, *138*, 4657-4664.

[125] W. Zhao, D. Qian, S. Zhang, S. Li, O. Inganas, F. Gao and J. Hou, *Adv. Mater.* **2016**, *28*, 4734-4739.

[126] Z. Li, W. Zhang, X. Xu, Z. Genene, D. Di Carlo Rasi, W. Mammo, A. Yartsev, M. R. Andersson, R. A. J. Janssen and E. Wang, *Adv. Energy Mater.* **2017**, *7*, 1602722.

[127] F. Huang, Y. H. Niu, Y. Zhang, J. W. Ka, M. S. Liu and A. K. Y. Jen, *Adv. Mater.* **2007**, *19*, 2010-+.

[128] Z. a. Li, X. Lou, H. Yu, Z. Li and J. Qin, *Macromolecules* **2008**, *41*, 7433-7439.

[129] M. R. P. Jeremiah K. Mwaura, David Witker, Nisha Ananthakrishnan, and a. J. R. R. Kirk S. Schanze, *Langmuir* **2005**, 10119-10126.

[130] J. Yang, A. Garcia and T.-Q. Nguyen, *Appl. Phys. Lett.* **2007**, *90*, 103514.

[131] R. Søndergaard, M. Helgesen, M. Jørgensen and F. C. Krebs, *Adv. Energy Mater.* **2011**, *1*, 68-71.

[132] W. Yu, H. Zhang, Z. Fan, J. Zhang, H. Wei, D. Zhou, B. Xu, F. Li, W. Tian and B. Yang, *Energy Environ. Sci.* **2011**, *4*, 2831.

[133] Q. F. Dong, W. L. Yu, Z. F. Li, S. Y. Yao, X. Y. Zhang, B. Yang, C. Im and W. J. Tian, *Sol. Energy Mater. Sol. Cells* **2012**, *104*, 75-80.

[134] T. T. Larsen-Olsen, T. R. Andersen, B. Andreasen, A. P. L. Böttiger, E. Bundgaard, K. Norrman, J. W. Andreasen, M. Jørgensen and F. C. Krebs, *Sol. Energy Mater. Sol. Cells* **2012**, *97*, 43-49.

[135] Z. Liu, L. Liu, H. Li, Q. Dong, S. Yao, A. B. Kidd Iv, X. Zhang, J. Li and W. Tian, *Sol. Energy Mater. Sol. Cells* **2012**, *97*, 28-33.

[136] C. C. Chueh, K. Yao, H. L. Yip, C. Y. Chang, Y. X. Xu, K. S. Chen, C. Z. Li, P. Liu, F. Huang, Y. W. Chen, W. C. Chenb and A. K. Y. Jen, *Energy Environ. Sci.* **2013**, *6*, 3241-3248.

[137] B. Meng, H. Song, X. Chen, Z. Xie, J. Liu and L. Wang, *Macromolecules* **2015**, *48*, 4357-4363.

[138] S. Subianto, N. Dutta, M. Andersson and N. R. Choudhury, *Adv. Colloid. Interface. Sci.* **2016**, *235*, 56-69.

[139] Z. Zhang, X. Zhang, J. Zhang, X. Gong, Y. Liu, H. Lu, C. Li and Z. Bo, *RSC Adv.* **2016**, *6*, 39074-39079.

[140] T. L. Nguyen, C. Lee, H. Kim, Y. Kim, W. Lee, J. H. Oh, B. J. Kim and H. Y. Woo, *Macromolecules* **2017**, *50*, 4415-4424.

[141] C. H. Duan, W. Z. Cai, B. B. Y. Hsu, C. M. Zhong, K. Zhang, C. C. Liu, Z. C. Hu, F. Huang, G. C. Bazan, A. J. Heeger and Y. Cao, *Energy Environ. Sci.* **2013**, *6*, 3022-3034.

[142] M. Lv, M. Lei, J. Zhu, T. Hirai and X. Chen, *ACS Appl. Mater. Interfaces* **2014**, *6*, 5844-5851.

[143] D. Ma, M. L. Lv, M. Lei, J. Zhu, H. Q. Wang and X. W. Chen, *ACS Nano* **2014**, *8*, 1601-1608.

[144] Z. George, Y. X. Xia, A. Sharma, C. Lindqvist, G. Andersson, O. Inganas, E. Moons, C. Muller and M. R. Andersson, *J. Mater. Chem. A* **2016**, *4*, 2663-2669.

[145] W. Z. Cai, C. M. Zhong, C. H. Duan, Z. C. Hu, S. Dong, D. R. Cao, M. Lei, F. Huang and Y. Cao, *Appl. Phys. Lett.* **2015**, *106*, 233302.

[146] X. Liu, P. Fu, D. Tu, Q. Yang, S. Yu, X. Guo and C. Li, *J. Mater. Chem. A* **2018**.

[147] M. Kertesz, C. H. Choi and S. Yang, *Chem. Rev.* **2005**, *105*, 3448-3481.

[148] J. R. Platt, *J. Chem. Phys.* **1961**, *34*, 862-863.

[149] V. D. Neff, *J. Electrochem. Soc.* **1978**, *125*, 886-887.

[150] R. J. Mortimer, A. L. Dyer and J. R. Reynolds, *Displays* **2006**, *27*, 2-18.

[151] R. J. Mortimer, *Ann. Rev. Mater. Res.* **2011**, *41*, 241-268.

[152] W. T. Neo, Q. Ye, S.-J. Chua and J. Xu, *J. Mater. Chem. C* **2016**, *4*, 7364-7376.

[153] J. Jensen, M. Hosel, A. L. Dyer and F. C. Krebs, *Adv. Funct. Mater.* **2015**, *25*, 2073-2090.

[154] H. Yashima, M. Kobayashi, K. B. Lee, D. Chung, A. Heeger and F. Wudl, *J. Electrochem. Soc.* **1987**, *134*, 46-52.

[155] X. Lv, W. Li, M. Ouyang, Y. Zhang, D. S. Wright and C. Zhang, *J. Mater. Chem. C* **2017**, *5*, 12-28.

[156] S. Mi, J. Wu, J. Liu, J. Zheng and C. Xu, *Org. Electron.* **2015**, *23*, 116-123.

[157] S. Ming, S. Zhen, K. Lin, L. Zhao, J. Xu and B. Lu, *ACS Appl. Mater. Interfaces* **2015**, *7*, 11089-11098.

[158] J. Y. Lee, S.-Y. Han, I. Cho, B. Lim and Y.-C. Nah, *Electrochem. Comm.* **2017**, *83*, 102-105.

[159] Z. Xu, L. Kong, Y. Wang, B. Wang and J. Zhao, *Org. Electron.* **2018**, *54*, 94-103.

[160] J. L. Bredas and G. B. Street, *Acc. Chem. Res.* **1985**, *18*, 309-315.

[161] L. Beverina, G. A. Pagani and M. Sassi, *Chem Commun (Camb)* **2014**, *50*, 5413-5430.

[162] A. L. Dyer, M. R. Craig, J. E. Babiarz, K. Kiyak and J. R. Reynolds, *Macromolecules* **2010**, *43*, 4460-4467.

[163] C. M. Amb, J. A. Kerszulis, E. J. Thompson, A. L. Dyer and J. R. Reynolds, *Polym. Chem.* **2011**, *2*, 812-814.

[164] A. L. Dyer, E. J. Thompson and J. R. Reynolds, *ACS Appl. Mater. Interfaces* **2011**, *3*, 1787-1795.

[165] K. L. Cao, D. E. Shen, A. M. Osterholm, J. A. Kerszulis and J. R. Reynolds, *Macromolecules* **2016**, *49*, 8498-8507.

[166] P. M. Beaujuge, C. M. Amb and J. R. Reynolds, *Acc. Chem. Res.* **2010**, *43*, 1396-1407.

[167] L. León and J. Mozo, *Trends Anal. Chem.* **2018**, *102*, 147-169.

[168] S. Hellström, P. Henriksson, R. Kroon, E. Wang and M. R. Andersson, *Org. Electron.* **2011**, *12*, 1406-1413.

[169] B. C. Thompson, P. Schottland, K. Zong and J. R. Reynolds, *Chem. Mater.* **2000**, *12*, 1563-1571.

[170] P. M. Beaujuge and J. R. Reynolds, *Chem. Rev.* **2010**, *110*, 268-320.

[171] X. Xing, C. Wang, X. Liu, L. Qin, E. Wang and F. Zhang, *Electrochimica Acta* **2017**, *253*, 530-535.

[172] A. M. Osterholm, D. E. Shen, J. A. Kerszulis, R. H. Bulloch, M. Kuepfert, A. L. Dyer and J. R. Reynolds, *ACS Appl. Mater. Interfaces* **2015**, *7*, 1413-1421.

[173] Z. C. He, B. Xiao, F. Liu, H. B. Wu, Y. L. Yang, S. Xiao, C. Wang, T. P. Russell and Y. Cao, *Nat. Photon.* **2015**, *9*, 174-179.

[174] J. You, L. Dou, K. Yoshimura, T. Kato, K. Ohya, T. Moriarty, K. Emery, C. C. Chen, J. Gao, G. Li and Y. Yang, *Nat. Commun.* **2013**, *4*, 1446.

[175] J. Remmele, D. E. Shen, T. Mustonen and N. Fruehauf, *ACS Appl. Mater. Interfaces* **2015**, *7*, 12001-12008.

[176] S. A. Sapp, G. A. Sotzing, J. L. Reddinger and J. R. Reynolds, *Adv. Mater.* **1996**, *8*, 808-811.

[177] P. Chandrasekhar, B. J. Zay, G. C. Birur, S. Rawal, E. A. Pierson, L. Kauder and T. Swanson, *Adv. Funct. Mater.* **2002**, *12*, 95-103.

[178] P. Chandrasekhar US Patent 5 995 273. **1999**.

[179] X. Xu, P. Cai, Y. Lu, N. S. Choon, J. Chen, B. S. Ong and X. Hu, *Macromol. Rapid Commun.* **2013**, *34*, 681-688.

[180] S. Tang, P. Murto, X. Xu, C. Larsen, E. Wang and L. Edman, *Chem. Mater.* **2017**, *29*, 7750-7759.

[181] P. Murto, S. Tang, C. Larsen, X. Xu, A. Sandström, J. Pietarinen, B. Bagemihl, B. A. Abdulahi, W. Mammo, M. R. Andersson, E. Wang and L. Edman, *ACS Appl. Energy Mater.* **2018**, *1*, 1753-1761.

[182] F. A. Nagia and R. S. R. El-Mohamedy, *Dyes and Pigments* **2007**, *75*, 550-555.

[183] Jean-Luc Brédas, David Beljonne, Veaceslav Coropceanu and Jérôme Cornil, *Chem. Rev.* **2004**, *104*, 4971-5003.

[184] M. R. P. Jeremiah K. Mwaura, David Witker, Nisha Ananthakrishnan, Kirk S. Schanze, John R. Reynolds, *Langmuir* **2005**, *21*, 10119-10126.

[185] J. Liu, E. N. Kadnikova, Y. Liu, M. D. McGehee and J. M. J. Fréchet, *J. Am. Chem. Soc.* **2004**, *126*, 9486-9487.

[186] F. C. Krebs and H. Spanggaard, *Chem. Mater.* **2005**, *17*, 5235-5237.

[187] M. Helgesen, S. A. Gevorgyan, F. C. Krebs and R. A. J. Janssen, *Chem. Mater.* **2009**, *21*, 4669-4675.

[188] M. Helgesen, R. Sondergaard and F. C. Krebs, *J. Mater. Chem.* **2010**, *20*, 36-60.

[189] J. L. Brusso, M. R. Lilliedal and S. Holdcroft, *Polym. Chem.* **2011**, *2*, 175-180.

[190] B. Sun, W. Hong, H. Aziz and Y. Li, *J. Mater. Chem.* **2012**, *22*, 18950.

[191] C. Liu, S. Dong, P. Cai, P. Liu, S. Liu, J. Chen, F. Liu, L. Ying, T. P. Russell, F. Huang and Y. Cao, *ACS Appl. Mater. Interfaces* **2015**, *7*, 9038-9051.

[192] Z.-H. Guo, N. Ai, C. R. McBroom, T. Yuan, Y.-H. Lin, M. Roders, C. Zhu, A. L. Ayzner, J. Pei and L. Fang, *Polym. Chem.* **2016**, *7*, 648-655.

[193] C. Liu, W. Xu, Q. Xue, P. Cai, L. Ying, F. Huang and Y. Cao, *Dyes Pigments* **2016**, *125*, 54-63.

[194] P. Vahdani, X. Li, C. Zhang, S. Holdcroft and B. J. Frisken, *J. Mater. Chem. A* **2016**, *4*, 10650-10658.

[195] M. Bergmann and L. Zervas, *Chem. Ber.* **1932**, *65*, 1192-1201.

[196] L. A. Carpino, *Acc. Chem. Res.* **1973**, *6*, 191-198.

[197] J. Mei, K. R. Graham, R. Stalder and J. R. Reynolds, *Org. Lett.* **2010**, *12*, 660-663.

[198] E. Wang, W. Mammo and M. R. Andersson, *Adv. Mater.* **2014**, *26*, 1801-1826.

[199] Y. Liu, J. Zhao, Z. Li, C. Mu, W. Ma, H. Hu, K. Jiang, H. Lin, H. Ade and H. Yan, *Nat. Commun.* **2014**, *5*, 5293.